Studies on Performance of Ultra High Speed Free-Space Optical Communication Systems

超高速光空間通信システムにおける伝播特性の研究

February 2007

Graduate School of Global Information and Telecommunication Studies
Waseda University

Kamugisha KAZAURA

Graduate School of Global Information and
Telecommunication Studies (GITS),
Waseda University
94 Waseda University Bldg.,
1011 Okuboyama, Nishi Tomida,
Honjo Shi, Saitama
Tel. +81-495-24-6420
Fax +81-495-24-6645

PREFACE

The work presented in this thesis was carried out at Matsumoto Lab, Graduate School of Global Information and Telecommunication Studies, Waseda University. The thesis covers a research project supported by the National Institute of Information and Communications Technology of Japan (NICT) and was carried out in collaboration with various institutions and organisation.

ACKNOWLEDGEMENTS

I am highly indebted to many individuals who have helped me to accomplish this work. First and foremost, I would like to extend my sincere gratitude to my supervisor, Prof. Mitsuji Matsumoto, for providing me with a conducive research environment and immense support during the duration of my studies at GITS, Waseda University. Prof. Matsumoto invaluable contribution apart from directing my research work also includes his kind advice and encouragement throughout.

I would also like to convey my special thanks to my doctoral thesis review panel which included Prof. Takuro Sato and Prof. Shigeru Shimamoto both of GITS, Waseda University, Prof. Katsuyuki Utaka of the School of Science and Enginerring, Waseda University and Prof. Nobuo Nakajima of University of Electro-Communication. I am grateful for their kind acceptance to be reviewers and judges of my doctoral thesis as well as their helpful constructive criticism.

I am deeply indebted to all the members of the FSO project including Mr. Toshiji Suzuki, Mr. Kazunori Omae, Mr. Kazuhiko Wakamori, Mr. Yoshinori Arimoto, Mr. Koichi Takahashi, Mr. Tadaaki Murakami and Mr. Hideki Matsumoto for always being ready to share their extensive knowledge and provide expert opinion. Their valuable technical input is well appreciated.

I would like to extend special thanks to my dear friend, Dr. Edward Mutafungwa, for his infinite suggestions and tireless effort in assisting and contributing in this research work.

I am very grateful to my estemeed past and present colleagues at Matsumoto Lab over the years. I very much appreciate the kind inputs and suggestions I received from Mr. Liu Jun, Mr. Horacio Sanson, Mr. Mohammad Shah Alam, Ms. Ara Shamim Shawkat, Mr. Christian Sousa, Mr. Bekkali Abdelmoula, Mr. Marcus Lucas da Silva and Mr. Hiroyuki Mori. Your presence and friendship simply gave me the support I needed.

Many thanks to all the GITS faculty members and staff who helped and steered me in the correct path to conduct my research and achieve successful results.

I would be remiss if I don't mention the Tanzania community living in Japan especially Amb. E. Mtango who always provided me advice and moral support.

I would also like to thank the Ministry of Education, Culture, Sports, Science and Technology of Japan for the scholarship which enabled me to come and pursue graduate studies in Japan.

And finally, my deepest thanks to Katrine for her constant support. Likewise, my sincerest thanks to my family who have encouraged and stood behind me throughout my studies.

TABLE OF CONTENTS

LIST OF TABLES

LIST OF FIGURES

LIST OF ACRONYMS

A/D	Analogue/Digital
ANSI	American National Standard Institute
AO	Adaptive Optics
AOA	Angle-of-Arrival
APD	Avalanche Photodiode
BER	Bit error rate
BERT	Bit error rate tester
BS	Beam Splitter
BWAN	Broadband Wireless Access Network
CCD	Charge-coupled device
CENELEC	European Committee for Electrotechnical Standardization
DFB	Distributed feedback laser
DSL	Digital Subscriber Line
DSP	Digital Signal Processing
DWDM	Dense Wavelength Division Multiplexing
EC	Evolutionary Computation
EDFA	Erbium-Doped Fiber Amplifier
EFS	Error Free Seconds
FEC	Forward Error Correction
FFS	Free Form Surface
FFT	Fast Fourier Transform
FL	Fuzzy Logic
FO-CDMA	Fiber Optic Code Division Multiple Access
FOV	Field of View
FPM	Fine Pointing Mirror

FSO	Free Space Optical
FTTB	Fiber to the Building
FTTC	Fiber to the Curb
FTTH	Fiber to the Home
FTTN	Fiber to the Node
FWA	Fixed Wireless Access
GaAlAs	Gallium Aluminum Arsenide
GEO	Geostationary Orbit
HC	Hard Computing
ICSA	Infrared Communication Systems Association
IEC	International Electrotechnical Commission
IEEE	Institute of Electrical & Electronics Engineers
IM/DD	intensity Modulation/Direct Detection
InGaAs	Indium-Gallium-Arsenide
IrDA	Infrared Data Association
JISC	Japan Industrial Standard Committee
LAN	Local Area Network
LMDS	Local Multipoint Distribution Service
MEMS	Micro Electro-Mechanical Systems
ML	Maximum Likelihood
MLSD	Maximum Likelihood Sequence Detection
MMW	Millimeter Wave
MNNP	Multi-Layer Neural Network Predictor
MOR	Meteorological Optical Range
MPE	Maximum Permissible Exposure
MSE	Minimum Square Error
NA	Numerical Aperture
NC	Neural Computing
NICT	National Institute of Information and Communications Technology
O/E	Optical/Electrical
OC	Optical Carrier

OOC	Optical Orthogonal Codes
PAN	Personal Area Network
PID	Proportional Integral Derivative
P-MP	Point to Multipoint
PPM	Pulse Position Modulation
PR	Probabilistic Reasoning
PRBS	Pseudo Random Bit Sequence
PSK	Phase Shift Keying
QAPD	Quadrature Avalanche Photodiode
RoFSO	Radion on Free Space Optics
rms	root mean square
SC	Soft Computing
Si APD	Silicon Avalanche Photodiode
Si PIN	Silicon PIN detector
Si QD	Silicon Quadrant Detector
Si QPD	Silicon Quandrant Photodiode
SMF	Single Mode Fiber
SONET	Synchronous Optical Network
SPGD	Stochastic Parallel Gradient Descent
TA	Transimpedence Amplifier
TCP/IP	Transmission Control Protocol/Internet Protocol
TCU	Tracking and Control Unit
TDMA	Time Division Multiple Access
UWB	Ultra-Wideband
WDM	Wavelength Division Multiplexing
WiMAX	Worldwide Interoperability for Microwave Access
WLAN	Wireless Local Area Network
WMAN	Wireless Metropolitan Area Network

LIST OF SYMBOLS AND NOTATION

A, A_{RX}, A_{TX}	Antenna aperture (receive and transmit aperture)
A_{avg}	Aperture averaging factor
A_f	Diameter of radiation pattern in focal plane
a_t	Effective radius
D	Propagation distance
l_0	Inner scale
L_0	Outer scale
L_G	Geometric loss
k	Optical wave number ($k = 2\pi/\lambda$)
λ	Wavelength
σ_I^2	Normalized intensity variance (scintillation index)
d_0	Correlation length of intensity fluctuation
τ_0	Correlation time of intensity fluctuation
τ	Transmittance
I	Intensity
γ	Attenuation coefficient
α_m	Molecular absorption coefficient
α_a	Aerosol absorption coefficient
β_m	Molecular scattering coefficient
β_a	Aerosol scattering coefficient
L	Attenuation (Loss)
ε	Discerment threshold
V	Visibility distance
C_n^2	Refractive index structure constant
r_c	Beam centroid motion

W_{LT}	Long term beamwidth
W_{ST}	Short term beamwidth
f	focal length
σ_A^2	log-amplitude variance
$\Phi(K)$	Refractive index fluctuations spectrum
$\sigma_{\ln x}^2$	Large-scale log-irradiance variance
$\sigma_{\ln y}^2$	Small-scale log-irradiance variance
β_0	Rytov variance
ΔD	Optical path difference
ΔS	Phase shift
ΔS_{RMS}	Root-mean-square image displacement
V_x	Actuator drive voltage x-direction
Vy	Actuator drive voltage y-direction
N	Number of neurons in input layer
R	Number of neurons in hidden layer
T	Number of neurons in output layer
b_j	Bias at the jth hidden neuron
w_{ji}	Connection weight between ith input and jth hidden neuron
f_h	Activation function
β	Regression analysis correlation coefficient
α	Regression analysis y-intercept
r	Regression analysis slope
$< >$	Ensemble average

SUMMARY

Free-space optical (FSO) communication systems are increasingly being adapted to provide high-speed, improved capacity, cost effective, secure and easy to deploy wireless networks. These systems have proven to be an attractive technology for broadband wireless communication when optical fiber links are unavailable or their deployment is simply not feasible (cost prohibitive). This thesis presents experimental work and results on the design, evaluation, prediction and comparison of a new ultra high speed FSO system performance in operational environments.

Currently, the typical channel capacity for optical fiber transmission is from 2.5 Gbps to 40 Gbps, and so far there is no deployed wireless communication network which can deliver this kind capacity. Innovative broadband wireless technologies (for both fixed and mobile applications) operating in the RF, microwave and millimeter wave regions of the electromagnetic spectrum are currently being deployed or are under active research investigations. These technologies include IEEE 802.11 based WLAN systems, IEEE 802.16 based WMAN (WiMAX) systems and ultra wideband (UWB) PAN systems. Unfortunately, these advanced wireless technologies still do not meet the capacity of current optical fiber transmission. Therefore, there is a need for a flexible full optical wireless network (free-space optical communication system) which can provide capacity equivalent to optical fiber.

Conventional FSO systems operate near the 800 nm spectral range and before transmission through the space, the optical signal is converted to electrical signal by the optical transceiver. The electrical signal is amplified by a laser driver and the modulated light from the laser diode is directed through space. At the receiver the optical beam is focused to a photo detector then converted to electrical signal. The electrical signal is again converted back to optical for transmission through

optical fiber. Unfortunately, optical devices using the 800 nm spectral range can not operate above 2.5 Gbps because of the power limitations imposed for eye safety. In order to overcome these bandwidth and power limitations, 1550 nm wavelength is selected for new ultra-high speed FSO systems and its advantages apart from being eye safe include, reduced solar background radiation and compatibility with existing optical fiber technology infrastructure. By using the 1550 nm wavelength, multi-gigabit per second wireless transmission can be achieved by leveraging the technology developed for long haul optical fiber communication e.g. erbium-doped fiber amplifier (EDFA) and wavelength division multiplexing (WDM) as well as advanced optical sources and detectors.

In this thesis, experimental studies on a newly designed FSO communication system operating at 1550 nm wavelength where the optical beam is emitted directly from the fiber termination to free-space and then coupled directly to fiber (usually single mode fiber SMF) at the receiver point is presented. The need for converting the optical signal to electrical and vice versa is omitted. The merits of this wireless communication system include being data rate and protocol independent thus the necessity of reconfiguring the transceivers is eliminated when the nature of the transmit signal changes due to varying bit rates, signal format (analogue or digital) or wavelength channel. The key technology in this kind of FSO communication system is a high-speed beam tracking and control mechanism which is able to suppress the effects of atmospheric turbulence so as to couple as much of the received optical beam to the SMF core having a diameter of about 10 μm. Therefore it is important to investigate the free-space atmospheric propagation properties necessary in the design, evaluation, prediction and comparison of FSO system performance in operational environments. The design of the high-speed beam tracking and control mechanism is a key element.

The primary goal of this thesis is to experimentally study the design and performance of a new ultra high-speed FSO communication system. It is well known that atmospheric turbulence, aerosols and molecular absorption affect the propagation of optical waves in the atmosphere. Atmospheric turbulence effect, manifested as beam wander and scintillation, is the major source of errors in FSO communication links often causing link quality deterioration and sometimes unavailability. Most of the techniques used to improve FSO communication system performance work by suppressing atmospheric turbulence which is a major source of deep signal fades. The experimental study is

conducted using a 1 km link FSO communication system setup in the Waseda campus area.

A relative simple technique for atmospheric turbulence mitigation is introduced. The technique utilizes a fast beam tracking miniature fine pointing mirror (FPM). The FPM function is to control and steer the beam to the fiber connection port. The advantages of using the miniature FPM for atmospheric turbulence mitigation compared to the other techniques is that the FPM can improve the FSO system performance with less complexity and minimum electronic overhead and at the same time maintaining a compact size antenna of about 10 cm cubed.

A method to determine the FPM optimum tracking speed has been proposed. This method determines the tracking speed by measuring the received signal intensity fluctuations as a result of atmospheric induced scintillations effects and comparing it with the signal variations caused by angle-of-arrival (AOA) fluctuations. The frequency response characteristics for the two measured data set (after performing FFT to the time series data) show similarity in the magnitudes of intensity fluctuation. From this result, an approximation for the antennas' fast beam steering FPM tracking speed has been determined. In this case, the FPM tracking speed is chosen to respond faster than the AOA fluctuations and is set to 1 kHz. The beam intensity fluctuations because of AOA fluctuations were suppressed remarkably.

The ultra high-speed FSO communication system performance evaluation in terms of bit-error-rate (BER) after setting the antenna tracking speed to 1 kHz was conducted. The improvement in atmospheric turbulence suppression is evident from the reduced errors and continuous stable full-duplex (bi-directional) transmission at 2.5 Gbps and 10 Gbps has been demonstrated under clear and quiet weather conditions.

A comparison on the performance of free-space optical systems operating in the 800 nm and 1550 nm wavelengths is presented. Up to now, there is no comprehensive long term statistical analysis data collected comparing the atmospheric turbulence effects on the performance and propagation characteristics of conventional 785 nm and new 1550 nm wavelength FSO communication systems deployed in the same environment. In this thesis an opportunity to conduct such experiment by measuring and analyzing collected data over a long period of time was presented.

The thesis also focuses on long-term experimental measurement, characterization and quantifying the effects of atmospheric turbulence experienced on ultra high speed FSO communication

system. Among the results after careful observation of the measurement data is that the magnitude of atmospheric induced scintillation fluctuation is not only determined by high temperature, but rather the difference between the ground and the air temperature. When this temperature difference is high, the degree of scintillation fluctuation is also high. Also by comparing the atmospheric turbulence measurement during arbitrary chosen summer and winter months, it was shown that the midday maximum of refractive index structure constant parameter, C_n^2, could change by a factor of 2.3. Therefore, the increased occurrence of bursts errors in the ultra high speed FSO system during the summer months, because the FPM could not suppress the strong atmospheric turbulence ($C_n^2 > 10^{-13}m^{-2/3}$).

And finally, this thesis explores a method to suppress burst errors which occur in periods of strong atmospheric turbulence ($C_n^2 > 10^{-13}m^{-2/3}$). Under such events, the FPM signal fading suppression capability is diminished. Therefore in order to avoid signal fading in such situation, the use of a soft-computing (SC) based multi-layer neural network predictor (MNNP) is proposed. The SC based tools are used for the prediction of key parameters of the FSO communication system. Measured data collected from the experimental FSO communication system is used as training and testing data for a proposed MNNP used to predict future parameters. From simulation studies, the parameters values predicted using the proposed tool show acceptable conformity with the original measurements. This demonstrates that soft-computing based tools can be used to enhance the performance and reliability of FSO communication systems especially in periods of strong atmospheric turbulence when the antenna tracking and control unit temporary looses it tracking capability.

CHAPTER 1

INTRODUCTION

In contrast to electrical communications, transmission of information in an optical format is carried out not by frequency modulation of the carrier but by varying the intensity of the optical power. Similar to radio frequency spectrum, two classes of transmission medium can be used: an atmospheric channel or a guided wave channel. Optical transmission using guided wave channel, commonly known as optical fiber communication, was first deployed in 1974 and their transmission capacity has experienced a 10-fold increase every 4 years [1]. Several major technology advances have spurred this growth including the emergence of erbium-doped fiber amplifiers (EDFAs) [2], wavelength-division multiplexing (WDM) and optical sources and photodetectors capable of working on higher wavelengths.

To further enhance the capacity of optical networks (by employing efficient wavelength utilization methods) various optical techniques have been introduced including fiber optic code-division multiple-access (FO-CDMA) using optical orthogonal codes (OOCs) and their variation [3], [4]. FO-CDMA have received much attention due to their simple structure and compatibility with today's intensity-modulation direct-detection (IM/DD) fiber optic transmission [5]. Moreover, further improvement techniques including methods to enable dynamic provision of bandwidth available in optical networks within acceptable cost bounds are being carried out. For example, architectures for improved scalability for handling more connections (increased capacity) in WDM networks have been explored in [6].

Early development of free-space optical (FSO) communication, also known as optical wireless communications, was directed toward space-based applications [7]. Due to the relative immaturity of laser technology and flawed system demonstrations, research in free-space optical communication experienced a decline in interest. The ever increasing power of computer and data-storage

devices in the mid and late 1990's and the rapid proliferation of information exchange desired by institutions such as commerce, finance, education, health, government, security and entertainment renewed interest in FSO communication. By this time, optical fiber communication had been well established and researchers had found ways to utilized these efficient, cost-effective components for FSO systems.

The increase use of bandwidth intensive application like streaming audio and video, high-speed web access and massive data downloads has brought about requirements of networks which can meet this demand in terms of data rates and capacity. Higher speed telecommunication applications such as Time Division Multiplexed (TDM) circuits (OC-48 and greater) and Gigabit Ethernet has become part of today's mainstream enterprise network environment thus driving the demand worldwide wireless bandwidth increasing beyond 622 Mbps [8]. Various competing wireless technologies have been proposed and standardized to support this array of advanced data services. These include systems operating in the millimeter wave band (60 GHz), ultra wide band (UWB) technologies, and other RF and micro wave technologies. Free space optical (FSO) communication systems represent one of the most promising approaches for addressing the emerging broadband network requirements [9], [10]. The increase demand of wireless links which are easier, faster and less expensive to deploy has revived the interest in the use of free-space optics in digital transmission of signal in the atmosphere [8, 11–18].

1.1 Background of Free Space Optical Communication

Depending on the deployment scenario and application, FSO communication systems are suitable for terrestrial and space based communication. In the case of terrestrial communication, FSO systems are usually deployed for last mile access, enterprise connectivity, fiber backup and long haul. For space based communication, FSO systems are applied for inter-satellite communication, manned spacecraft, data broadcasting satellites and satellite and ground station communications.

Current available FSO systems can be classified into two categories depending on the operating wavelength. There are systems which operate near the 800 nm wavelength band and those that operate near the 1550 nm. However, FSO systems which operate near the 800 nm are incompatible with most current high capacity optical fiber systems. Because of the power and bandwidth limitations imposed on optical devices operating in the 800 nm wavelength, they can not operate at a data rate above 2.5 Gbps. Reasons for selecting 1550 nm wavelength for FSO systems include eye safety,

reduced solar background radiation and compatibility with existing technology infrastructure. By using FSO system operating near the 1550 nm wavelength, high data rates can be achieved by leveraging the technology developed for long haul optical fiber communication e.g. erbium-doped fiber amplifier (EDFA) and wavelength division multiplexing (WDM).

The next generation of ultra high-speed free-space optical (FSO) communication systems will utilize seamless connection of free-space and optical fiber links operating at 1550 nm. By directly coupling the received beam into an optical fiber (usually single mode fiber) the FSO communication system signal throughput is greatly enhanced. Seamlessly coupling a free-space beam to optical fiber a bandwidth and protocol transparent communication link is achieved. In this regards, the need for reconfiguration of the transceivers is eliminated when the nature of the transmit signal changes due to varying bit rates, signal format (analogue or digital) or wavelength channel.

1.2 Free Space Optical Communication techniques

In attempts to improve the reliability of FSO communication systems researchers have pursued a variety of system architectures. FSO system use intensity modulation/direct detection (IM/DD) technique or on-off keying (OOK) to transmit information. This is simply turning the optical source on when transmitting "1" bits and turning the optical source off when transmitting "0" bits. It is a low over head technique because no attempt is made to ensure the integrity of the signal and allows FSO systems to be designed as a bandwidth and protocol transparent physical layer link. This transmission scheme attempts to collect enough photons at the receive to correctly detect "1" and "0" bits. Atmospheric turbulence may easily prevent the detection of a sufficient number of photons to correctly interpret the received bits [19].

Atmospheric turbulence causes fluctuation in both the intensity and the phase of the received optical beam, impairing the link performance thus leading to an increase in the link error probability [20], [21–24]. Researchers have come up with various techniques to improve the performance of FSO communication links. These include techniques which where developed over the years to mitigate atmospheric turbulence induced effects on imaging systems, like improving the quality of stellar telescopes. These techniques, also applicable in FSO systems, include post processing techniques and adaptive optics. The later consist of deformable mirrors, wave-front sensors and actuator commands computer to sense and correct wave-front deformation in real time [25], [26]. Atmospheric induced intensity fluctuations i.e. signal fading can also be reduced by using aperture

averaging (when using large receive apertures) and diversity techniques like using multiple transmit and/or receive apertures [27].

1.3 Main research contribution

The primary research contribution presented in this work is in the methods of measuring, characterization and quantifying the influence of atmospheric effects relevant in the design of a FSO communication system and primarily in the design of the antenna tracking system. The results are used in the evaluation, prediction and comparison of FSO communication system performance in operational environment.

The optical beam tracking and control system is crucial in determining the performance and reliability of FSO communication system. Atmospheric turbulence manifested as beam wander and scintillation is the major source of FSO link deterioration and errors. A technique to avoid deep signal fades by suppressing atmospheric turbulence effects is proposed and experimentally demonstrated. The technique uses a fast beam tracking miniature fine pointing mirror (FPM). The FPM has the vital function of controlling and steering the received beam to the SMF connection port. It works by receiving information on beam position changes from a position sensitive silicon quadrant detector (Si-QPD) utilized for fine tracking. The merit of using the fast beam tracking miniature FPM for atmospheric turbulence mitigation compared to the other techniques is that the FPM manages to improve the FSO system performance with less complexity and minimum electronic overhead while maintaining compact size antenna.

Another contribution of this research work is in methods of measuring and quantifying the external parameters which influence the performance of FSO systems, especially the parameters related to the system deployment environment. These external parameters include atmospheric turbulence effects which contribute to the performance deterioration of FSO communication links. A method to determine the optimum antenna miniature FPM tracking speed is studied and proposed. This is determined by measuring the received signal fluctuations as a result of scintillations effects then making comparisons with the signal variations caused by angle-of-arrival (AOA) fluctuations. The frequency response characteristics for the two collected data show similarity in the magnitudes of intensity fluctuation. From the power spectrum at various frequencies, the optimum antenna FPM tracking speed can be approximated which in this case was found to be 1 kHz.

The miniature FPM signal fading suppression capability is reduced in situations of strong

atmospheric turbulence ($C_n^2 \geq 10^{-13} m^{-2/3}$). As a result, burst errors occur in the link. In order to avoid deep signal fading in such situation, the use of a soft-computing (SC) based multi-layer neural network predictor (MNNP) is proposed. The SC based tools can be used for the prediction of key parameters of the FSO communication system. The data collected from the experimental FSO communication system is used as training and testing data for a proposed multi-layer neural network predictor used to predict future parameters. From the simulation studies, the parameters values predicted using the proposed tool show acceptable conformity with the original measurements. This demonstrating that soft-computing based tools can be used to enhance the performance of FSO communication systems especially in periods of strong atmospheric turbulence when the antenna tracking and control unit temporary looses it tracking capability.

1.4 Organization of the Thesis

This thesis is organized in 5 chapters detailing the theory, experimental work including design, evaluation and analysis as well as performance enhancements techniques for ultra high-speed FSO communication systems. The primary goal of the thesis have been outlined in section 1.3. The rest of the thesis is organized as follows:

Chapter 2 provides an overview of FSO communication systems. The marits for deploying FSO systems over other wireless technology is outlined. The advantages of FSO communication over RF or millimeter wave (MM-wave) systems include the potential of providing fiber like capacity. A detailed description of conventional FSO systems operating in the 800 nm spectral range and new FSO system using 1550 nm wavelength is presented. The design and performance advantages of new FSO systems over conventional systems include increased capacity, bandwidth and data rate transparent because of the seamless coupling of free-space beam directly to optical fiber and compatibility with existing widely deployed optical fiber infrastructure. This chapter also describes techniques used to improve the performance and reliability of FSO communications systems as well as the proposed technique using a miniature fine pointing mirror (FPM). Details of the optical antenna design and tracking mechanism used in this experimental system are described. A method to determine the optimum FPM antenna tracking speed is given and atmospheric turbulence suppression capability by the FSO communication system by using a fast beam tracking mechanism is presented.

In chapter 3, the detailed experimental performance evaluation including results and analysis

of the FSO communication system is given. First the setup and specifications of the FSO systems used in this experiment are outlined. The atmospheric effects like optical power attenuation, beam wander and scintillation which influence the propagation of FSO beam in the atmosphere are measured and characterized. The effects of atmospheric turbulence by comparing data collected on different seasons and weather conditions is analysed and presented. It is observed that the degree of scintillation fluctuation is greater when the difference between the ground and air temparature is highest which is usually during midday. Also by comparing the atmospheric turbulence measurements during arbitrary chosen summer and winter months it was shown the midday maximum of refractive index structure constant parameter, C_n^2, can change by a factor of 2.3.

Also a comparison of intensity fluctuation as a result of scintillation effect and angle-of-arrival (AOA) fluctuation is conducted and the results show similarity in the power spectrum and this information is used in determining the miniature FPM tracking speed of 1 kHz. Comparisons of the propagation characteristics for a conventional 785 nm wavelength FSO system and a new ultra high-speed full duplex FSO system operating in the 1550 nm wavelength is presented. The BER and fiber received power characteristics under various weather conditions is also conducted and analyzed. A stable and reliable performance of the new ultra high-speed FSO communication system is observed under quiet and clear weather conditions. Whereas, under strong atmospheric turbulence conditions ($C_n^2 \geq 10^{-13} m^{-2/3}$), heavy rain and snow event or when there is poor visibility, the system performance deteriorates.

In Chapter 4, a performance enhancements technique for the free-space optical communication systems is proposed and investigated. The techniques applies soft-computing (SC) based tools. The possibility of using SC to assist the current tracking mechanism in suppressing burst errors which occur in the system in periods of strong atmospheric turbulence is explored and presented. Under such conditions the FPM signal fading suppression capability is reduced. The description of the proposed SC-based multi layer neural network predictor (MNNP) is outlined. The different possible implementation architectures with the current antenna tracking and control unit are investigated. Experimentally measured data is used as training data for the proposed MNNP used to predict future parameters. From simulation studies, the predicted values using the MNNP show conformity with the original measurements which demonstrates that this system is feasible.

And finally Chapter 5 provides the concluding remarks of this thesis work. Critical analysis of the results is presented and areas of future research are outlined.

CHAPTER 2

FSO COMMUNICATION SYSTEMS

Traditionally, information has been relayed over cable, fiber and copper lines, but recently it is now increasingly being relayed over air, i.e., through wireless transmission. New wireless communication methods and services have been enthusiastically adopted by people throughout the world since Gugliemo Marconi first demonstrated radio's ability to provide continuous contact with ships sailing the English channel in 1897 [28]. The mobile communication industry has experienced tremendous growth in recent years fueled by digital and RF circuit fabrication improvements, new large-scale circuit integration and other miniaturization which make portable radio equipment smaller, cheaper and more reliable [29]. The scarcity of spectrum in the RF band due to the increase number of wireless devices operating in this band and the demand for broadband wireless access technology has compelled a shift for the use of higher frequency (in the millimeter wave region) and optical band of the electromagnetic spectrum [30], [31]. Broadband wireless access network (BWAN) systems are emerging as a new and growing area of telecommunications, since the ability to provide access without extensive installation of copper or fiber infrastructures make wireless technology well suited for broadband services.

Free-space optical (FSO) links can be used to setup FSO communication networks or to supplement radio and optical fiber networks [32]. It is a good solution for broadband wireless for closing the "last mile" connectivity gap throughout metropolitan networks. FSO communication systems are suitable in dense urban areas and are ideally suited for urban applications. The advantages of FSO communications include quick link setup, license free operation, high transmission security, high bit rates, full duplex transmission and protocol transparent. Figure 2.1 depicts the current trend in wireless communication technology and the relative position of FSO communication.

To date, various wireless technologues (as shown in Figure 2.1) have been developed and are

used for personal area networks (PANs) and local area networks (LANs). These technologies have different data rates and coverage distance. Therefore depending on the deployment scenario, intended application and the cost benefit analysis, some technologies can be more suitable than others. FSO systems can offer data rates from 10's of Mbps to several 10's of Gbps with distance ranging from a few meters to 10 km and more. It is the only wireless communication technology capable of providing the capacity offered by optical fiber transmission systems i.e. above 2.5 Gbps data rate. It's disadvantages when compared to other wireless communication systems is the propagation distance. For terrestrial application, FSO systems propagation is limited up to several 10's of kilometers because of atmospheric effects and can not propagate through obstacles.

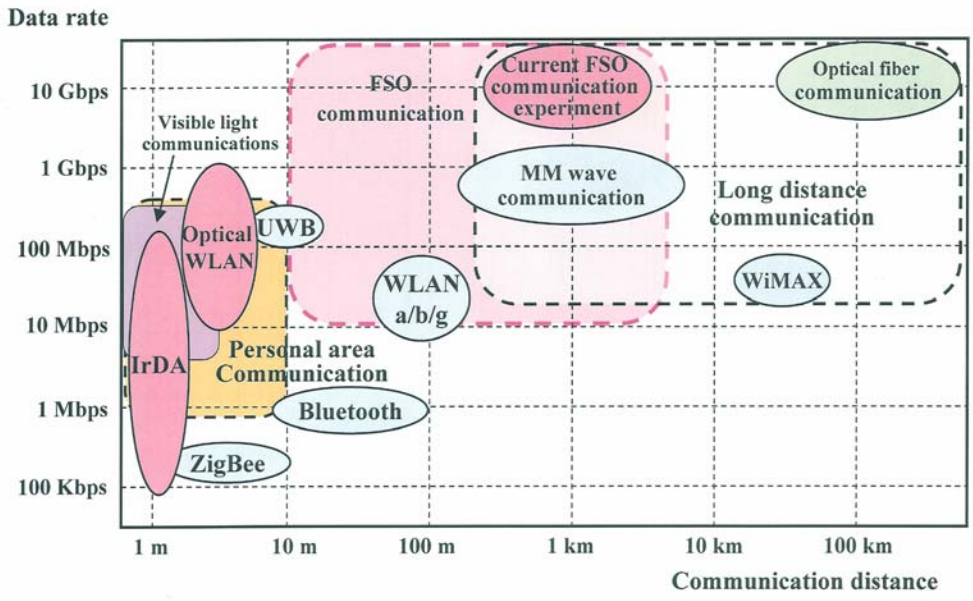

Figure 2.1: Wireless communication technology map

The frequency of various RF carriers vary from 550 kHz (AM radio) to the highest mm-waves (about 60 GHz) where as the infrared carrier frequencies are about 10,000 times higher. Since the information bandwidth is a direct function of carrier frequency, the broadband capabilities of free space optical systems are significantly higher than RF and with WDM technology several of hundreds times higher [33]. Table 2.1 summarizes some of the trade-offs between RF and IR.

Parameter	RF	IR	Implications
Max bandwidth	Limited	Unlimited	
Subject to regulation	Yes	No	Delays
Propagation through obstacles	Yes	No	Security
Dominant noise	Other users	Background	Limits range
Thresholds	-60 dBm	-40 dBm	LMDS easier with RF
Weather effects	Rain	Fog	Up to -120 dB/km
Side lobes	Yes	No	Interference
Health issues	Possible	No	Eye safety limits

Table 2.1: Trade-offs between RF and IR

Apart from terrestrial application of FSO communication systems, the application of FSO for ground to space communication has been extensively researched and applied. Compared to horizontal path links exceeding 10 km range, space-to-ground links for satellite laser communications involve beam propagation through lower air mass where the impact of atmospheric turbulence effects is less severe than that encountered on horizontal links. On the other hand, space-to ground links involve dynamic tracking and pointing strategies in order to maintain line-of-sight and compensate for space platform vibrations and jitter. Ground to geo-stationary orbiting (GEO) spacecraft is an exception where the line-of-sight is also essentially static [34].

Ultra high-speed FSO communication systems capable of offering multi gigabit per second data rates is achieved by leveraging the mature technology developed for long haul optical fiber technology [13], [35], [36]. These major technology advances which also spurred the growth of optical fiber technologies include the development of optical sources and photodetectors capable of operating at different wavelengths [1]. FSO technology roadmap is depicted in Figure 2.2[1]. From as early as 1990, FSO communication systems which could offer data rates of up to several 10's of megabits per second where commercially available. The achievable FSO systems data rates have been gradually increasing with the increasing adaptation of optical fiber technology and penetration of fiber into the access network such as FTTx (the most common architectures being fiber-to-the-home (FTTH), fiber-to-the-building (FTTB), fiber-to-the-curb (FTTC), and fiber-to-the-node (FTTN)) [38].

[1] Adapted from [37]

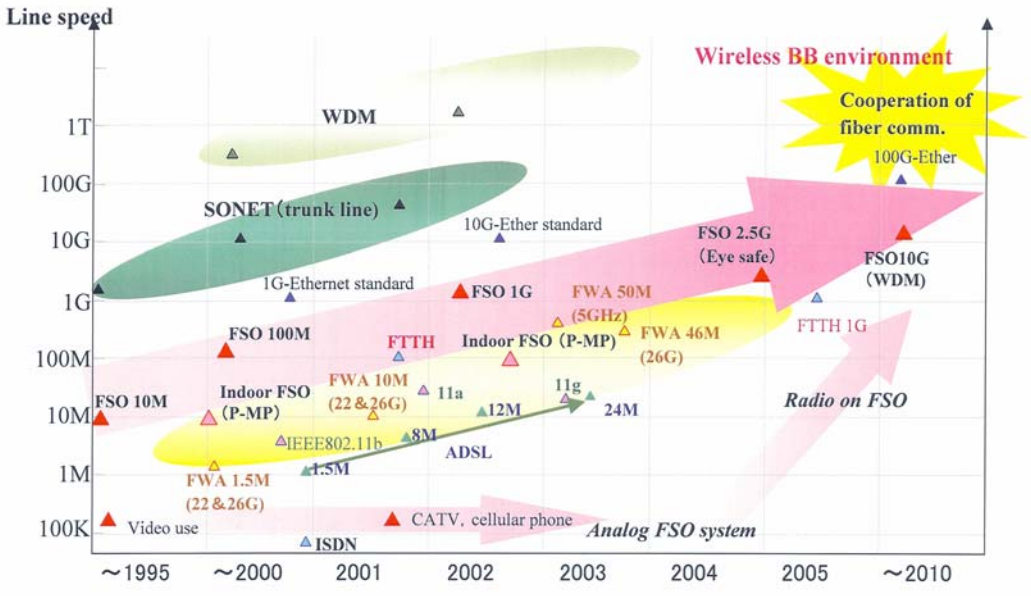

Figure 2.2: FSO technology roadmap (Adapted from ICSA Techn. Group)

Commercially available FSO communication systems offer capacities in the range of 100 Mbps to 2.5 Gbps and demonstration of a system capable of offering 160 Gbps using 1550 nm wavelength over 200 m has been reported in [39]. The research work covered in this thesis is development and experimental demonstration of a FSO communication system capable of providing a single channel 1550 nm wavelength 10 Gbps transmission link. As future work, this system can be investigated for investigations in developing a Radio on FSO (RoFSO) system capable of providing a free space for heterogeneous wireless services in free space optics [40]. RoFSO can realize a universal platform to quickly and effectively provide ubiquitous wireless services (e.g. for rural areas). Services can be connections for cellular basestations, digital TV, WLAN access points and other wireless services.

2.1 FSO communication technology

FSO is the transmission of a modulated visible or infrared (IR) beam through the atmosphere to obtain broadband communications. Several transmission windows are available for FSO transmission through the atmosphere. In the most commonly used atmospheric windows for FSO, the most common absorbing particles are water (H_2O), carbon dioxide (CO_2) and ozone (O_2). A typical absorption spectrum is shown in Figure 2.3[2]. Well known windows exist between 720 and 1550 nm,

[2] Adapted from [41]

some with narrow boundaries. The region between 700 - 2000 nm is dominated by water vapour absorption, whereas the region from 2000 - 4000 nm is dominated by a combination of water and carbon dioxide absorption [13]. In the figure, the molecule responsible for each absorption band is shown in the upper part.

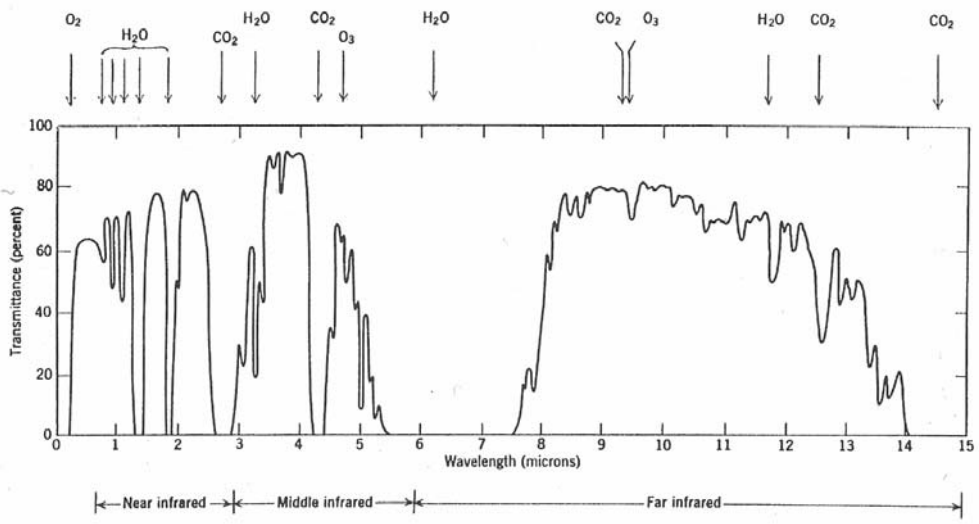

Figure 2.3: Atmospheric transmittance measured over a sea level 1820 m horizontal path

In traditional FSO systems, a fiber transceiver converts an electrical signal to optical signal. The electrical signal is amplified by a laser driver providing enough current to drive the laser diode. Modulated light from the laser diode is directed through space to the corresponding receiver which focuses the beam onto a commercially available photo detector like silicon avalanche photodiode (Si APD) or a silicon PIN photodiode (Si PIN PD). The photo detector converts the optical signal to electrical signal. After noise filtering and reshaping the electrical signal is converted at the fiber transceiver back to an optical signal. This process is depicted in Figure 2.4. Most FSO optical systems operating in this way operate near the 800 nm wavelength band and have been demonstrated to be able to transmit data rates up to 2.5 Gbps. However, because of power and bandwidth limitations of the optical devices it is not possible to operate above this data rate [24].

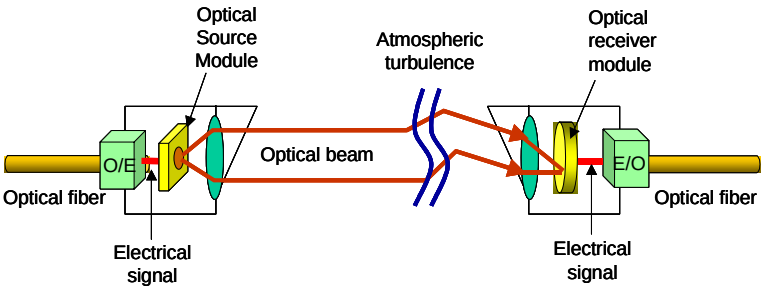

Figure 2.4: FSO system using O/E and E/O conversion

In order to overcome the bandwidth and power limitations imposed by optical devices for FSO communication systems outlined above, technology which gave a major boost to fiber transmission capacity is applied. With the advent of optical amplifiers in 1989 like gallium aluminum arsenide (GaAlAs) based solid-state optical amplifiers and erbium-doped fiber amplifiers (commonly called EDFAs) operating at around 1550 nm together with the use of wavelength division multiplexing (WDM) offered further boost to fiber transmission capacity [1], [2]. The basis of WDM is to use multiple light sources operating at slightly different wavelengths to transmit several independent information streams over the same fiber. By applying these technologies and seamlessly connecting a free space optical beam to single mode fiber (SMF), which is the most widely deployed fiber technology, a FSO system capable of offering higher data rates in terms of several gigabits per second is attained. The neccessity of converting the signal from optical-to-electrical (O/E) and vice versa is eliminated. By directly coupling the received beam into an optical fiber the FSO communication system the signal throughput is greatly enhanced. Seamlessly coupling a free-space beam to an optical fiber (SMF) a bandwidth and protocol transparent communication link is achieved. Figure 2.5 shows the process of a FSO system operating without any O/E or E/O conversion. Commercially available off the shelf detectors like InGaAs detectors for operation in the 1550 nm wavelength that support bandwidth of 10 Gbps and beyond are employed.

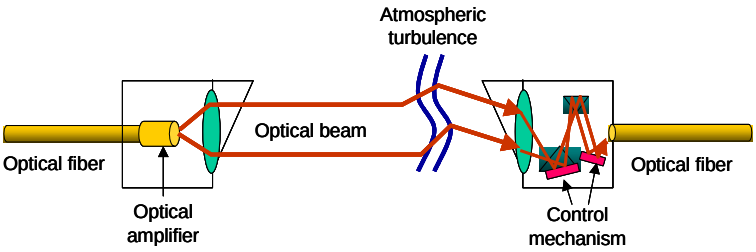

Figure 2.5: FSO system using seamless connection of FSO beam to fiber

It should be noted that several factors are usually considered when selecting wavelength for FSO communication systems. Optical fiber technologies use either 1310 nm or 1550 as transmitting wavelength. Unfortunately, the 1310 nm wavelength is a poor choice for free-space transmission because of high atmospheric absorption near 1310 nm for water vapour [13]. Also the availability of EDFA and laser diodes for DWDM operating in this wavelength is limited. The important advantage of using the 1550 nm wavelength for FSO resolve around power, distance and eye safety. Optical beams at 1550 nm tend not to reach the retina of the eye, being mostly absorbed by the aqueous fluid of the eye preventing it traveling to the retina and inflict damage[3]. Regulating agencies allow longer wavelengths beams to operate at higher power than 800 nm beams by about two order of magnitude. The power increase can boost link lengths by a factor of at least five while maintaining adequate signal strength for proper link operation. Thus for high data rates, long distances, poor propagation conditions (like fog), or combination of these conditions, 1550 nm is considered to be quite applicable[4]. Therefore there are compelling reasons for selecting 1550 nm FSO systems due to laser eye safety, reduced solar background radiation, and compatibility with existing technology infrastructure and/or support higher data rates.

As more practical and robust FSO systems are being devoloped, the design desicion has been based on specifying the 1550 nm as the nominal wavelength. This specification is not only based on the eye-safety issues outlined above but also on the number of practical and cost related advantages of 1550 nm which have been argued in more detail in [46].

The case for 1550 nm operation is so compelling that most FSO companies which initially designed systems operating in the 800 nm spectral range, including companies like LightPointe (FlightStrata^{TM} and FlightLite^{TM} line of products) [47], TeraBeam, Inc. (TeraOptic^{TM}) [48], [49], fSONA (SONAbeam^{TM} products) [16], Canon (Canonbeam^{TM}) [50], Hamamatsu Photonics Corp. (Photoliner^{TM}) [51] and MRV Communications, Inc. (TereScope^{TM}) [52] among others, are actively developing commercially available systems operating in the 1550 nm spectral range.

[3] All the laser beams transmitted through the atmosphere should be at irradiance levels well below the maximum permissible exposure (MPE) levels at the exit apertures specified by respective entity responsible for laser safety standard. The International Electrotechnical Commission (IEC) publishes international standards related to all electrical equipment, including laser and laser equipment (IEC60825-1) [42]. In the US, the American National Standards Institute (ANSI) publishes standards for laser use (ANSI Z136-1) [43]. In Europe, the European Committee for Electrotechnical Standardization (CENELEC) [44] is the responsible entity while the Japan Industrial Standard Committee (JISC) [45] is the responsible entity.

[4] FSO community has also suggested operation in the longer wavelength transmission windows between 3 - 5 μm and 8 - 14 μm due to excellent characteristics of atmosphere. However recent studies have shown no significant advantages of using these longer wavelengths windows and also the availability of light source and detectors operating in this wavelength is very limited.

2.2 Techniques for improving reliability of FSO systems

Free-space optical communication through atmospheric turbulence has been under active research and various methods have been proposed to mitigate turbulence-induced communication signal fading. The wave-front distortions arising from these optical inhomogeneities caused by turbulence as the FSO beam propagates through the atmosphere may severely impact the performance of FSO communication systems resulting in communication link deterioration, i.e., an increase of the number of errors in the received signal. The bit error rate (BER), a the major communication system performance metric, depends on both short-term errors resulting from electronic-circuit related noise and the turbulence induced long-term random breaks (up to tens of milliseconds) in communication data traffic known as atmospheric signal fading [26]. By using various data coding techniques developed for RF and wired communication systems the short-term data losses can be recovered [53]. In contrast, atmospheric-turbulence-induced deep signal fading represents a unique and significantly more challenging problem, which cannot be solved using conventional data coding techniques without sacrificing communication system efficiency, i.e., data throughput rate [26].

In practical FSO communication systems, various techniques have been developed or are applied to mitigate atmospheric effects such as scintillation or beam wander. These techniques include adaptive optics (AO), use of large receive apertures (aperture averaging), diversity techniques and fast tracking antennas [10]. Adaptive optics techniques, originally developed for atmospheric compensation in astronomical sites, restores the distorted wave-front to its original state before it was destroyed by atmospheric turbulence. Although AO have shown limited success, they require bulky and computation-intensive systems to achieve wave-front sensing and correction.

Communication techniques utilized to mitigate turbulence-induced intensity fluctuations, i.e., signal fading in FSO communications systems are described in more detail in the following subsection.

2.2.1 Aperture averaging

The decrease in scintillation with increasing telescope collecting area, known as aperture averaging, had been recognized in early astronomical measurements made in the 1950's [54]. More recently, aperture averaging effects have been studied in the context of laser beam propagation through atmospheric turbulence [55] Ch. 6. Aperture averaging is considered to be a low overhead technique for mitigating the effects of atmospheric turbulence in FSO communication systems which can

be designed using techniques that add nearly no power, bandwidth, size or weight overhead to the overall design. In [19] the behavior of aperture averaging in weak and strong turbulence condition by comparing the experimental data with available models for plane and spherical wave propagation where carried out and new expressions for the aperture averaging factor in weak turbulence proposed.

The amount of intensity fluctuation varies with the size of the receiver. Aperture averaging is the effect of receiver size on the intensity variance [55]. The aperture averaging factor A_{avg} is defined as the ratio of the normalized intensity variance (σ_I^2) of fluctuations of receiver A_{RX} to that of a point receiver. The signals are normalized by the square of the average signal. For a plane wave with small inner scale, $l_0 << (D/k)^{1/2}$, where D is the propagation length and $k = 2\pi/\lambda$ is the wave-number, the aperture averaging factor may be approximated by [23]

$$A_{avg} = \frac{\sigma_I^2(A)}{\sigma_I^2(0)} = \left[1 + 1.062\left(\frac{kA^2}{4D}\right)\right]^{-7/6} \tag{1}$$

A receiver must be large enough to collect sufficient power and reduce scintillation effects at a given range, but must also be small enough to be of practical size [56]. Because of a nonlinear reduction in scintillation with increasing the diameter, the receiver does not need to be of a very large diameter. It should be noted that as turbulence becomes more severe, aperture averaging becomes more effective in reducing the intensity variance, but only up to a point.

Two useful parameters describing turbulence induced fading are d_0, the correlation length of intensity fluctuations and τ_0, the correlation time of intensity fluctuations. When the receiver aperture, A_{RX}, can be made larger than the correlation length, d_0, then turbulence-induced fading can be reduced substantially by aperture averaging [13].

2.2.2 Diversity techniques

Because it is not always possible to satisfy the condition $A_{RX} > d_0$, alternative techniques have been proposed for mitigating fading in the regime where $A_{RX} < d_0$ [57]. Diversity technique is one of the alternative techniques proposed for mitigating atmospheric turbulence induced fading. The use of diversity techniques increases the likelihood that the detected signal will be read correctly by propagating the optical wave-front in at least two distinct ways. Diversity can occur in the form of spatial diversity (requiring multiple transmitters and/or receivers), temporal diversity (requiring signal to be transmitted twice, separated by a time delay) and wavelength diversity (requiring the

transmission of data on at least two distinct wavelengths).

In [57] an alternative technique for mitigating fading in the regime where $A_{RX} < d_0$ are proposed. The techniques are based on the statistical properties of turbulence-induced signal intensity fading as a function of both temporal and spatial coordinates. In the temporal domain employing a single receiver, if the receiver has knowledge of the marginal fading distribution, but knows neither the temporal fading correlation nor the instantaneous fading state, a maximum-likelihood (ML) symbol-to-symbol detection is used. If the receiver knows the joint temporal fading distribution, but not the instantaneous fading state, the receiver can use a ML sequence detection (MLSD) technique to mitigate turbulence induced fading. By using the proposed techniques to mitigate turbulence induced fade, [58] demonstrated the technique in a 500m terrestrial link using OOK to yield signal to noise ratio gains of 2.4 for MLSD.

In the spatial-domain techniques at least two receivers must be employed to collect the signal light at different positions or from different spatial angles. To maximize the diversity reception gain, the multiple receivers should be placed as far apart as possible, so that the turbulence-induced fading is uncorrelated at the various receivers. However, in practice. it may not always be possible to place the receivers sufficiently far apart therefore in [57] making use of the spatial correlation of turbulence-induced fading, an optimal ML detection scheme for correlated spatial diversity reception was derived.

Even though diversity techniques are promising, they do require significant electronic overhead in the retiming and synchronization process [19].

2.2.3 Adaptive optics

Adaptive optics (AO) technology was initially developed for atmospheric compensation in astronomical observation sites, whose locations are selected specifically in view of low turbulence-induced distortions [26]. Wave-front distortions can be mitigated, in principle, with adaptive optics, i.e., real-time wave-front control, reducing the likeliness of signal fading [59–63].

Adaptive optics are designed to measure wave-front errors continuously and correct them automatically. The corrections are made by special computer controlled deformable mirror that can change its shape to correct the wave-front errors in the system. The wave-front errors are measured by a highly accurate system called a wave-front sensor that provides correction signal to the mirror. The complete assembly of wave-front sensor, deformable mirror, computer, control hardware and software form an adaptive optic system.

Adaptive optics is used in FSO communication systems to:

- Dynamically correct wave-front distorted by the atmosphere
- Suppress optical signal fades
- Precisely steer beam to receiver
- Precisely couple both end of the link for maximum signal to noise ratio.

However, adaptive optics technology, which has been primarily utilized in astronomical imaging, needs to be adapted to the requirements of free-space optical communication systems and their specific challenges.

In [26] a non-conventional adaptive optics approach that optimizes the optical signal that could be coupled into a single-mode fiber after propagating along a 2.3 km near-horizontal atmospheric path is proposed. The technique is unrestricted to wave-front measurements, which are difficult under the strong scintillation conditions, but is based on the direct optimization of a performance quality metric, e.g., the communication signal strength, with a stochastic parallel gradient descent (SPGD) algorithm. The experimental adaptive optics system comprising of a beam-steering and a higher-resolution wave-front correction unit with a 132 actuator micro-electro mechanical system (MEMS) piston-type deformable mirror controlled by a VLSI system implementing the SPGD algorithm is employed

2.2.4 Coding techniques

It is also possible to improve the reliability of FSO system by utilizing coding schemes used in RF and wired communication systems. Channel coding refers to the class of signal transformation designed to improve communications performance by enabling the transmitted signal to better withstand the effects of various channel impairments, such as noise, interference, and fading. These signal processing techniques are used to accomplish desirable system trade-offs (e.g. error performance versus bandwidth, power versus bandwidth) [64], [65].

Suggestions of using error correcting codes such as convolution codes for free-space optical communication systems has been proposed in [66]. It has been shown (in [66]) that the convolutional code and hard-decision Veterbi decoding can yield coding gain of 1-2 dB in turbulent atmosphere. In [67] two turbo coded atmospheric optical systems: turbo-coded atmospheric optical subcarrier PSK and a turbo-coded atmospheric optical pulse position modulation (PPM) system have been

proposed. Both turbo coded atmospheric optical systems exhibit better performance in terms of BER when compared to convolutional coded atmospheric optical systems.

Although coding provides an additional layer of information security, studies have shown that even the best Forward Error Correction (FEC) codes cannot negate the effect of atmospheric turbulence alone [67–72]. FEC codes insert check bits into the data stream which contribute an additional power and bandwidth overhead on the system. Coding schemes are more suitable in recovering short term data losses [64].

2.3 Atmospheric turbulence mitigation using proposed FPM technique

To compensate for atmospheric turbulence induced signal fading, the antenna used in the experiment utilizes a fast beam tracking miniature fine pointing mirror (FPM) to control and steer the received beam to the SMF connection port. The major incentive of incorporation of a FPM is the active prevention of long term data loss by compensating or at least mitigating atmospheric turbulence induced wave-front phase distortion. Compared to the techniques outlined above, the merit of the FPM employed in the experimental antenna is that it manages to improve the FSO system performance and reliability with less complexity and minimum electronics overhead while maintaining the antennas' compact size.

The operation of the FPM mirror is almost similar to conventional adaptive optics approach for atmospheric compensation. It is based on wave-front sensing but rather than reconstructing the deformed waveform, the FPM acts to corrects the beam position changes as a result of AOA fluctuations by measuring beam spot movement on a quad-detector (QD) and calculating the control signal for the actuators of the wave-front corrector. The FPM has been demonstrated to be suitable for compensating lowest-order aberrations i.e., wave-front tip and tilt by stabilizing the beam centroid location in the focal plane focused to the fiber coupling point [73]. High wave-front aberrations beyond tip and tilt errors severely impact the fiber coupling efficiency, high resolution phase compensation is required in addition to beam steering in order to avoid (mitigate) signal fading.

In this doctor thesis a method to determine the approximate FPM tracking speed suitable to mitigate the effects of atmospheric turbulence experienced on the FSO beam as it propagates through the atmosphere has been proposed. The method is based on measuring the effects of

atmospheric turbulence on the beam intensity changes as a result of angle-of-arrival (AOA) [74], [75]. By comparing the power spectrum of the beam intensity variations as a result of AOA fluctuations caused by atmospheric turbulence to the intensity fluctuation as a result of scintillation effects, the approximate miniature FPM tracking speed of 1 kHz has been determined. The proposed antenna tracking speed is implented in the antenna tracking and control unit and the FSO system performance is evaluated under various weather and atmospheric conditions. From the experimental results, the system has demonstrated stable and reliable performance under clear and quite weather conditions. Satisfactory performance under light rain is demonstrated with intermittent power fades.

2.4 FSO antenna description

Next generation or new free-space optical communication systems will require compact, light-weight antennas with superior tracking and acquisition capabilities. These FSO systems will not only be applied for terrestrial communication but also for space communication such as optical feeder links, inter-satellite links, stratospheric platforms and also for terrestrial FSO links [76]. The optical antenna used in this experiment offers full-duplex (bi-directional) seamless connection of free-space and fiber system. An optical beam is emitted directly from a single mode fiber (SMF) termination to free-space using the optical antenna. At the receiver, the transmitted optical beam is focused (using the antenna optics) directly to a SMF then sent down the fiber to the photo detectors. In this system, the neccessity of converting the optical signal from electrical to optical or vice versa for transmitting or receiving through space is omitted. Furthermore, this system is protocol independent, thus the need for reconfiguration of the transmitting antenna is eliminated even when the nature of the transmitted signal changes due to varying bit-rate, wavelength division multiplexing (WDM) or optical analogue signal transmission [36], [77].

The narrow transmission beam of a free-space optical signal makes alignment of FSO communication terminals difficult as compared to the wider beam RF systems. Therefore FSO systems are faced with the challenge of designing effective tracking and acquisition mechanism to maintain the transceiver alignment. In the subsequent subsections the detailed design of the optical antenna considered to be ideal for next generation ultra high-speed FSO communication systems as well as tracking and acquisition method is given.

2.4.1 Optical antenna design

The design of the optical antenna is one of the most important key issues in FSO communication system. The basic design concept of a FSO antenna is like that of an astronomical telescope. Several types of telescope design are applicable for FSO communication. The most common are Cassegrain and Gregorian telescopes. The main difference between the two optical systems is that Gregorian telescopes employs a concave secondary mirror located beyond the focus of the primary mirror. This mirror arrangement results in longer tube lengths, as the distance between the mirrors is slightly more than the sum of their focal lengths, which is the reason why Cassegrain systems are more common [78]. Techniques for designing compact antennas suitable for FSO communication are described in [78–80]. The important characteristics include high efficient, compactness and simplicity [79], [81].

The optical antenna used in this experiment is a new compact optical system, which is a modified Cassegrain telescope [82]. This antenna is ideally suited for free-space optical communications but it also has many applications like inter-satellite communication, manned spacecrafts, data broadcasting satellites and for optical feeder links between satellites and ground stations [76]. The compact telescope is created from a standard Cassegrain system by using free form surface (FFS) mirrors with a magnification factor of 20. The primary mirror and secondary mirror are arranged in off-axis to avoid center obstruction which typically occurs in the design of a Cassegrain type telescope. The advantage of the three mirror design is that it removes all the major aberrations such as spherical aberration, astigmatism and comma aberrations [80]. Also this design is free from chromatic aberration but its fabrication is extremely complicated [83].

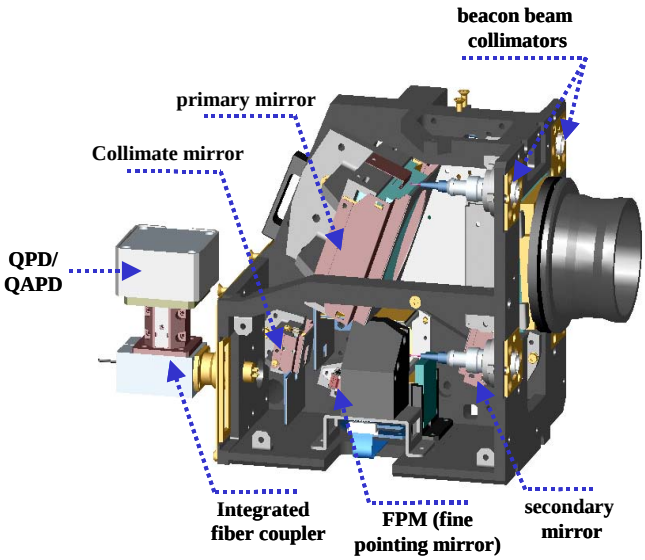

(a)

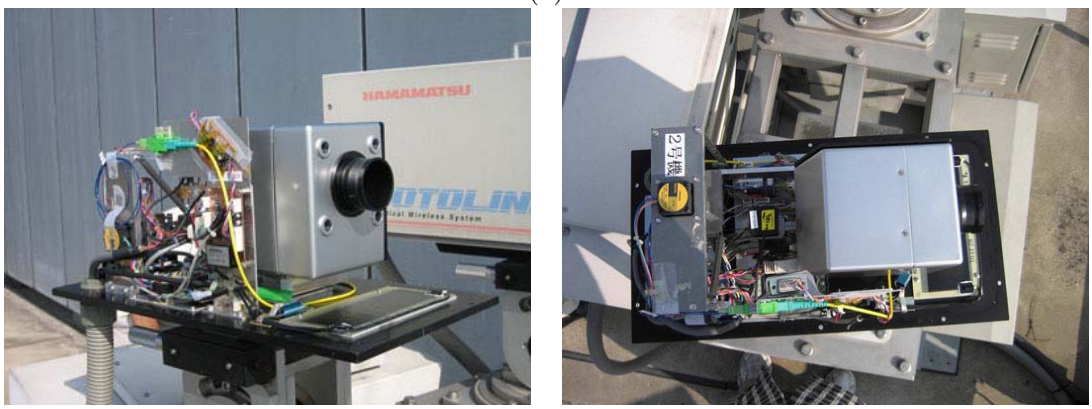

Side/front view Top view

(b)

Figure 2.6: Optical antenna (a) internal structure and (b) antenna mounted on gimbal mechanism with cover removed (Reproduced courtesy of Olympus and NICT)

Parameter specification	Value
Aperture diameter, A	40 mm
Angular magnification	20
Diffraction limit imaging	0.2 deg at 1550 nm
Transmitted wavefront accuracy	< 0.3 μm (rms)
Mirror reflectivity	> 98 % at 780 - 1600 nm

Table 2.2: Specifications of FFS mirror optical system

The internal structure of the optical antenna is shown in Figure 2.6(a) and Figure 2.6(b) shows the antenna mounted on the gimbal mechanism. The antenna specifications are summarized in Table 2.2. The optical system components layout in the antenna showing the arrangement of the

triple mirrors is shown in Figure 2.7 (a) depicting the top view and Figure 2.7 (b) the side view. A tilted windowpane is placed at the antenna aperture (not shown in he figures) to prevent return light caused by internal reflection.

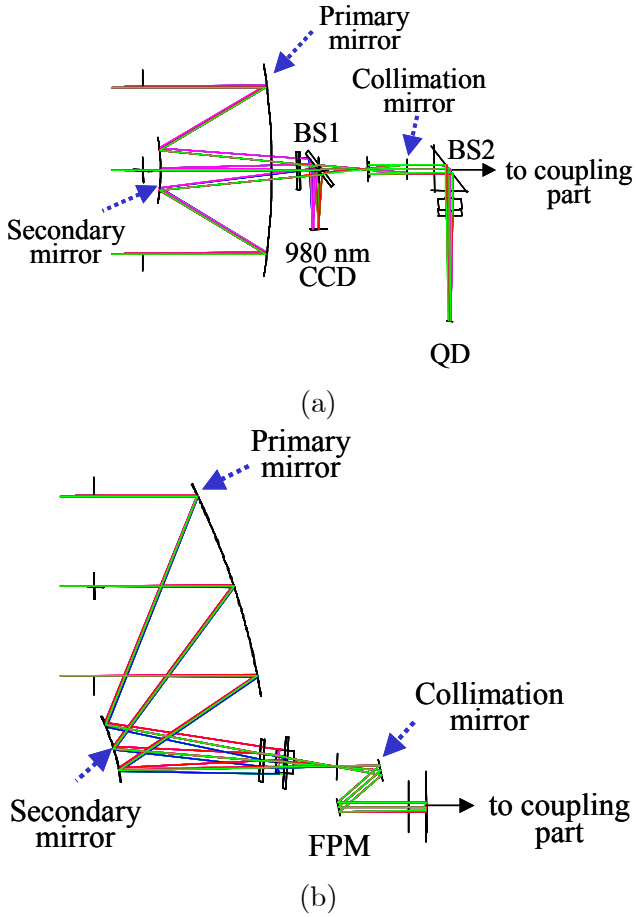

Figure 2.7: Optical system components showing optical path (a) top view and (b) side view

The antenna's transmit and receive aperture is 40 mm. A 1550 nm wavelength beam is used for data reception and transmission while a 980 nm wavelength beam is utilized as a beacon for tracking purpose. The beacon light is emitted from four output windows placed on the four corners in front of the antenna. The antenna uses automatic active tracking mechanism implemented with a CCD camera for rough tracking or initial alignment and a silicon quadrant detector (Si-QD) for accurate/fine tracking. The field-of-view (FOV) of the CCD is +/- 0.72 degree in azimuth (horizontal) direction and +/- 0.54 degree in elevation (vertical) direction [83]. The optical antenna has a wide imaging FOV at the acquisition sensor (CCD) as well as diffraction limited performance

at the fine tracking and fiber coupling port[5]. Coupling of transmitted optical beam directly to the SMF is accomplished by fine pointing mirror (FPM) which is a two axis gimbal flat mirror with a voice coil actuator. The position of aperture in front of the primary mirror is the entrance pupil and the reflector of the FPM is located on the exit pupil which is conjugate with the entrance pupil. The FPM is small, low on power consumption and has a fast enough response to counteract potential optical beam impairments as a result of atmospheric effects or base motion at the installation site. Table 2.3 summarizes the specifications of the FPM.

Parameter specification	Value
Mirror aperture	2.3 mm $\times$ 2.8 mm
Tilt angle range	Az: $\pm$ 6.5 deg; El: $\pm$ 7.8 deg
Sensitivity of angular sensor	150 mV/deg
Tilt angle accuracy	< 0.02 $m$rad
Wavefront accuracy of mirror	0.04 λ rms
Range of motion	2-axis (tip/tilt)

Table 2.3: Specifications of FPM

As beam splitters this antenna employs pellicle beam splitters[6] (BS1 and BS2 shown in Figures 2.7). Dichroic mirrors[7] can also be used as beam splitters. BS1 reflects part of the beacon beam onto a position sensitive detector, in this case a Si-CCD sensor. The signal is sent to the gimbal stage controller for rough tracking. The BS2 reflects the beacon beam to a QD which is used to track small angle deviations, i.e. fine tracking. The beam splitters are transparent to the 1550 nm data beam. The close loop feedback control mechanism used in the automatic tracking keeps the receive beam on target. Furthermore, it helps the FPM to keep track of variations in the angle-of-arrival (AOA) of the data beam so as to take corrective action to steer the 1550 nm data beam to the SMF connection port (FOV 0.2 deg).

The wave-front accuracy of the telescope is measured to be less than 1/10 waves at 1550 nm wavelength. The overall optical losses from the telescope aperture to the SMF is measured to be 4.9 dB. The primary reason for this loss can be attributed to at least because of imperfect mirror processing accuracy.

[5] Two types of quadrant detectors are utilized in the antennas used in this experiment; one is a silicon avalanche photodiode (Si-QAPD) with a 1 mm circular aperture and the other is a quadrant Si-photodiode (Si-QPD) with a 2 mm square aperture. The FOV of the QAPD and APD is +/- 125 μradian and +/- 250 μradians respectively.

[6] Pellicle beamsplitters are constructed from thin, nitrocellulose films that are stretched and cemented to rigid supporting rings. Unlike thicker beamsplitters, pellicle beamsplitters have the major advantage of eliminating second surface reflections by making them coincident with the original beam.

[7] A mirror used to reflect light selectively according to its wavelength.

2.4.2 Tracking and acquisition

One of the key challenges with FSO systems is maintaining transceiver alignment. FSO transceivers transmit highly directional and narrow beams of light that must impinge upon the receive aperture of the transceiver at the opposite end of the link. A typical FSO transceiver transmits one or more beams of light, each of which can vary from 5 - 8 cm in diameter at the transmitter (depending on the transmitter aperture) and typically spreads to roughly 1 - 5 m in diameter at a range of 1 km. Adding to the challenge is the fact that FSO receivers have a limited FOV, which can be thought of as the receiver's "cone of acceptance" and is similar to the cone of light projected by the transmitter. For a FSO link to function, it is very important that both the transmitted beam of light and the receive FOV cone encompass the transceiver at the opposite end of the link [10].

In order to transport as much light power as possible to the opposite receiver the beam is usually narrow (a few tens of μrad) therefore tracking and acquisition is one of the important design issues of FSO based communication systems. A slight mispointing of such narrow beam could cause a complete interruption of the communication link. Numerous methods for coarse and fine tracking and automatic acquisition have been developed. These methods include the use of servo motors, stepping motors, voice coils, mirrors, quad detectors, CCD arrays and even liquid crystals and micro-electromechanical systems (MEMS) [13]. Beam pointing errors are significant despite the fact that in terrestrial based FSO application the distance involved between remote sites are much smaller as compared to outer space (satellite) systems. For operation over moderate distances and moderate data rates, wide beam transmission systems without tracking feature are a cost effective and reliable solution, although the wider beam results in increased loss of transmission power.

More advance systems use auto tracking whereby the beam is automatically realigned toward the opposite receiver. Auto trackers incorporate a mechanism that detects the position of the beam at the receiver side and a counter measure that controls and keeps the beam on the receiver detector. Most tracking system use a beacon beam (980 nm in the experimental system setup in Waseda University) that is separate from the data carrying beam (1550 nm) and it is important that the data and beacon beam are lined up in the same direction. Automatic tracking often uses a close loop feedback control mechanism to keep the receive beam on target as shown in Figure 2.8.

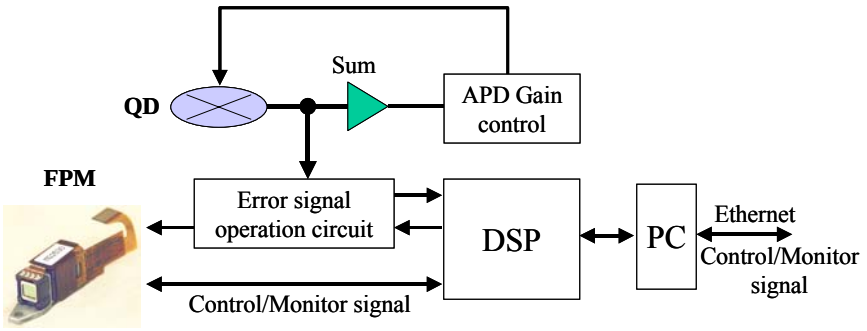

Figure 2.8: Tracking system block diagram

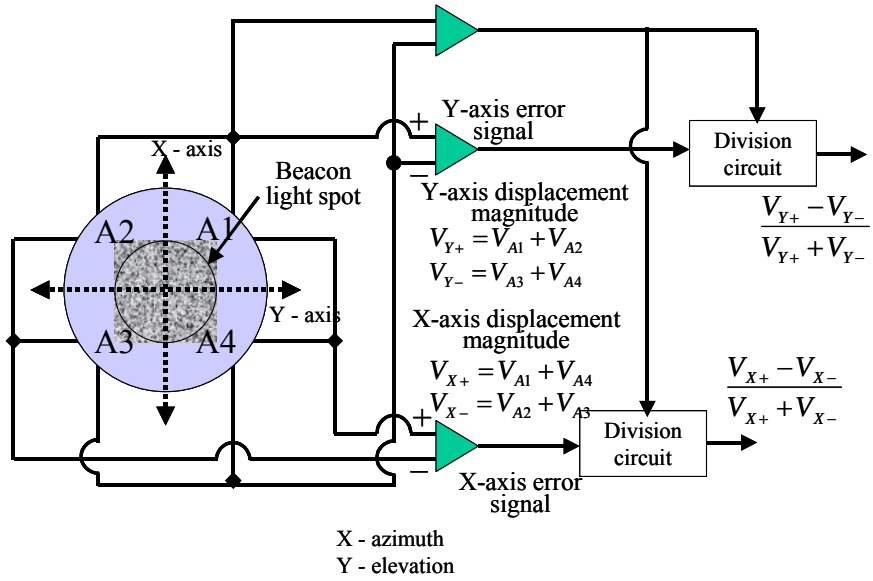

Figure 2.9: Block diagram of tracking system error signal generation for QPD/QAPD

Combining two tracking methods, one for initial alignment and coarse tracking and a second for fine tracking, a more effective tracking mechanism can be realized. By using charge coupled devices (CCD) position sensor, a software or digital signal processor (DSP) can perform the actual position detection and analysis and feeds the information back to the system for counter measures such as moving the steering mirror or gimbal. Combination the CCD detector with a quad detector (QD) can offer even better beam positioning. With a quad detector the incoming light from a remote location is focused onto the detectors by using an external optic devices such as a lens or mirror. A more illustrative description of the tracking mechanism error signal formation is presented in the schematic in Figure 2.9.

The detector (shown in Figure 2.9 with a circular aperture) consists of four separate single detector elements arranged in a matrix. The four elements collects the light separately, and when

the signal output from all four detectors is the same then the spot is located exactly at the middle of the detector array. If the light spot moves, the amount of light collected by each different detector element will be different, resulting in variation of the level of the output signal. By analyzing and comparing these four individual output signals the direction of the spot movement on the surface of the detector array can be determined. This procedure is relative fast because only four different output levels have to be analyzed. Quad detectors are normally applied to track small angle deviation (fine tracking) because if the light spot leaves the detector surface the system loses its tracking capability. Typical intensity distribution at QPD/QAPD for initial setting and on site measurement is shown in Figure 2.10.

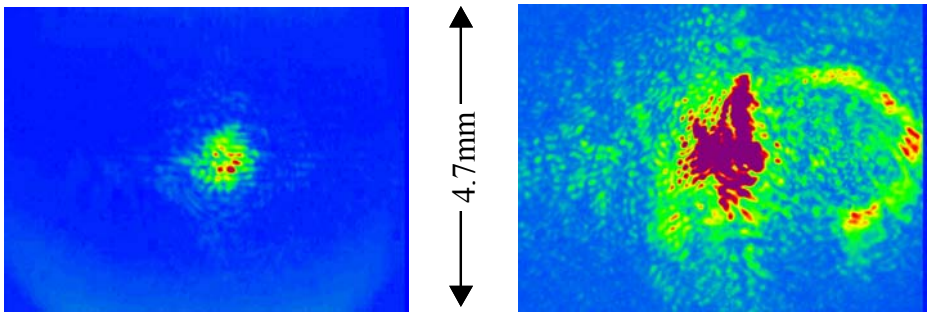

Figure 2.10: Typical intensity distribution at QPD/QAPD

In the optical antenna used in the experiment the information on the arrival beam position fluctuations is provided by the QD in order for the FPM to counteract the changes so as to always lead the horizontal optical axis to the fiber connection port and therefore achieving a feedback control setup. The FPM tracking speed is chosen to be able to compensate the effects of random AOA fluctuation as a result of atmospheric turbulences on the received beam and steer most of the received optical beam to the 8 - 10 μm core diameter of the SMF. Taking into consideration the narrow acceptance angle of SMFs (core diameter of 8.2 μm and a numerical aperture of 0.13 the fiber connection incident angle is $\pm$7.47 degrees), the V_x and V_y error tolerance is low since the sensitivity of the FPM angular motion in azimuth and elevation angles is only about – 150 mV/deg and + 150 mV/deg respectively.

2.4.3 Atmospheric turbulence suppression

The FPM fluctuation pointing/tracking jitter suppression response characteristics for the azimuth axis is shown in Figure 2.11. From the figure, it can be observed that it is possible to achieve more

than 40 dB suppression at the frequency less than 100 Hz. A sharp mechanical resonance caused by the mirror mass and it supporting spring appears at 80 Hz.

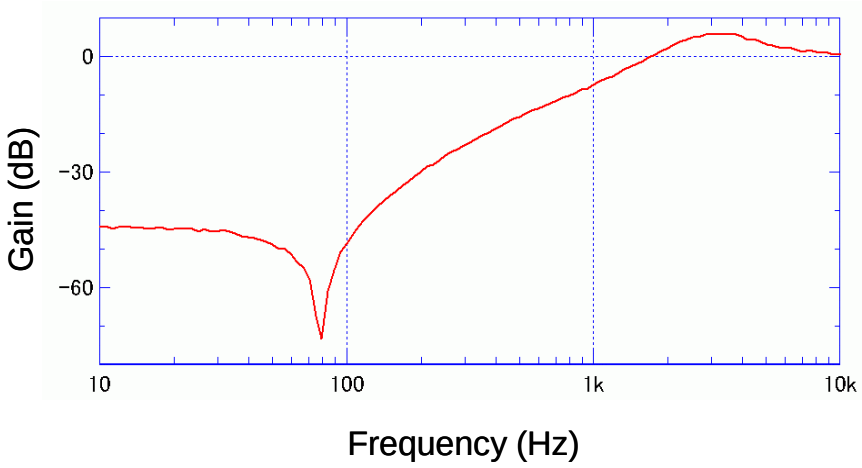

Figure 2.11: Relationship between tracking speed and suppression magnitude

The optimum antenna FPM tracking speed for atmospheric suppression is obtained from the measured beam intesity fluctuations as a result of scintillation effects and angle-of-arrival fluctuations (described in more detail in subsection 3.2.4). The selected optimum tracking speed should enable the FPM to steer and focus most of the received beam to the SMF. In the experimental setup the approximate FPM tracking speed was set to 1 kHz. The improvement in the fiber received power is depicted in Figure 2.12. The figure shows the result for accurate tracking by controlling the beam AOA changes. Figure 2.12 top shows the fiber received power when the antennas' FPM tracking is set to OFF and Figure 2.12 bottom shows fiber received power when the antennas' FPM tracking speed is set to 1 kHz. From the figure it can be observed that the FPM manages to steer most of the received beam to the SMF and thus shows improvement in the fiber received power as depicted in Figure 2.12 bottom. This demonstrates the FPM tracking system reduces the pointing errors which reduces the atmospheric induced scintillation effects.

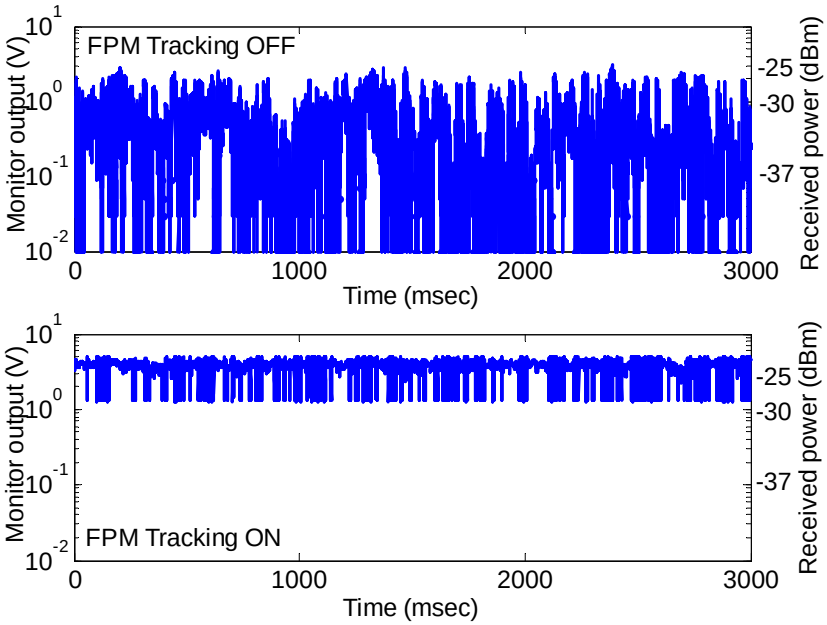

Figure 2.12: Fiber received power top – antenna tracking set to OFF, bottom – FPM tracking set to 1 kHz.

A demonstration the FPM turbulence suppression characteristics is shown in Figure 2.13. This figure shows the FPM angular fluctuation during a shock disturbance applied to the antenna module, captured using a digital oscilloscope. The shock disturbance is shown by the magnitude variation of the tracking signal in the Azimuth and Elevation direction. The subsequent vibrations because of the schock can easily be absorbed by the FPM corrective response depicted by a disturbance free (almost no changes in the 1550 nm measured signal intensity shown in the figure). This demonstrates that the fast response of FPM is capable of suppressing the beam intensity fluctuations as a result of AOA fluctuations.

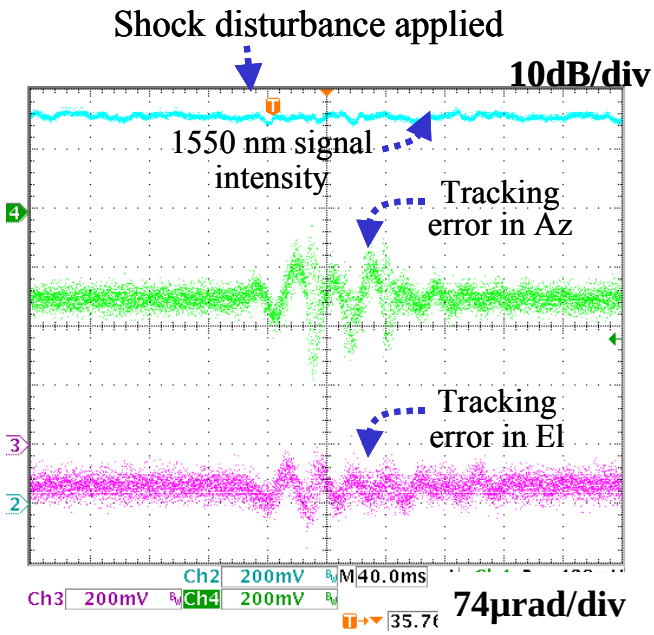

Figure 2.13: FPM angular fluctuation during turbulence

2.5 Conclusion

In this chapter an overview of FSO communication systems has been outlined. Because of the power and bandwidth limitations of optical devices operating near the 785 nm wavelength, FSO systems using this wavelength can not operate above 2.5 Gbps data rate. To overcome these limitation the 1550 nm wavelength has been selected as the operating wavelength for new FSO systems. A new FSO system operating at 1550 nm which seamlessly connects an free-space optical beam to a SMF has been discussed. The advantages of this system include data rate and protocol transparency and it is readily compatible with existing optical fiber transmission infrastructure.

Also in this chapter various techniques currently adapted in commercial and experimental FSO systems for atmospheric turbulence mitigation have been presented. Atmospheric turbulence is known to be the major source of errors in FSO communication systems. The design of the FSO optical antenna used in this experiment has been outlined and its capability for atmospheric turbulence mitigation using the FPM has been described in detail. By setting the antennas' FPM tracking speed to 1 kHz, it has been demonstrated that the beam intensity fluctuations has a result of AOA changes can be markably suppressed. In the next chapter, the experimental performance results of the FSO system after setting the antenna FPM to 1 kHz will be presented.

CHAPTER 3

EXPERIMENTAL PERFORMANCE RESULTS AND ANALYSIS

For any given FSO system, its performance can be determined by considering several system parameters which can be divided into two categories: internal parameters (or system specific parameters) and external parameters (non-system specific parameters). These parameters are not independent but are linked together in specifying the overall FSO system performance [84].

The external parameters which influence the performance of FSO system include atmospheric effects such as attenuation, beamwander, beam spreading and scintillation. These effects can reduce the link availability and may introduce burst errors in the system. Several techniques, discussed in the previous chapter, can be used to reduce intensity fluctuations caused by scintillation and beam wander. These techniques include and are not limited to large receive apertures, multiple transmit aperture and fast tracking antenna [22], [85]. For a FSO system to achieve a given system performance in terms of bit error rate (BER) it is important to measure and quantify the amount of scintillation fade margin required to be inbuilt in the FSO system. An additional margin is also necessary for atmospheric attenuation [86].

In this chapter the experiment system setup is described and extensive performance evaluation of the system under various weather conditions is also presented. The atmospheric effects are measured, characterized and quantified. The results have been used in the evaluation, prediction and comparison of FSO system performacne in deployment environment. The effects on the system performance metric like BER and fiber received power are described and correlated with the weather condition and atmospheric events.

3.1 Experimental setup

The experimental system is setup in the Waseda University campus area situated in Shinjuku ward, Tokyo city for a terrestrial, nearly horizontal FSO link spanning 1 km. The transceivers are installed on rooftop of buildings at two different Waseda University campuses. Figure 3.1 shows a satellite view of the test area. Two free-space optical antennas were set on the rooftop of a 10 floor building in the Nishi Waseda campus and the corresponding antennas on the rooftop of a 9 floor building with a clear line of sight between the transceivers on the top of these two buildings. Both antennas are connected to control and data acquisition system placed in the experimental setup room which records all the data. From Figure 3.1 it is observed that the FSO propagation path travels over low rising residential, office or campus buildings, therefore the transmitted beam may likely experience higher probability of scintillation from ground heating and heating from these buildings.

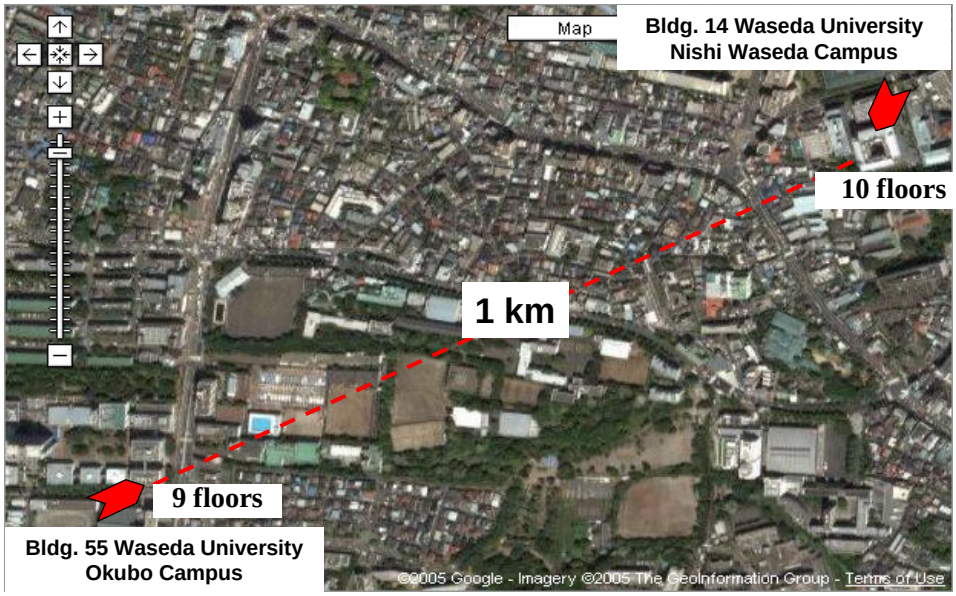

Adapted from http://maps.google.com/

Figure 3.1: Satellite view of the test area

The basic configuration of the experimental setup is shown in Figure 3.2. Because the light is fiber coupled at both ends, the EDFA receive electronics and other measurement and data collection devices can be conveniently placed inside the building. The fibers are run to the respective rooftops and then coupled directly to the transceivers as depicted in Figure 3.2.

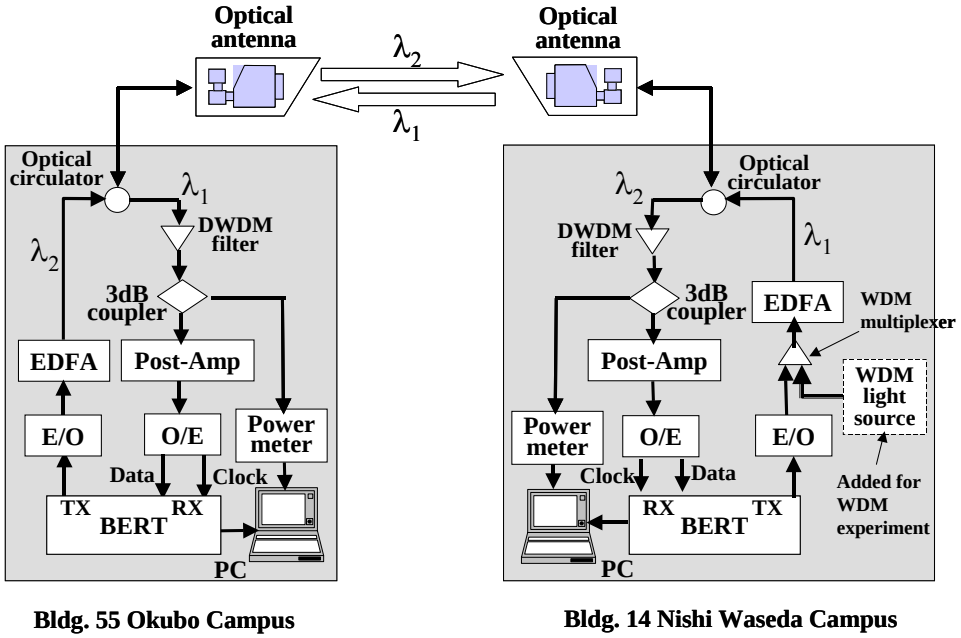

Figure 3.2: Experimental setup FSO system performance evaluation

The experimental hardware setup including data collection and other measurement devices are place in the experiment room as shown in Figure 3.3 and corresponding devices on the rooftop of the building are depicted in Figure 3.4. The collected data include weather data (visibility, temperature, precipitation and fog), optical power attenuation and ascintillation (for 785 nm wavelength FSO syatem), bit error rate (BER) and the optical receive power for the 1550 nm wavelength FSO system.

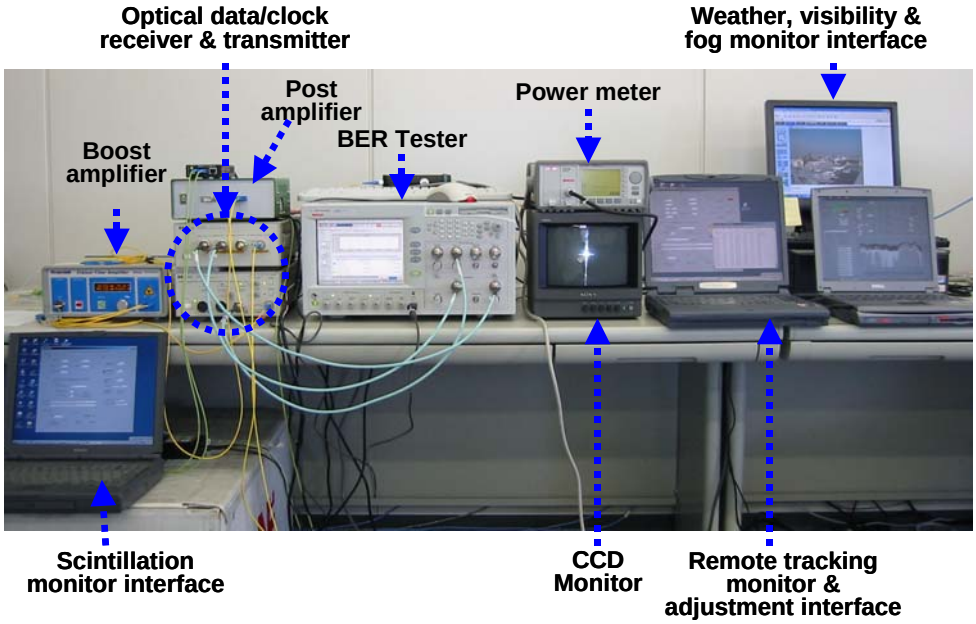

Figure 3.3: Experimental hardware setup in the laboratory

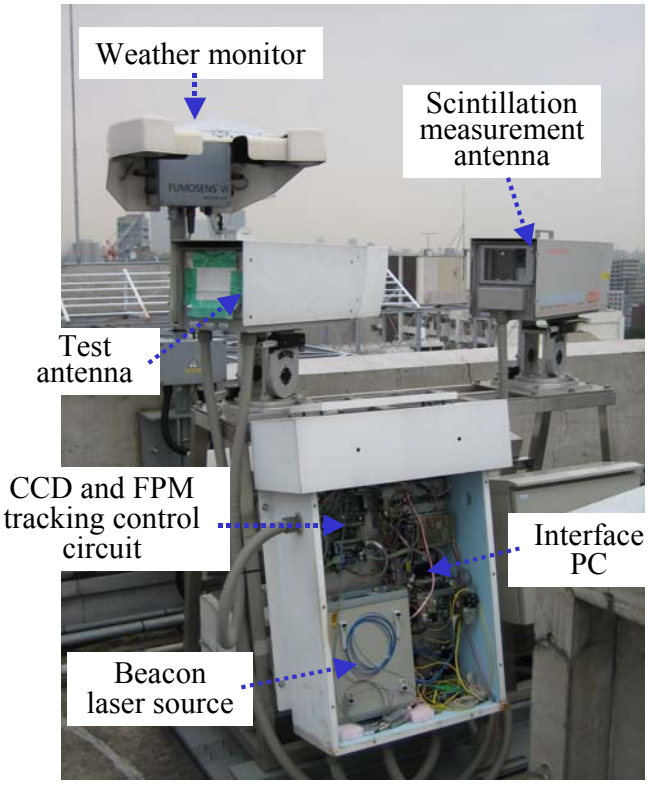

Figure 3.4: Device setup of the rooftop of building 55 in Okubo campus showing test antenna (left), an optical power attenuation and scintillation effects measurement antenna(right), weather monitoring device and temperature controlled box containing electronics, PC and beacon source

A summary of the FSO communication system specifications as well as the tracking beacon CCD and QAPD tracking specifications are outlined in Table 3.1, 3.2 and 3.3 respectively. The data summarized in the tables is the initial design specification when the experimental system was first installed. The theoretically calculated antenna optical losses was about 3.5 dB but the experimentally measured internal antenna optical losses was 4.9 dB. In table 3.1 the internal optical losses of 10 dB represents the total losses for both the antennas (they are similar in design). The experimental system optical losses of 10 dB quoted in Table 3.1 represents the losses at both optical antenna installation sites (Nishi Waseda and Okubo campuses) which include cabling (rooftop top to laboratory) and splitter losses.

Parameter specification	Value
Wavelength (λ)	1550 nm
Transmit power	100 mW (+20 dBm)
Transmit/Receive aperture (A)	40 mm
Beam spread angle	94.5 μrad ($\Delta\theta = 2.44\lambda/D$)
Propagation distance (D)	1 km
Elevation angle	0^o
Beam spreading loss (Geometric loss)	10.5 dB
Internal optical losses	10 dB (5 dB for each antenna)
Experimental system optical losses	6 dB (for both sites)
Minimum received power	-30 dBm (at 2.5 Gbps)
Link margin	23.5 dB

Table 3.1: 1550 nm FSO communication system design specifications

Parameter specification	Value
Wavelength (λ)	980 nm
Transmit power	60 mW (x4) +23.8 dBm
Beam spreading angle	8.7 mrad
Propagation distance (D)	1 km
Receive aperture (A)	40 mm
Beam spreading losses	46.7 dB
Internal optical losses	7.5 dB
Minimum receive power	-60 dBm
Link margin	29.6 dB

Table 3.2: Tracking beacon CCD specifications

Parameter specification	Value
Wavelength (λ)	980 nm
Transmit power	60 mW (x4) +23.8 dBm
Beam spreading angle	8.7 mrad
Propagation distance (D)	1 km
Receive aperture (A)	40 mm
Beam spreading losses	46.7 dB
Internal optical losses	7.8 dB
Minimum receive power	-50 dBm
Link margin	19.6 dB

Table 3.3: Tracking beacon QAPD specifications

3.2 Atmospheric effects

When a free-space optical beam propagates through the atmosphere it experiences deterioration and deformation of its wave-front caused from small scale, randomly localized changes in the atmospheric index of refraction [21]. Refractive index inhomogeneities of the turbulent air cause wave-front distortions of optical waves propagating through the atmosphere, leading to such effects as beam spreading, beam wander, and intensity fluctuations (scintillations). These distortions are responsible for severe signal fading in free-space optical communications systems and therefore compromise link reliability [27].

The foundations of the study of atmospheric turbulence were laid in the late 1960s and 1970s [20], [54], [87], [88]. To date there are still inconsistencies in applying these theories to experimental systems and demonstrating acceptable correlations with experimental results. The primary disconnect in turbulence theory is between the reliability of theory in the weak turbulence regime and the lack of consistent theory in the intermediate and strong turbulence regimes. A free-space optical (FSO) communication system is expected to perform in both weak and strong turbulence conditions. Because of the shortcomings of theory, more empirical approach to determining ways of improving link performance through experiments and data analysis will fill gaps in the theory, and potentially result in the development of new theories are required [56]. Atmospheric turbulence has been studied extensively and various theoretical models have been proposed to describe turbulence induced image degradation and intensity fluctuations (i.e., signal fading) [89–92].

In this experiment work, an optical antenna using 785 nm wavelength is set up to record the atmospheric effects including beam intensity fluctuations as a result of scintillation and beam wander. Also, a weather measurement device is installed to record weather data including temperature, precipitation, visibility and fog. The weather data was used to correlate atmospheric events and the performance of the FSO system. The equipment setup on the rooftop is depicted in Figure 3.5. A camera to capture live pictures was also installed.

Figure 3.5: Devices setup on the rooftop of building 55 Okubo Campus

3.2.1 Atmospheric attenuation

Atmospheric attenuation has a strong influence on the weather condition, visibility etc. Atmospheric attenuation of FSO systems is typically dominated by fog but can also be dependent upon low clouds, rain, snow, dust, and various combinations of each [10]. The effects of weather condition on visibility and range can be seen in Figure 3.6, which presents a series of photographs taken on a clear, cloudy and rain day. The first photo (Figure 3.6 (a)) shows clear atmospheric conditions with a visibility range of over 20 km as measured with a nephelometer[1] mounted at the camera site. This corresponds to an attenuation of between 0.06 to 0.19 dB/km according to the International Visibility Codes for Weather Conditions and Precipitation [13]. The distant buildings and structures are clearly visible, even though they are several kilometers away. The second photo (Figure 3.6 (b))depicts cloudy event, at which time visibility is measured at approximately 5.36 km (2.58 dB/km). The near buildings are still visible although some of the further buildings and landmarks are obscured. In the third photo taken during rain event, the visibility range is approximately 1.09 km (12.65 dB/km), and buildings in the foreground are completely obscured. In the third photo shown in Figure 3.6 (c) some of the rain water collect on the camera window thus contributing to obscuring the vision. The same also occurs on the FSO transceiver window

[1] An instrument which measures the scattering function of particles suspended in a medium in order to determine the visual range through the medium.

during heavy rain condition and it usually contributes significantly to the attenuation in the link.

(a) (b) (c)

Figure 3.6: Visibility under different weather conditions (a) clear day - no overcast, (b) cloudy day and (c) rainy day

The attenuation of an optical beam traveling through the atmosphere due to both absorption and scattering is described by Beer's Law. In general, the transmittance, τ, of radiation in the atmosphere as a function of distance, D, is given by Beer's Law, as [21]

$$\tau = \frac{I(D)}{I_0} = \exp(\text{-}\gamma D) \ , \tag{2}$$

If the attenuation coefficient, γ, is a function of the path, then the above equation becomes

$$\tau = \exp\left[-\int_0^D \gamma(D) dD\right] \tag{3}$$

The attenuation coefficient is determined by four individual processes: molecular absorption, molecular scattering, aerosol absorption and aerosol scattering. The atmospheric attenuation coefficient is

$$\gamma = \alpha_m + \beta_m + \alpha_a + \beta_a \ , \tag{4}$$

where α is the absorption coefficient, β is the scattering coefficient, and the subscripts m and a designate the molecular and aerosol processes, respectively[2]. Each coefficient in equation 4 depends on the wavelength of the free-space optical system [21].

Molecular absorption is very wavelength specific and can be avoided by careful choice of free-space optical wavelength. Molecular (Rayleigh) scattering is inversely dependent on the wavelength

[2]Absorption and scattering are deterministic effects that are fairly well known [55]. Software packages like LOWTRAN, FASCODE, MODTRAN, HITRAN, and LNPCWIN are commonly used to predict transmittance (attenuation) effects as function of wavelength, λ, based on a variety of conditions - metrological range, latitude (tropical, mid, artic), altitude, etc.

to the fourth power. The most severe attenuation is caused by turbid atmospheric effects, such as rain, fog or snow. Rain causes relatively wavelength-independent attenuation in the optical region, since droplet sizes are much larger than the wavelength. Snowflakes are also large compared with the wavelength, and it attenuation (geometric blockage) has the same magnitude to its effect on visibility. However, fog is composed of particles which range from under 0.1 μm to over 15 μm, and its attenuation effect is caused by Mie scattering, which is most severe for particles sizes comparable to the wavelength [93]

Due of the complicated and unpredictable nature of the atmospheric weather condition, it is difficult to estimate the optical wave attenuation with a specific weather phenomenon. Therefore, the term visibility is often used as a measure to express the optical wave attenuation in the atmosphere. Visibility can be described as the distance one can see horizontally based on seeing and recognizing such objects as buildings, bridges, or other landmarks. Discernment rate of 5% is called meteorological optical range (MOR), and it is synonymous with the visual range (weather term) observed at the meteorological observatory of every place. The attenuation, L, (expressed in dB/km) of electromagnetic waves as a result of particle size distribution in the air by Mie scattering is given by the following formula [94]

$$L = 4.343 \times 10^5 \gamma \text{ (dB/km)} , \tag{5}$$

If the distance D expressed in equation (2) is replaced by the visibility distance, V, the contrast discernment threshold value, ε, will be given by

$$\varepsilon = e^{-\gamma V} \tag{6}$$

When equation (6) is substituted to equation (5) above the following equation is obtained

$$L = 4.343 \ln(\frac{1}{\varepsilon})/V \text{ (dB/km)} , \tag{7}$$

If $\varepsilon = 0.05$ (MOR) is substituted into the above formula, then the equation becomes simply

$$L = \frac{13}{V} \text{ (dB/km)} , \tag{8}$$

An empirical simplified formula found in [21] which has been used in the FSO community for a long time to calculate the attenuation coefficient due to the Mie scattering considering wavelength

dependency is

$$L = \frac{17}{V} D \left(\frac{550}{\lambda} \right)^{\delta} \text{ (dB/km)}, \tag{9}$$

where $\delta = 0.585(V)^{1/3}$ for $V < 6$ km; $\delta = 1.6$ for $V > 50$ km; $\delta = 1.3$ for 6 km $< V <$ 50 km; and D is the propagation distance.

Both formulas (equations (8) and (9)) show close results to actual measurements of a FSO link range varying from several 100m to 5km [95].

3.2.2 Beam wander, scintillation and beam spreading

Atmospheric turbulence produces temporary pockets of air with slightly different temperatures, different densities, and thus different indexes of refraction. These air pockets are continuously being created and then destroyed as they are mixed. Data can be lost due to beam wander and scintillation as the free-space optical beam becomes deformed propagating through these index of refraction inhomogeneities. The significance of each effect depends on the size of these turbulence cells with respect to the free-space optical beam diameter[3]. If the size of the turbulence cells is larger than the beam diameter, the free-space optical beam as a whole will randomly bend, causing possible signal loss if the beam wanders off the receiver aperture as shown in Figure 3.7 (beam wander).

More commonly, if the size of the turbulence cells is smaller than the beam diameter, ray bending and diffraction will cause distortions in the laser beam wave-front. Small variations in the arrival time of various components of the beam will produce constructive and destructive interference and will result in fluctuation in the free-space optical beam intensity at the receiver similar to the twinkling of a distant star shown in Figure 3.7 (scintillation or intensity fluctuation).

[3] Atmospheric turbulence is usually measured in terms refractive index structure coefficient C_n^2. Because the air needs time to heat up, turbulence is typically greatest in the middle of the afternoon ($C_n^2 = 10^{-13}$ m$^{-2/3}$) and weakest an hour after sunrise or sunset ($C_n^2 = 10^{-17}$ m$^{-2/3}$). C_n^2 is usually largest near the ground, decreasing with altitude. To minimize the effects of scintillation on the transmission path, FSO systems are not installed close to hot surfaces [9].

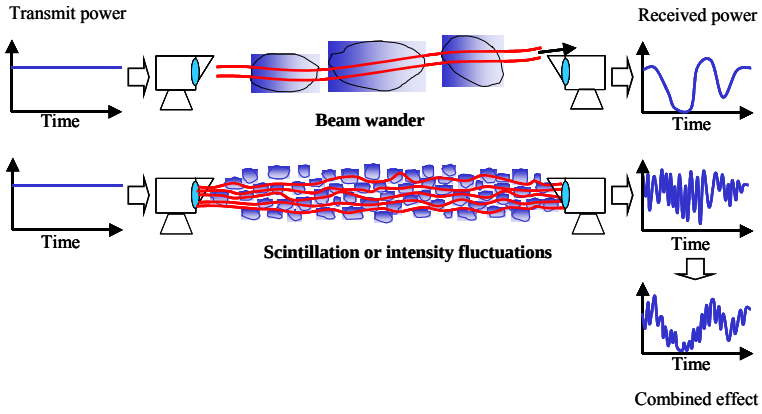

Figure 3.7: Beam wander and scintillation attributed to atmospheric turbulence.

The time scale of these fluctuations is comparable to the time it takes the volume of air to move across the beam path due to wind. Previous measurements of scintillation for a free-space optical beam propagating along a terrestrial path show that the fluctuations occur on the order of 1 ms to 10 ms [22]. It has been shown experimentally that beam wander has a time constant in the order of (beam size)/(wind speed), and this can be minimized with the use of a fast tracking transmitter [23]. Some experiments have shown that, depending upon the atmospheric conditions along the beam path, the magnitude of scintillation-induced fades reaches a maximum that does not continue to increase with distance [10], [96].

After a beam propagates through a length equal to a few transmitter diameters of turbulence atmosphere, the beam begins to wander randomly in the plane transverse to the propagation directions [97]. Beam wander is a result of the electromagnetic wave interacting with turbulent eddies of sizes on the order of the trasnmit aperture diameter [91]. The motion of the centroid of the beam, r_c, is defined by equation 10 [55]

$$\langle r_c^2 \rangle^{1/2} = \sqrt{W_{LT}^2 - W_{ST}^2} \tag{10}$$

where W_{ST} is the short term beam width, and W_{LT} is the long term beam width, shown in Figure 3.8.

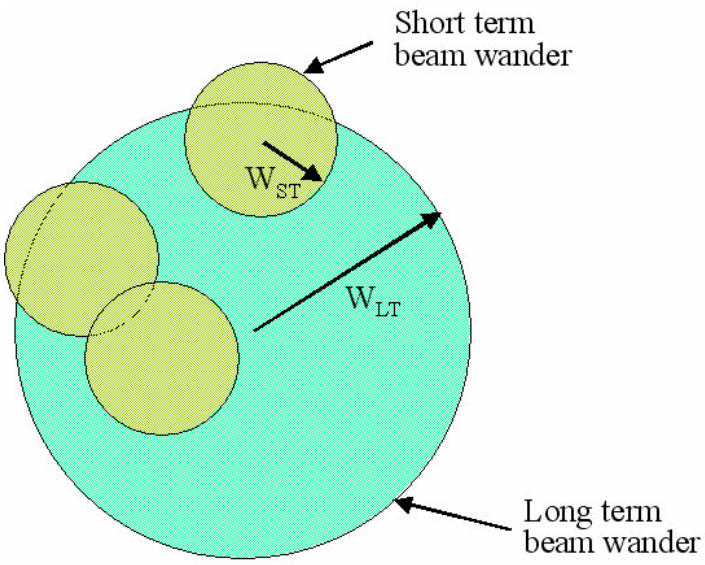

Figure 3.8: Beam wander at the receiver plane is characterized by the short term and long term beam widths

In addition to beam wander and scintillation discussed above, the beam will also spread in size beyond the dimensions attributed to usual diffraction spreading. This effect is sometimes described as beam breathing [21]. According to the diffraction theory, a focused beam from a uniformly illuminated circular aperture of diameter A produces a radiation pattern in the focal plane whose diameter is

$$A_f \simeq f\lambda/A \ , \tag{11}$$

where f is the focal length of the optical system and λ is the wavelength of the beam. The presence of atmospheric turbulence prevents achieving diffraction-limited (ideal) focal spot sizes.

The turbulence induced beam spread can be characterized by the effective radius, a_t, the distance from the center of the beam ($z = 0$) to where the mean intensity is down by $1/e$. The effective radius is given by [13]

$$a_t = 2.01 \left(\lambda^{-1/5} C_n^{6/5} z^{8/5}\right) \tag{12}$$

The wavelength dependence of beam spreading is not strong. The spot size can often be observed to be twice that of the diffraction-limited (ideal) beam diameter. Many FSO systems incur about 1 m beam spread per kilometer of distance. If a perfect medium is considered with no environmental attenuators present, beam spread would be the only distance limiting variable. Using a closed loop

control feedback mechanism, an active tracking mechanism that operates at a frequency faster than the beam wander frequency can be used to overcome beam wander and beam spread.

3.2.3 Scintillation, refractive-index structure constant parameter and angle-of-arrival fluctuation measurement

3.2.3.1 Scintillation measurement

Using the setup shown in the schematic depicted by Figure 3.9 intensity fluctuations and optical power attenuation caused by atmospheric turbulences as the beam propagates through the atmosphere is measured and recorded. Figure 3.10 shows a photograph of the antenna setup on the rooftop of building 14 in Nishi Waseda campus. The antenna shown on the left of the photo uses 785 nm wavelength and is used for measurement of atmospheric propagation characteristics of the 785 nm wavelength including scintillation, refractive index structure constant parameter (C_n^2) and optical power attenuation. The antenna seen on the right of the photo is the antenna under investigation which uses 1550 nm wavelength for data communication and a 980 nm wavelength beacon beam for antenna alignment and tracking purposes.

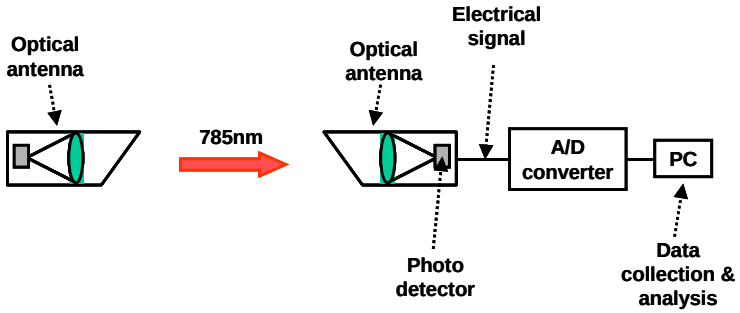

Figure 3.9: Atmospheric effects (scintillation and optical power attenuation) measurement setup block diagram.

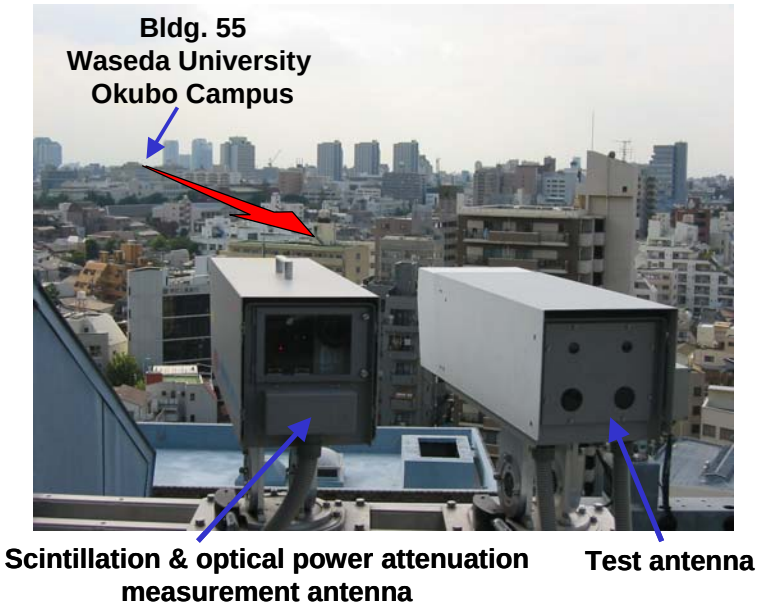

Figure 3.10: Experimental antenna placed on the rooftop of building 14 in Nishi Waseda Campus.

Typical intensity fluctuation (scintillation) data collected during the experiment is depicted in Figures 3.11 (a) and 3.12 (a). The figures show the 785 nm wavelength free-space optical beam intensity fluctuation as a result of atmospheric induced scintillation effect. The measured data is recorded in blocks of 3 second at a sampling rate of 10 kHz recorded continuously every 5 minutes intervals. Figure 3.11 (a) shows a times series plot showing the intensity fluctuation and Figure 3.11 (b) is a power spectrum of the times series after performing fast Fourier transformation on the time series data shown in Figure 3.11 (a). The fast Fourier transform equation is defined as

$$X(k) = \sum_{j=1}^{N} x(j)\, \omega_N^{(j-1)(k-1)} \,, \tag{13}$$

where $\omega_N = e^{(-2\pi i)/N}$ is the Nth root of unity.

The power spectrum shows the signal intensity at the different frequencies and can be used to determine the portions of the signal intensity falling within frequency bins. In this experiment, the power spectrum obtained from the intensity fluctuation measured time series data is important in determining the antennas' miniature FPM approximate optimum tracking speed for atmospheric turbulence mitigation.

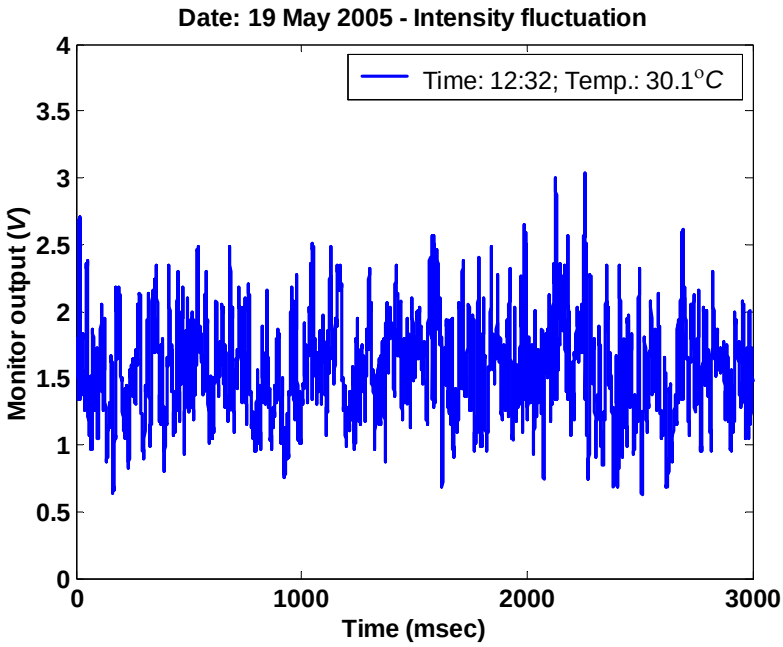

(a)

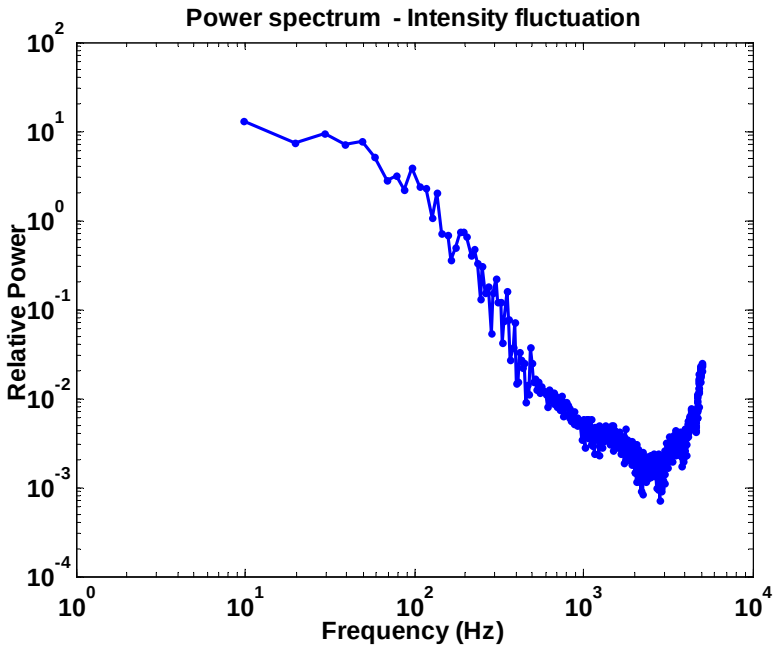

(b)

Figure 3.11: Measured beam intensity fluctuation (a) time series data (b) power spectrum of time series data in (a)

The magnitude of scintillation is considered to be a strong function of the time of day and ambient temperature. As an example of the variation of magnitude of scintillation, two data sets collected on the same day (19^{th} May 2005) but at different time is presented. The data shows the variation of the measured received signal intensity as a result of scintillation for two data sets collected at midday (12:07 pm with temperature of 32.6^{o}C) where scintillation is more pronounced and early evening (19:02, temperature 22.3^{o}C). The magnitude of the scintillation fluctuations can be observed to be higher during the afternoon (Figure 3.12(a) top) as compared to early evening (Figure 3.12(a) bottom).

The scintillation time series data can also been analyzed using a different method of producing probability density functions (pdf) by histogramming the data for different normalized intensity values as shown in Figure 3.12(b) [98]. Qualitatively, the wider the histogram, the greater the degree of received signal intensity fluctuations due to scintillation as demonstrated by the pdf curves of the time series data shown in Figure 3.12(a). To quantify the amount of scintillation, the variance or the width of the histogram can be calculated. This parameter is used as a good indicator of the degree of scintillation in the recorded data. For the time series data Figure 3.12(a) the variance calculated for data collected in the afternoon and in the early evening for this particular day is 0.1807 and 0.0481 respectively. The greater the variance, the wider the histograms, the greater the magnitude of power fluctuations and thus the deeper the scintillation fades.

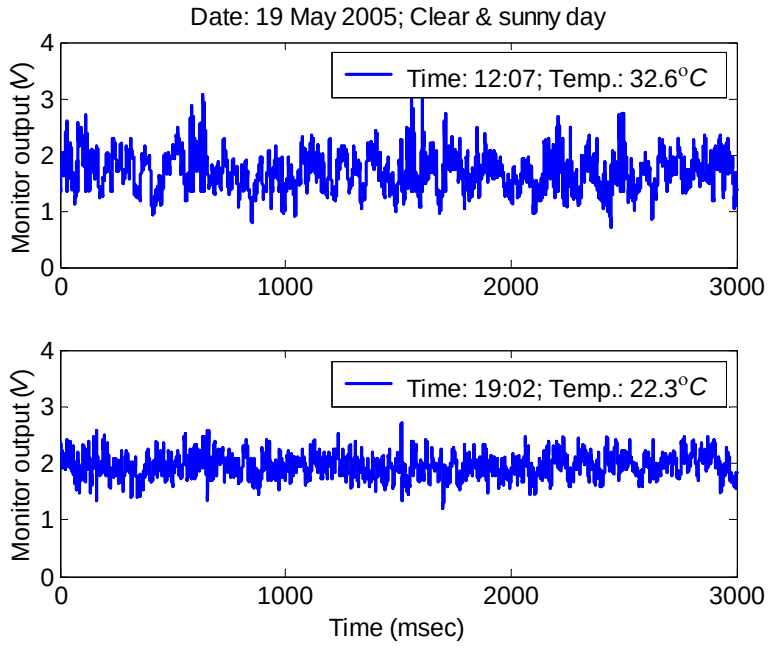

(a)

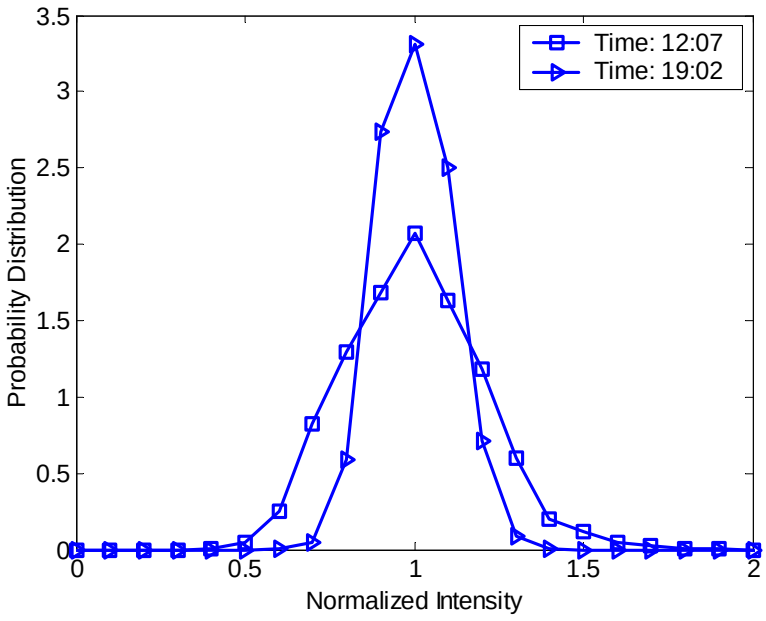

(b)

Figure 3.12: Measured beam intensity fluctuation (scintillation) (a) time series data top - afternoon; below - early evening and (b) Probability density function of the measured intensity fluctuation time series data

Comparable data depicting the intensity variation with different weather conditions including clear sunny day (no overcast), cloudy day and rainy day are shown in Figures 3.13, 3.14 and 3.15 respectively. Figure 3.13, shows the collected data for intensity fluctuation on a day when the weather condition is considered to be clear and sunny (no overcast). From the probability density function figure (see 3.13(b)) the width of the histogram for the data collected at midday (12:30 pm) is wider than for the data collected in the early morning and evening. This demonstrates the higher degree of signal fluctuation as a result of scintillation during the mid afternoon than early morning and evening.

For the case of cloudy weather condition, the difference between the days' maximum and minimum temperature is usually not very high. From Figure 3.14(b) the width of the histogram for the data collected at different periods during the day are almost similar. Therefore there is very little difference in the degree of signal fluctuation as a result of scintillation. This phenomenon is almost the same for the data collected on a rainy day as depicted in Figure 3.15.

A more comprehensive analysis of the measured intensity fluctuationdata is presented in the subsequent section which attempts to quantify the magnitude of atmospheric turbulence using the refractive index structure constant parameter, C_n^2. The refractive index structure constant parameter is considered as the most critical parameter along the propagation path in characterizing the effects of atmospheric turbulence [55].

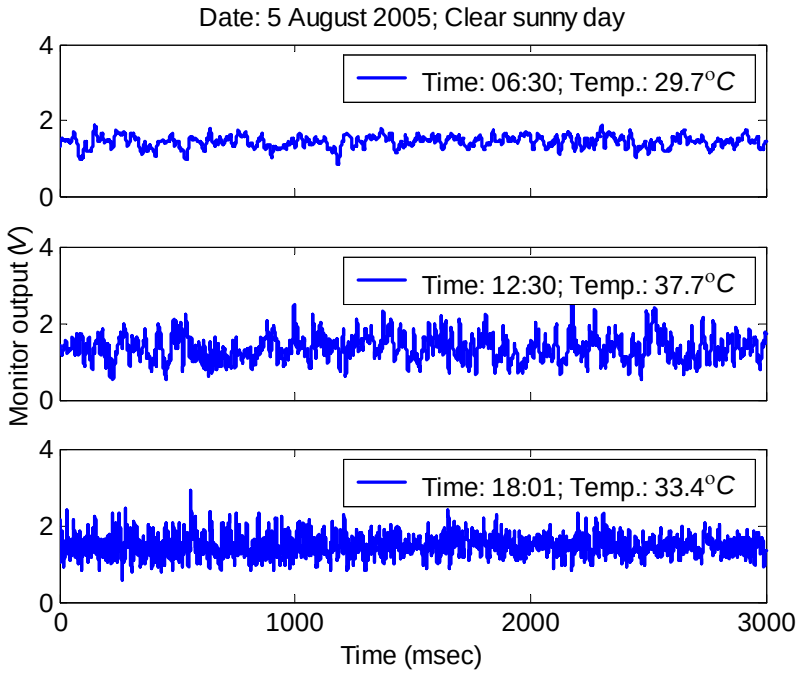

(a)

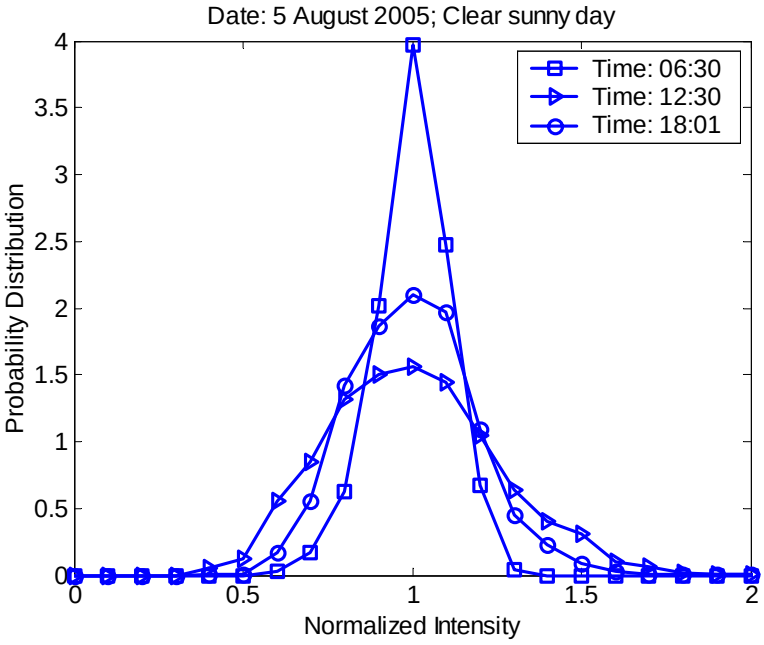

Figure 3.13: Measured intensity fluctuations at different times collected on a clear sunny day (a) time series data and (b) pdf of the time series data in (a).

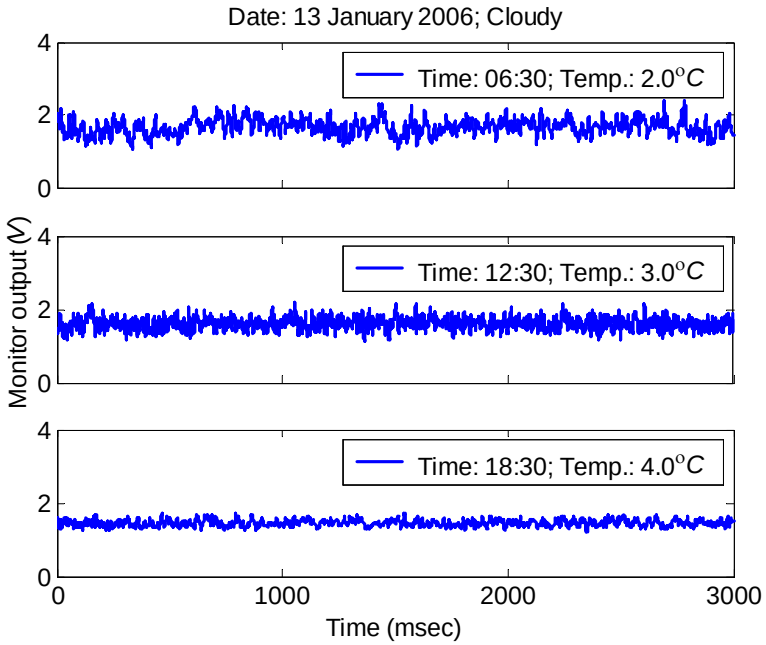

(a)

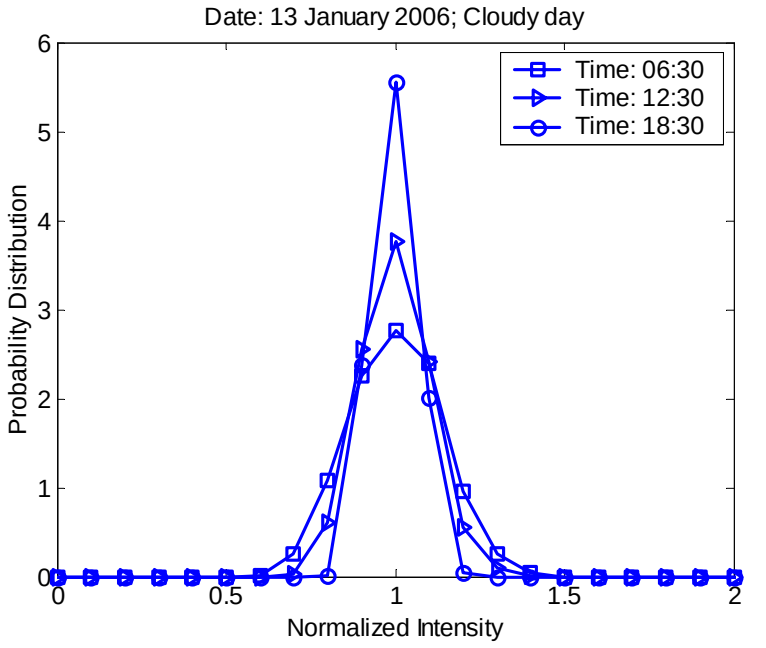

(b)

Figure 3.14: Measured intensity fluctuations at different times collected on a cloudy day (a) time series data (b) pdf of the time series data in (a).

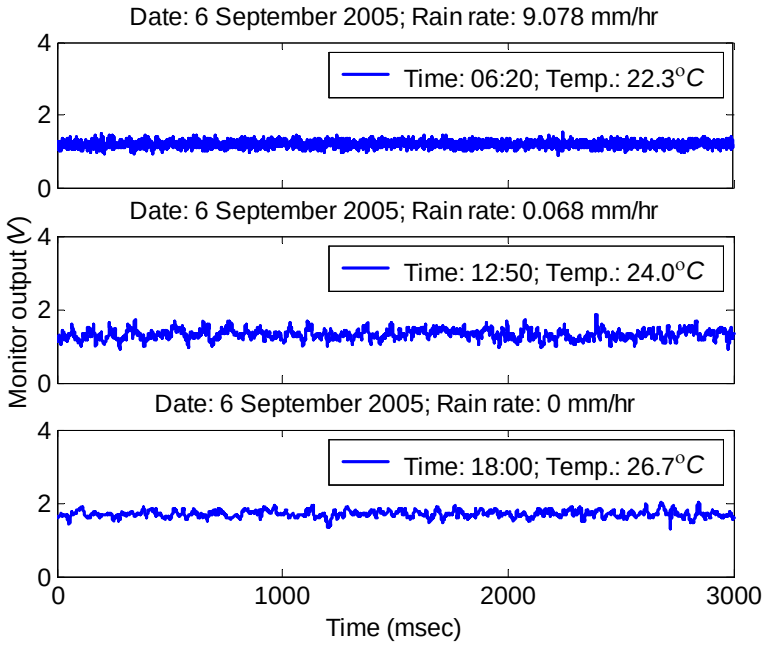

(a)

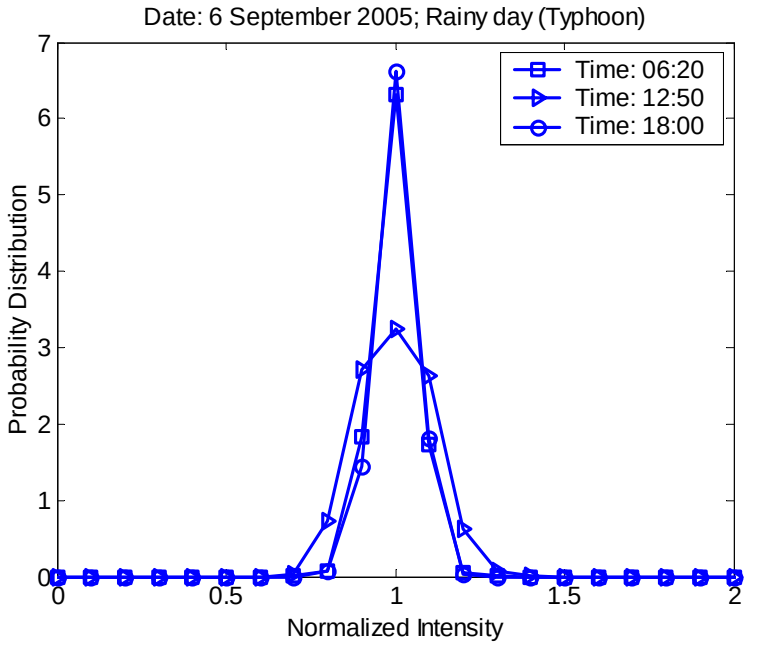

(b)

Figure 3.15: Measured intensity fluctuations at different times collected on a rainy day (a) time series data (b) pdf of the time series data in (a).

Figure 3.16 compares intensity variations for data taken near the same time but on different days with different weather conditions including clear day, cloudy day and rainy day. From the pdf plots in Figure 3.16(b), the amount of scintillation is observed to be higher during clear sunny day (data collected on 28^{th} June 2005) and lower for the data collected during a rain or cloud events (4^{th} and 8^{th} July 2005 respectively). This further demonstrates that a higher amount of scintillation will most likely occur on hot days when the temperature variations are usually higher than in cloudy or rainy day when the temperature difference between the days maximum and minimum temperature are usually not so big. The strength of atmospheric turbulence depends on the net radiation which is sensitive to cloudiness.

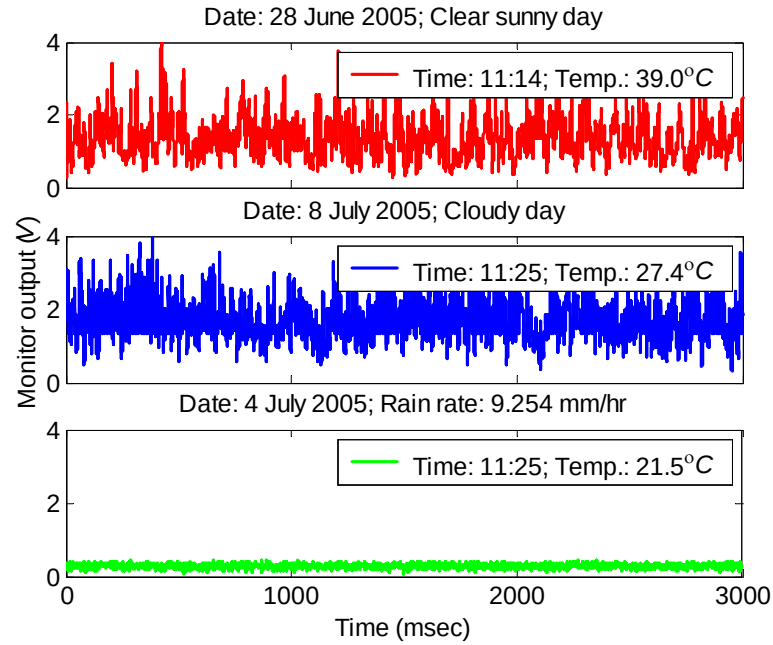

(a)

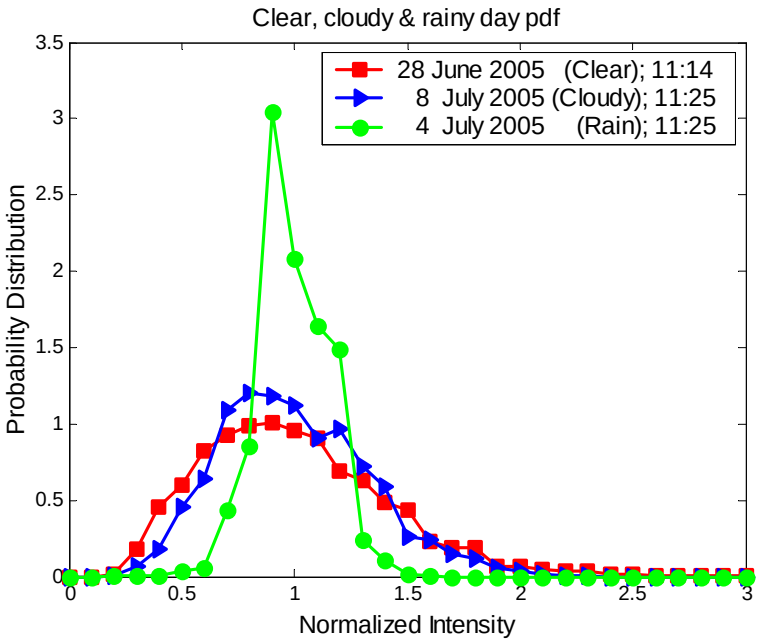

(b)

Figure 3.16: Measured intensity fluctuations taken at the same time but on different days with varying weather conditions (a) time series data (b) pdf of the time series data in (a).

Figure 3.17 and 3.18 show the degree of scintillation fluctuation with temperature both averaged per hour for a period of 24 hours. The plotted data has been collected on different days representing two different seasons (19^{th} May and 19^{th} September 2005 representing summer and 19^{th} Nomber 2006 and 11^{th} January representing winter season). In both cases the weather condition is the same i.e. clear (no overcast). As noted earlier, it is observed that the magnitude of scintillation is a strong function of the time of day and ambient temperature. As predicted, for both season measured data the scintillation was at its worst around midday (between 12:00 and 13:00 pm), which is indicated by the high degree of scintillation fluctuation. The scintillations decrease to minimums near sunrise and sunset. This results agrees with the theory that scintillation is directly related to the difference of the air and ground temperature. During the day, the ground heats up from the sun. The maximum difference between ground and air temperature occurs in the early afternoon. This difference in temperature creates the most turbulence in the air and thus the maximum scintillation as evidenced in Figures 3.17 and 3.18. At sunrise and sunset, the ground and air temperature are approximately equal, thus reducing air turbulence and in effect scintillation.

In the results depicted in Figure 3.17 and 3.18 significant diurnal and seasonal variations are clearly demonstrated. In a study conducted by [99] it was observed that the peak-to-peak scintillations are very much higher on hot still days, especially before heavy rainfall (as high as 12 dB); and it could drop to a low value immediately after heavy rain (less than 4 dB). This is consistent with the results in the variations of degree of scintillation fluctuation for the data recorded in the Waseda University experimental FSO communication system.

This information explains why free-space communication outages may occur in the early afternoon because of increased scintillation levels. Since scintillation is a significant problem, most FSO communication equipments are usually installed as high above the ground as possible, since scintillation level decreases with height.

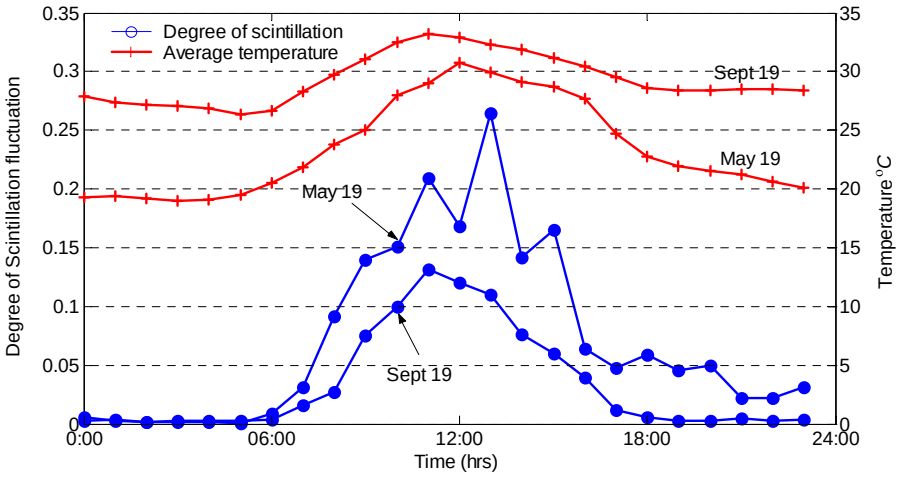

Figure 3.17: Variation of degree of scintillation with temperature in hot weather condition

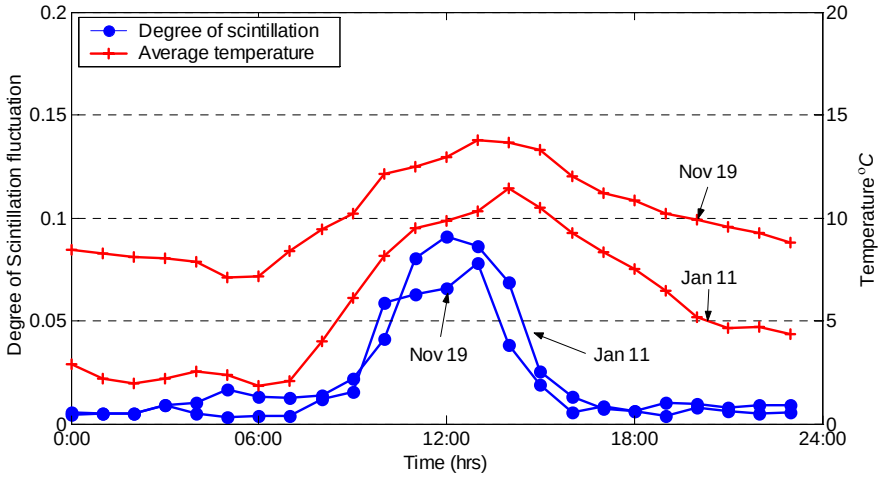

Figure 3.18: Variation of degree of scintillation with temperature in cold weather condition

3.2.3.2 Refractive-index structure constant parameter measurement

The refractive-index structure parameter, C_n^2, is considered the most critical parameter along the propagation path in characterizing the effects of atmospheric turbulence. It can be deduced in a variety of way, but is usually defined as the proportional constant in the index of refraction structure function. That is, under statistically homogeneous and isotropic turbulence, the index of refraction structure constant function exhibits the asymptotic behaviour [55]

$$S_f(D) = C_n^2 D^{2/3}, \text{ for } l_0 \ll D \ll L_0 \tag{14}$$

and

$$S_f(D) = C_n^2 l_0^{-4/3} D^{2/3}, \text{ for } D \ll L_0 \tag{15}$$

where D is the scalar distance between two points in space.

As described earlier and demonstrated using experimentally measured data, temperature and humidity fluctuations are known to be the primary mechanism affecting the index of refraction and thus atmospheric turbulence (degree of scintillation fluctuation). In day time, the solar radiation warms up the ground and the air. The temperature gradient between the ground and atmosphere results in turbulent vertical air streams. From earlier result, it has been shown that the temperature gradient is generally greatest at noon when the ground is warmer than the overlaying air, thus increasing C_n^2. At daytime wind causes air mixing and therefore decrease the inhomogeneity of temperature and hence decreases C_n^2. Increasing wind also enhances the dissipation of ground heating, which causes decreasing temperature gradient and C_n^2. As noted earlier, the strength of atmospheric turbulence depends on the net radiation which is sensitive to cloudiness. When the air temperature is closest to the ground temperature, mainly at sunrise, C_n^2 has a minimum value. At night there is no heating of the ground hence the temperature gradient is smaller and the vertical heat flux decreases. Typical variation of C_n^2 during the day is depicted in Figure 3.19. Overlaid in the same figure is the days temperature variations which helps to emphasis the temperature dependence of C_n^2.

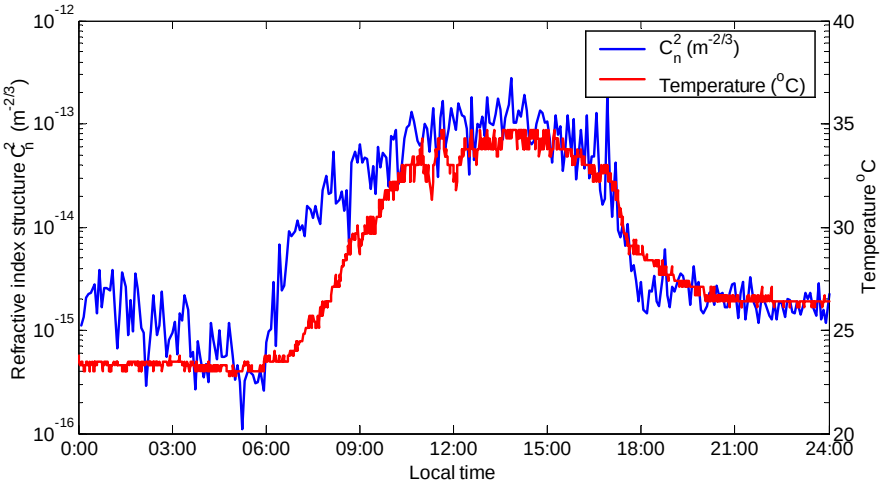

Figure 3.19: A typical variation of Cn2 with temperature during the day measured on 12 September 2005

In the case of laminar temperature flux (horizontal flux), the C_n^2 values are very low. If the temperature of the ground is lower than the air, wind causes vertical temperature flux, which result in turbulent flux and strong turbulence of short duration. This result in a strong oscillation of C_n^2 values, an effect that is know as intermittence. Higher wind velocity increases this effect. In experimental studies conducted by [100, 101] for measurement of C_n^2 values in two different climatic regions (moderate climate and arid/semiarid climate) it was found that intermittence can be observed mainly at night in winter and over snow-covered ground.

Measurement of C_n^2 values has been performed using the setup shown in Figure 3.9. The measured data of intensity fluctuations as a result of scintillation effects is used to provide the C_n^2 values integrated over the 1 km optical path length. From the theory of schintillation it is known that the path averaged C_n^2 in weak-scattering region can be measured by the irradiance (or amplitude) scintillation of a monochromatic wave propagating through the atmosphere [96,102,103]. The variance of the log-amplitude, σ_A^2, for a spherical wave propagating through a statistically homogeneous and isotropic refractivity field is given by

$$\sigma_A^2(D) = 4\pi^2 k^2 \int_0^D dz \int_0^\infty dK K \Phi(K) \times \sin^2\left(\frac{K^2 z\,(D-z)}{2kD}\right), \tag{16}$$

where k is the wave number of the radiation ($k = 2\pi/\lambda$), D is the path length, and $\Phi(K)$ is the three dimensional spectrum of the refractive index fluctuations. The most commonly accepted form of the spectrum of refractive turbulence is that of Kolmogorov [96] i.e.,

$$\Phi(K) = 0.033 C_n^2(z) K^{-11/3}. \tag{17}$$

Inserting Equation (17) into Equation (16), we obtain

$$\sigma_A^2(D) = 0.124 \cdot k^{7/6} D^{11/6} C_n^2, \tag{18}$$

The normalized intensity variance, σ_I^2, or scintillation index, is defined by

$$\sigma_I^2 = \frac{\left\langle [I - \langle I \rangle]^2 \right\rangle}{\langle I \rangle^2} \tag{19}$$

The relation between the log-amplitude variance and the scintillation index for $\sigma_A^2 \ll 1$ is given by

$$\sigma_I^2 = \exp\left(\sigma_{\ln I}^2\right) - 1 = \exp\left(4\sigma_A^2\right) - 1 \approx 4\sigma_A^2 \tag{20}$$

$$\sigma_I^2 = 0.5k^{7/6}D^{11/6}C_n^2 = \beta_0^2 \tag{21}$$

where β_0^2 is the Rytov variance for a spherical wave. The Rytov variance is linearly proportional to C_n^2 and approximately proportional to the square of the optical path length D. This formula can be applied as long as the variance of log-amplitude does not become larger than the limit imposed by the Rytov approximation, $\sigma_A^2 \ll 1$. In agreement with the Rytov approximation, the variance β_0^2 increases linearly with C_n^2 only for low level turbulence. For higher levels, the experimental variance approaches a constant and indeed decreases slightly for higher levels of turbulence leading to the behaviour know as the saturation of scintillation [96].

Approximate expressions for calculation of the variance of normalized intensity fluctuations for strong path-integrated turbulence were derived by Churnside [102] and Andrews et al [55]:

Andrews et al. [55] derived formulas to calculate σ_I^2 which are valid for weak up to strong turbulence conditions. They assumed that the normalized irradiance can be expressed as $I = x \cdot y$, where x and y are statistically independent random quantities:

x arises from large-scale turbulent eddy effects (refractive radius $R_{ref} >$ Fresnel zone $(D/k)^{1/2}$) and y from statistically independent small-scale eddy effects (diffractive radius $R_{diffr} < (D/k)^{1/2}$).

The total scintillation index takes the form

$$\sigma_I^2 = \exp\left(\sigma_{\ln I}^2\right) - 1 = \exp\left(\sigma_{\ln x}^2 + \sigma_{\ln y}^2\right) - 1 \tag{22}$$

where $\sigma_{\ln x}^2$ and $\sigma_{\ln y}^2$ are large-scale and small scale log-irradiance variances, respectively.

In the case of a spherical wave and neglecting inner scale l_0 (assumin $l_0 = 0$ and outer scale L_0) the scintillation index is then given by

$$\sigma_I^2(D) \cong \exp\left[\frac{0.49\beta_0^2}{\left(1 + 1.11\beta_0^{12/5}\right)^{7/6}} + \frac{0.51\beta_0^2}{\left(1 + 0.69\beta_0^{12/5}\right)^{5/6}}\right] - 1 \qquad 0 \le \beta_0^2 \le \infty \tag{23}$$

By applying the above theory of scintillation to the experimentally measured data of intensity fluctuations, atmospheric turbulence statistics can be analysed for attempts to determine the values of C_n^2.

Example of the diurnal cycle of C_n^2 values measured during an arbitrarily chosen summer and winter months is plotted in Figure 3.20 and 3.21. The data was collected when there was no overcast sky. In both figures all months show the same characteristics diurnal cycle of C_n^2. Around noon the atmospheric turbulence was strongest, rising to values of about $3.35{\cdot}10^{-13}$ during summer period. Around sunrise, when the temperature stratification of the atmosphere was stable, the daily variation indicates a distinct minimum of C_n^2 with values of about $1.10{\cdot}10^{-16}$. Due to lower solar irradiance during the winter months the maximum C_n^2 was reduced to values less than $1{\cdot}10^{-13}$. By comparing these two data sets, the noon maximum changed by a factor of 2.3.

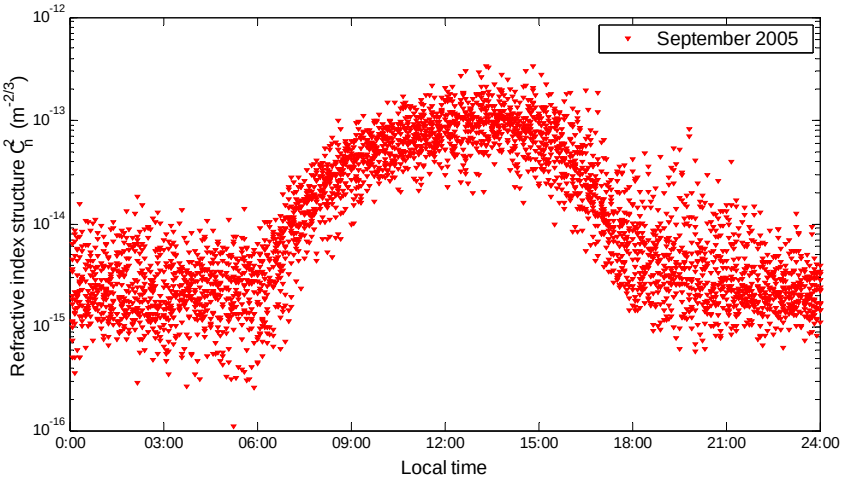

Figure 3.20: Diurnal cycle of Cn2 values measured during a one month period for the month of September 2005

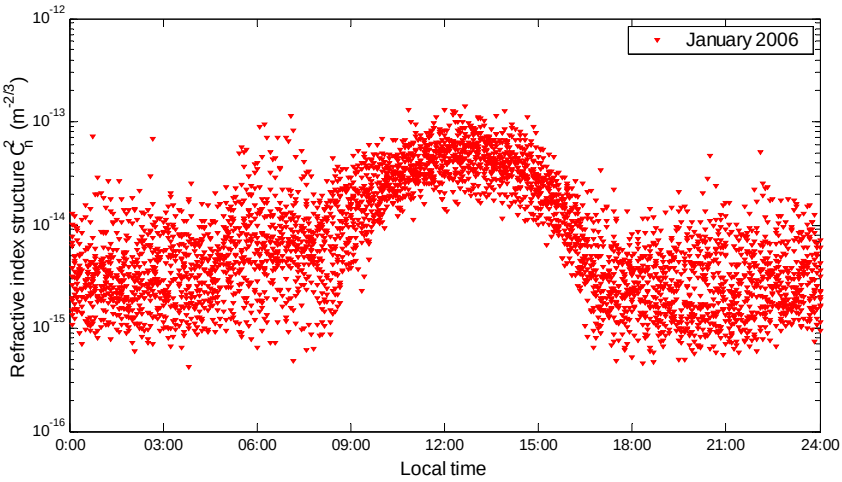

Figure 3.21: Diurnal cycle of Cn2 values measured during a one month period for the month of January 2006

Overcast sky additionally reduces the temperature gradient and hence C_n^2 value. Precipitation and clouds lead to 1-2 magnitude reduction in the noon magnitude. An example of this is shown in Figure 3.22 depicting values of C_n^2 measured during different weather conditions for the month of July 2005. In Figure 3.22 (a) for clear weather condition the diurnal cycle of C_n^2 can easily be observed, but in the case of cloudy and rainy weather conditions depicted in Figure 3.22 (b) and (c) the diurnal cycle of C_n^2 is barely discernable. Also noticeable is the reduction in the noons maximum values of C_n^2.

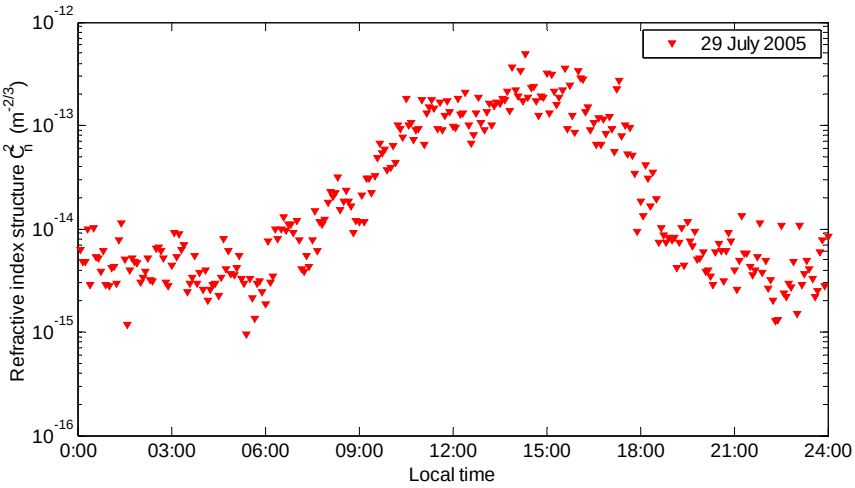

(a)

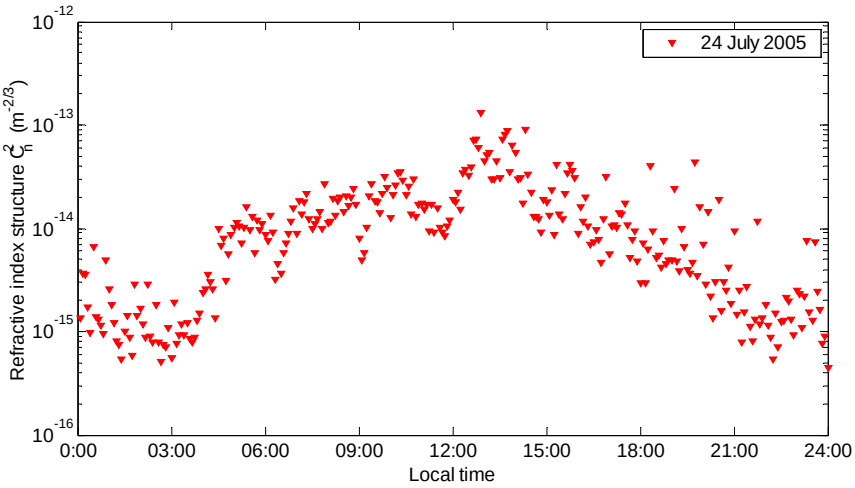

(b)

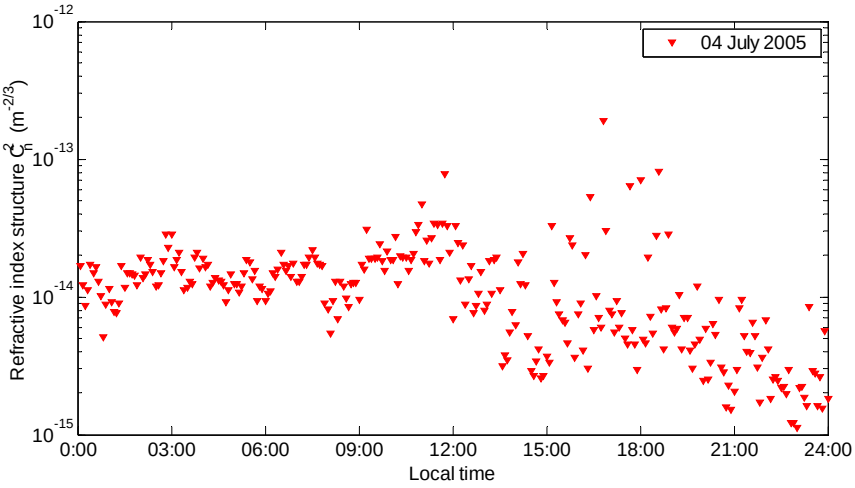

(c)

Figure 3.22: Cn2 values measured in different weather conditions (a) clear day, (b) cloud condition and (c) heavy rain

Since the atmospheric parameters and hence the atmospheric turbulence usually change as a function of time-of-day and season, their influence on the effectiveness of FSO systems can normally only be expressed in a statistical way. To provide a statistical data base for the atmospheric turbulence the cumulative frequency of occurence was calculated for a time period of one month. The time period of one month was arbitrary selected using data sets collected when there was no overcast sky (cloud or rain).

The cumulative frequency of occurence of C_n^2 evaluated values measured for a time period during September is shown in Figure 3.23. The cumulative frequency of occurence was calculated for two-hours time interval during three selected times of the day: around sunrise from (04:30 - 06:30), during day time (11:00 - 13:00) and during night time before midnight (21:00 - 24:00). At midday about 28.13 % of evaluated data indicate $C_n^2 > 1{\cdot}10^{-13}$ m$^{-2/3}$ (strong atmospheric turbulence) and 71.88 % indicate $1{\cdot}10^{-14} < C_n^2 < 1{\cdot}10^{-13}$ m$^{-2/3}$ (medium turbulence). In the case of evaluated C_n^2 values for January 2006 (shown in Figure 3.24) measured data, at midday less than 2 % of evaluated data indicate $C_n^2 > 1{\cdot}10^{-13}$ m$^{-2/3}$.

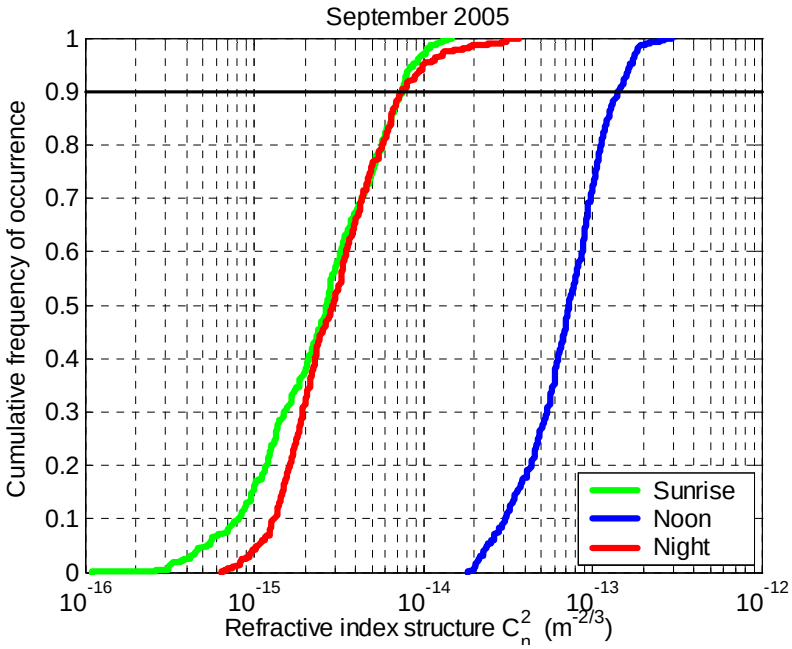

Figure 3.23: Cumulative frequency of occurence of evaluated Cn2 values measured for September 2005 at different time of day (sunrise , noon and night)

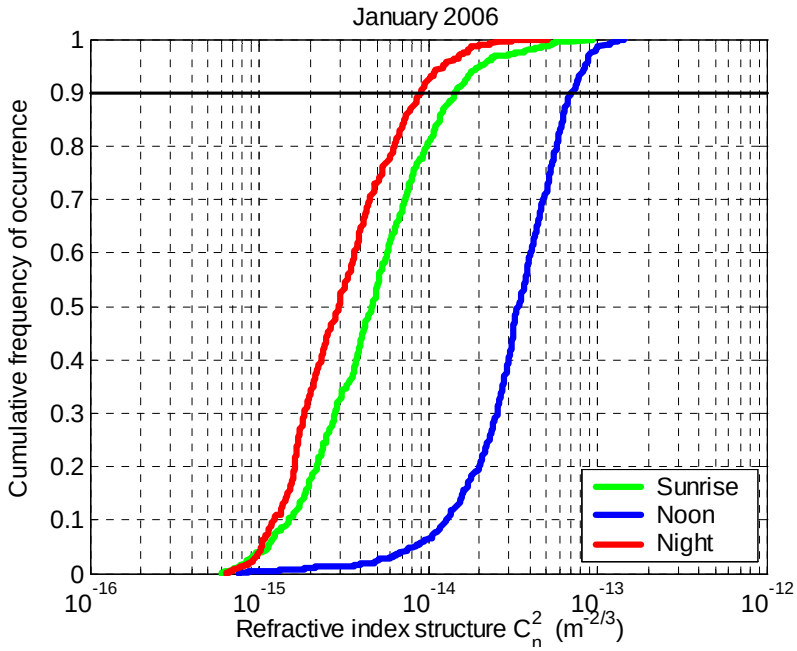

Figure 3.24: Cumulative frequency of occurence of evaluated Cn2 values measured for January 2006 at different time of day (sunrise , noon and night)

Figure 3.25 demonstrates examples for the cumulative frequency of occurence on a monthly basis for C_n^2 values for four difference selected months (September and November 2005 as well as January and March 2006). These months were selected because of the availability of measured data which could be evaluated collected on days which have no overcast (no clouds or rain) and an average of more than 6 hours of sunlight.

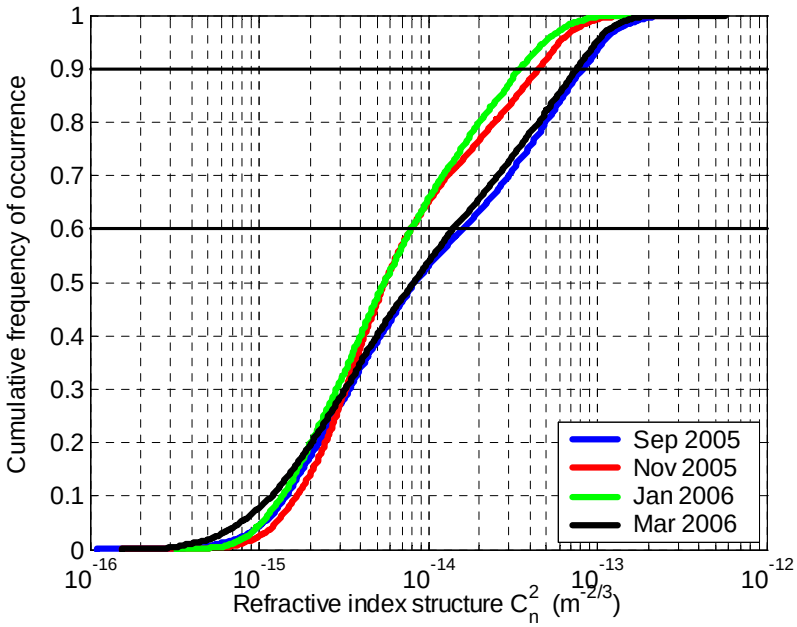

Figure 3.25: Cumulative frequency of occurence of Cn2 values measured for a time interval of one month during different seasons

Table 3.4 shows the occurence of C_n^2 for the different selected months. Because of the high solar irradiance, the occurence of strong atmospheric turbulence (values of C_n^2 greater than $6{\cdot}10^{-14}\mathrm{m}^{-2/3}$) for the months of September 2005 and March 2006 is much higher than for the months of November 2005 and January 2006.

	measured C_n^2 values (in $\mathrm{m}^{-2/3}$)	
Month	$C_n^2 > 6 \cdot 10^{-14}$	$6 \cdot 10^{-15} < C_n^2 < 6 \cdot 10^{-14}$
September 2005	16.12%	41.06%
November 2005	4.98%	42.48%
January 2006	2.91%	44.83%
March 2006	14.42%	41.67%

Table 3.4: Occurence of Cn2 values

It should be mentioned that the number of C_n^2 values for evaluation of turbulence measurements in this experiment varies and is always smaller than the theoretical number of measurements (288 measurements per day multiplied by the number of complete data files per month). This is because the weather situation can significantly change during short time period during certain months. Therefore only 50% - 70% of the theoretical amount of a monthly data set can be evaluated.

3.2.3.3 Angle-of-arrival fluctuation measurement

Image dancing, also called beam wander in the focal plane, is related to turbulence-induced phase fluctuations on the propagating optical wave. The angle-of-arrival[4] is a result of a phase shift along the receiver lens diameter that is manifested as optical path difference. The angle-of-arrival, α, is defined by [55]:

$$\alpha = \frac{\Delta D}{A} = \frac{\Delta S}{A} \text{ (in radians)} \tag{24}$$

where ΔD is the optical path difference and ΔS is the phase shift across a receiver aperture with diameter A. Using equation 24, the rms image displacement, $\Delta Srms$, is [55]:

$$\Delta S_{rms} = \langle \alpha^2 \rangle^{1/2} \; f = \left(2.91 C_n^2 D A^{-1/3}\right)^{1/2} \; f \text{ for } A \gg l_o \tag{25}$$

where f is the focal length of the optical receiver in meters.

The setup shown in Figure 3.26 is used to measure and record scintillation and beam intensity variations from angle-of-arrival (AOA) fluctuations caused by atmospheric turbulences as the beam propagates through the atmosphere.

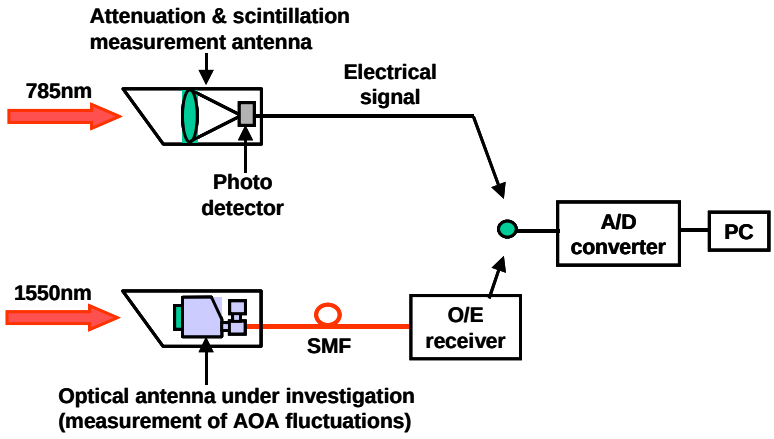

Figure 3.26: Measurement setup for scintillation and beam intensity variations as a result of AOA fluctuations measurement setup.

Experiment data collected for intensity changes of the 1550 nm wavelength signal caused by angle-of-arrival (AOA) fluctuation is shown in Figure 3.27(a). This measurement is made when the

[4] angle-of-arrival (AOA) can be defined as a measure of the direction of propagation of an optical/IR wave upon arrival at a receiver. It is the angle between the actual plane of the phase front at the receiver and some plane of reference.

antennas' FPM tracking is set to OFF. The spectral density of the measured intensity fluctuation as a result of AOA fluctuation at different frequencies if shown in Figure 3.27(b). The significance of measuring the intensity variations of the 1550 nm wavelength signal as a result of AOA fluctuations is to be able to compare with the intensity fluctuations caused by scintillation effects for the 785 nm wavelength signal outlined in the next section.

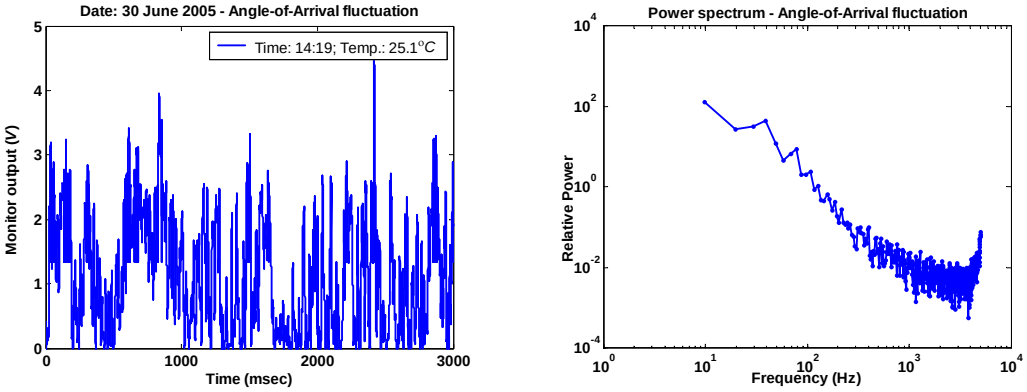

(a) (b)

Figure 3.27: Beam intensity variations as a result of angle-of-arrival fluctuations (a) time domain data and (b) frequency domain

3.2.4 Comparison of scintillation and angle-of-arrival fluctuations

Considering that the measurement for beam intensity fluctuations as a result of scintillation effect for the 785 nm wavelength optical beam is collected over the same propagation path (see figure 3.10) as the experimental 1550 nm wavelength FSO system, it can be assumed that statistically the atmospheric turbulence effects will influence the 1550 nm communication beam intensity variation because of AOA fluctuations in a similar way as the scintillation effect observed on the 785 nm wavelength beam [74]. So, bearing that in mind and considering the same atmospheric condition, measured data for the beam intensity variations as a result of beam AOA fluctuations and the scintillation effect is recorded. Figure 3.28 shows the measured time series data using the system setup shown in Figure 3.26.

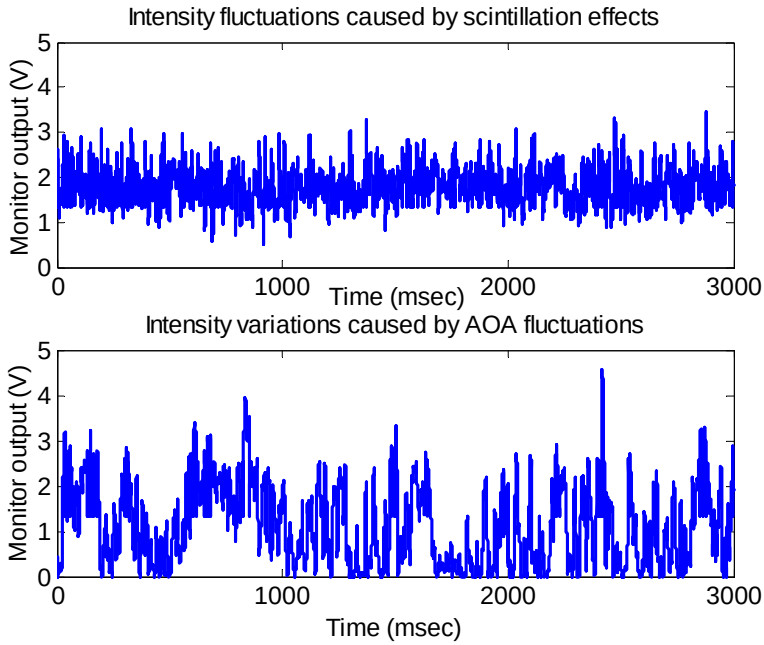

Figure 3.28: Beam intensity fluctuation caused by scintillation (top) and 1550 nm communication beam intensity variations as a result of AOA fluctuations (bottom).

Figure 3.28 top shows the intensity fluctuations as a result of scintillation effect for the 785 nm wavelength beam and Figure 3.28 bottom shows the 1550 nm beam intensity variations (in terms of detected voltage) because AOA fluctuations when the antenna tracking is set to OFF. Figure 3.29 shows the frequency response characteristics obtained by performing fast Fourier transform (FFT) on the time series data in Figure 3.28 and producing a power spectrum at various frequencies. It is observed that there is similarity between the frequency characteristics of the magnitude of intensity fluctuations as a result of scintillation effect and beam AOA fluctuations[5]. The main interest is to determine the rate of the free-space optical beam intensity fluctuation, especially for the values above 100 Hz. The approximate fine pointing mirror (FPM) tracking speed suitable to suppress this atmospheric turbulence fluctuation is determined from this results.

[5] In figure 3.29, the slopes of the two curves for frequency below 100 Hz are different in the degree of fluctuation (amplitude) because of the physical difference of the photo detector (PD) and SMF as optical beam acceptance surface (size) and possible optical beam acceptance angle.

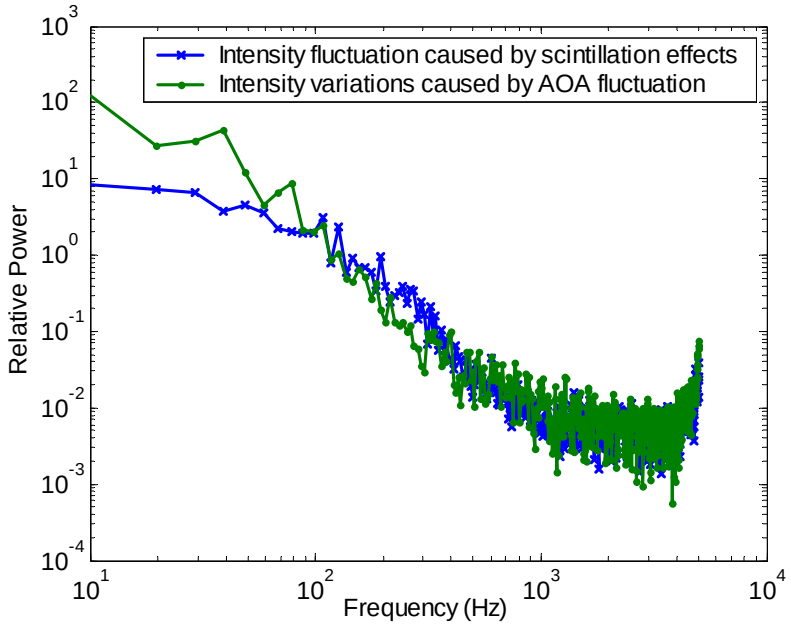

Figure 3.29: Relationship between intensity fluctuation caused by scintillation and 1550 nm communication beam intensity variations caused by AOA fluctuations.

From the above the FPM tracking speed which will enable the FPM to control and steer to a great extent the received 1550 nm data beam to the SMF can be accurately approximated. From the experimental results and observation of beam AOA fluctuations frequency characteristics the selected FPM antenna tracking speed should be above 500 Hz. In this case the tracking speed is set to 1 kHz which is currently considered to be the fastest tracking system for any available FSO communication system. The suppression of the intensity fluctuation as a result of atmospheric induced AOA changes was shown earlier in Figure 2.12 depicting the improvement in the fiber received power.

3.3 Comparisons of 785 nm and 1550 nm system

Taking advantage of the two antennas (operating in 785 nm and 1550 nm wavelengths) installed and operating in the same environment, comparative based performance studies on the propagation characteristics of the two FSO systems can be easily conducted. The comparisons is made considering data collected on the same atmospheric and weather condition. Therefore in this section atmospheric propagation characteristics comparison for the 785 nm and 1550 nm wavelength using field accumulated data is conducted. The performance under various weather conditions is

presented.

3.3.1 Atmospheric loss and receiver sensitivity

As outlined in the previous section, the atmosphere causes signal degradation and attenuation in a free-space optical system link in several ways including absorption, scattering (mainly Mie scattering), and scintillation. All these effects are time varying and will depend on the current local conditions and weather and together they contribute to channel fade. It is neccessary when setting up a communication link to calculate the link budget which will determine how far a transmitter and receiver can be placed while still maintaining enough margin to allow for specified minimum link availability (for example 99.9%). For a given distance, it is possible to determine the link fade margin which can help in judging the reliability of the link. In this section the link margin for the two systems (operating in 785 nm and 1550 nm wavelengths) is determined which will give a quantitative value of the amount of atmospheric loss the systems can be able to tolerate.

Figure 3.30 illustrates the sources of power loss throughout an FSO link. The losses include optical losses[6], connector losses, geometric losses[7] (beam spreading losses) as well as pointing losses and atmospheric losses.

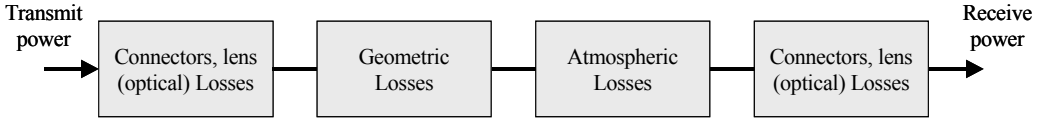

Figure 3.30: Sources of losses in a FSO link

Geometric losses, L_G, arises as a result of the divergence of the optical beam. These losses can be computed via the following formula

$$L_G(D) = 10^{*}\log\left\{\frac{A_{RX}}{A_{TX} + [D * \theta]}\right\}^2 , \tag{26}$$

where A_{RX} and A_{TX} are the receive and transmit antenna apertures measured in m, both 4 mm in the case of the 1550 nm antenna and 10 cm for the 785 nm antenna. D is the distance between the transmitter and receiver measured in km, $D = 1$ km in this case and θ is the divergence of the transmitted laser beam in $mrad$, $\theta = 94.5$ μrad for the 1550 nm wavelength antenna. These parameter values are included in Table 3.1

[6] Loss due to imperfect lenses and other optical elements (such as couplers).
[7] The term geometric loss refers to the losses that occur due to the divergence of the optical beam.

The link margin analysis for the two systems is shown in Figure 3.31. To determine the link budget, the above mentioned loses namely optical losses, geometric losses and atmospheric losses are taken into consideration. The link distance is 1 km therefore pointing loss is considered not too significant for the 785 nm system. And because the 1550 nm system uses automatic tracking the pointing loss can also be ignored.

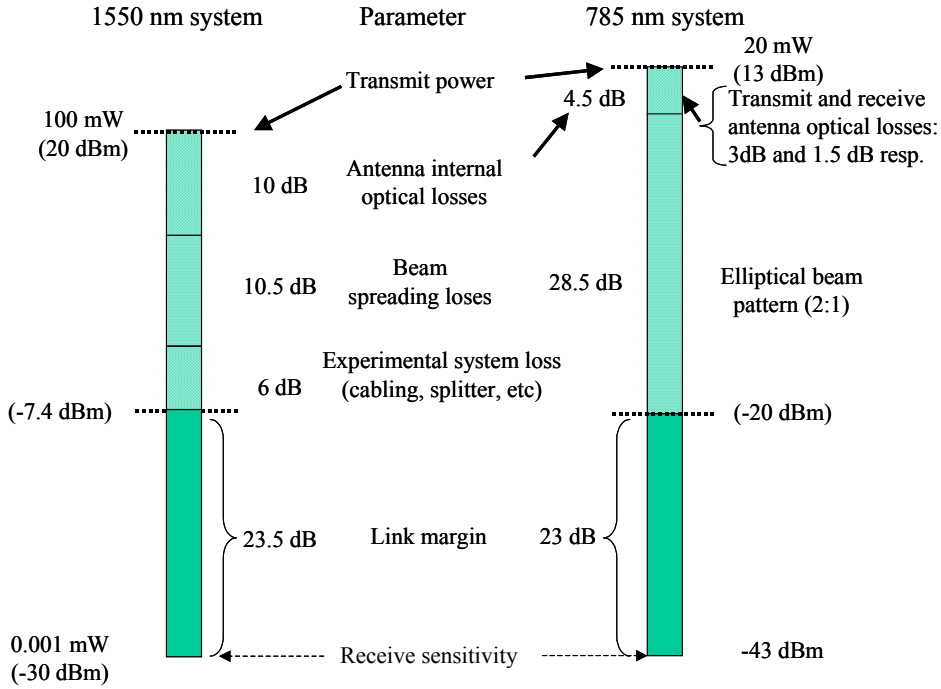

Figure 3.31: Link budget for 800 and 1550 nm systems

The specified receiver sensitivity applies to specific BER and the threshold that is chosen depends on the specific application. In this case for high data rate transmission, a BER threshold of better than 10^{-10} is considered. The receiver sensitivity for the 1550 nm system is -30 dBm for 2.5 Gbps digital transmission rate and a BER of 10^{-12} and for the case of the 785 nm system the receive sensitivity is -43 dBm for 155 Mbps. For both systems the link margin is about 23 dB, and this is what is available for to protect against fade events caused by atmospheric turbulence. When extending the link distance, consideration is focused on the additional loss by geometric loss (which is a function of the beam divergence angle) and the atmospheric turbulence. For the two system, the available margin is sufficient to protect against geometric loss and atmospheric turbulence for a distance of up to 2 km.

It should be noted that the above link margin has been determined from the initial design specifications of the systems. During the course of the experiment, in order to achieve better

performance, adjustments were made which varied the beam divergence (defocus was carried out). In the final analysis the measured beam divergence was 200 urad.

3.3.2 Propagation characteristics of 785 nm and 1550 nm system

The conventional free-space optical system used in this experiment operates in the 785 nm wavelength. After determining the system link margin, measurements of atmospheric propagation characteristics data were performed to evaluate the system performance in correlation with the weather condition. In [104, 105] comparison of propagation characteristics for 785 nm and 1550 nm wavelength systems under various weather conditions are reported. But, sufficient field experimental data has yet to be accumulated for evaluation of free-space optical system operating in the 1550 nm wavelength.

In this experimental work, an opportunity to verify full optical wireless system operating in the 1550 nm wavelength band for long term field test and at the same time comparing with the conventional 785 nm wavelength system is conducted. The data is correlated with meteorological data at the deployment environment.

3.3.2.1 Propagation characteristics during rain event

Figure 3.32 shows the performance characteristics for 785 nm and 1550 nm optical antenna system during rain event. As the visibility deteriorates from around 23:00 on 7^{th} January due to precipitation (rainfall), the received optical power is also attenuated. Figure 3.33 shows the optical power attenuation for the 785 nm and 1550 nm with visibility far the data which is shown in Figure 3.32.

For each wavelength (785 nm and 1550 nm), theoretical value for received optical power attenuation as a result of visibility is plotted using formula 9 which was introduced in section 3.2.1. The reference optical power is the value determined before the onset of rainfall. The results are shown Figure 3.33. The theoretical data for the two wavelengths are shown by curved lines while actual measured experimental data is plotted as $\circ$ and $\triangle$. For each wavelength, the theoretical and actual measured optical power attenuation show close correspondence. The correspondence between theoretical and measured values for the 785 nm and 1550 nnm wavelengths is not so big for visibility equal to or less than 1 km but it improves as the visibility increases. It is neccessary to point out that the time setting between the computers used to record the optical received power data for the two systems was different (about 10 minutes difference). This is the reason why the figures showing the comparison of the received optical power (Figures 3.32 and 3.34) show a slight

time-shifted correlation.

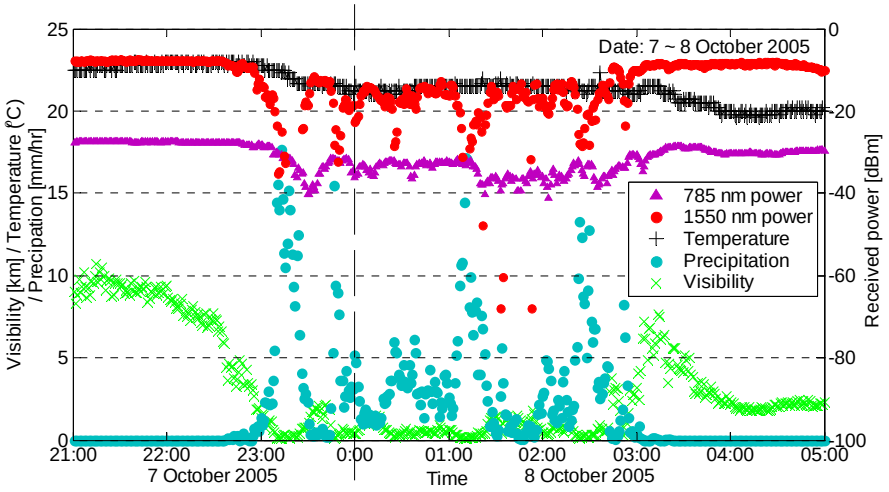

Figure 3.32: 785 nm and 1550 nm received power characteristics during rain event

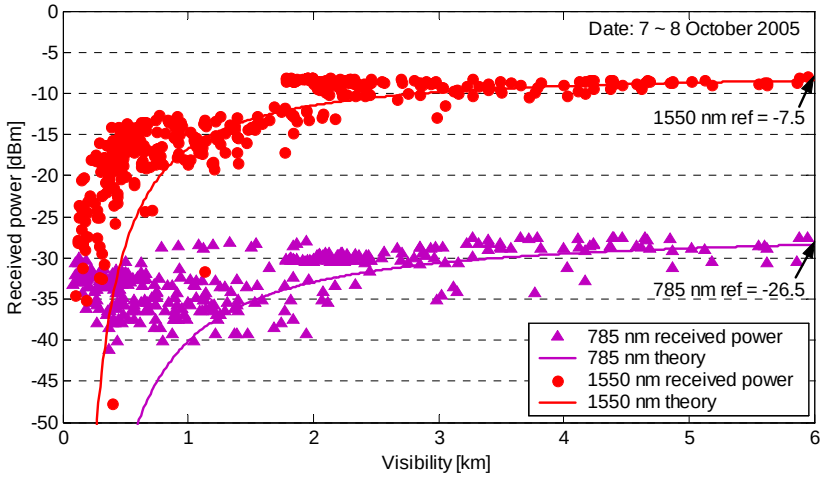

Figure 3.33: Received power and visibility characteristics during rain event

3.3.2.2 Propagation characteristics during snow event

An example for data collected for comparison of received power attenuation for a 785 nm and 1550 nm system during snow event is depicted in Figure 3.34 and 3.35. The occurrence of snow in the Tokyo area is rare compared to rainfall event, but this data was obtained on a day when there was an ample amount snow fall which occurred on the 21^{st} of January. 2006. From Figure 3.34 it is observed that the visibility starts to deteriorate from around 2:40 am because of snow. This results in attenuation of the received optical power for the 785 nm and 1550 nm systems. In addition,

around 4:40 am the 1550 nm antenna tracking circuit fails causing complete link cut-off. By setting the reference optical power equal to the power before the onset of snow, the relationship between the received optical power and visibility for actual measurement and theoretical calculated values is shown in Figure 3.35. Here the 1550 nm wavelength reference value is different from the previous data observed for rainfall event (8^{th} October 2005) above because of the system measurement and gain adjustment. This measurement data for optical attenuation because of snowfall for the 1550 nm wavelength seamless connection free-space optical system is insufficient because the tracking system fails completely. In addition, transmission quality evaluation for visibility lower than 2 km is important, but unfortunately because of the insufficient data, it is difficult to show the relationship between the actual measured data and the theoretical derived values.

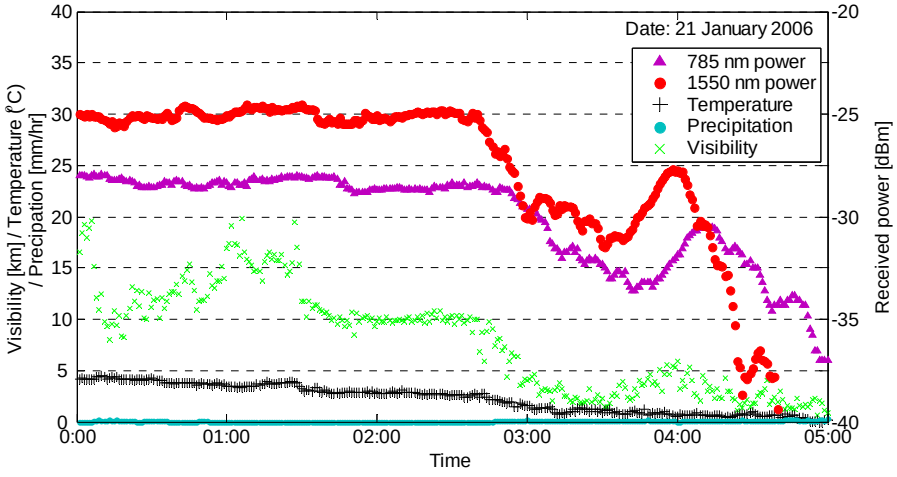

Figure 3.34: 785 nm and 1550 nm received power characteristics during snow event

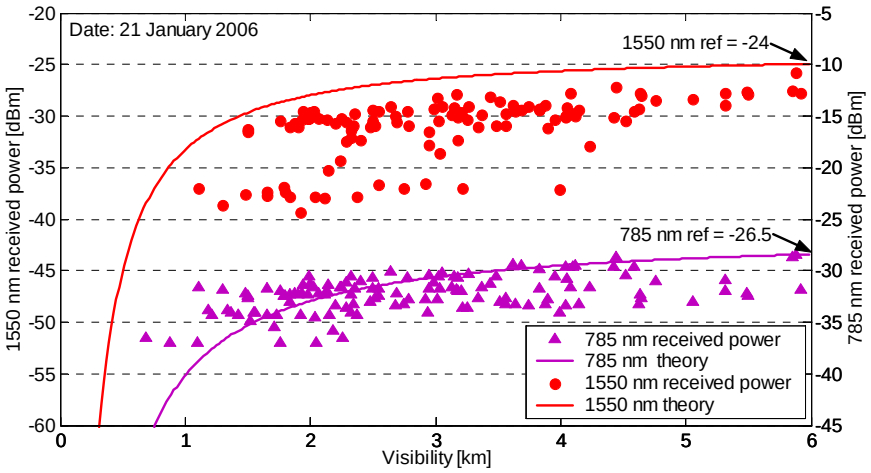

Figure 3.35: Received power and visibility characteristics during snow event

In this section, the propagation characteristics by comparison of optical power attenuation under the same atmospheric conditions (visibility and rain rate) for 785 nm and 1550 nm wavelength systems has been shown. When the optical power attenuation characteristic as a function of visibility was evaluated, the received optical power was confirmed to closely correspond to the theoretical value. Therefore, considering the same propagation path and data collected at the same time with the same condition, based on optical power measurement for 785 nm and 1550 nm wavelength systems, both wavelength comparison evaluation result (except for the full optical connection free-space optical system tracking problem) the 1550 nm attenuation characteristics using equation 9 (which shows similar results to equation 8) was confirmed. In other words, it has been verified that the expression used for conventional free-space optic link design in calculating the optical power attenuation can also be used for 1550 nm wavelength free-space optical system.

Furthermore, in this experiment, the 785 nm system uses a photo detector whereas in the 1550 nm system, the optical beam if coupled directly to the SMF. Therefore, in this case complete symmetric comparison evaluation is difficult and it is not easy to say which system is more superior or inferior. In the future, by accumulating more data, it is expected that more reasonable results can be obtained.

3.4 BER and received power experiment for 1550 nm system

3.4.1 BER and received power performance analysis

To evaluate the communication quality of the system a 2.5 Gbps and then later 10 Gbps Bit Error Rate Tester (BERT) pattern generator (Agilent Technologies N4906 Serial BERT) is used to directly modulate (on-off keying) a single frequency distributed feedback (DFB) laser at 1550 nm wavelength, with a 2^{23}-l pseudo random bit sequence (PRBS) pattern length (The PRBS pattern length for the 10 Gbps transmission test was set to 2^{7}-1). The data encoded optical signal, is amplified by a 100 mW (20 dBm) EDFA. At the receiver the received optical beam is focused by the FPM to the SMF. The optical circulator is used to isolate the transmitted and the received signals. At the reception side, the received signal is equally split into two arms by a single mode 3 dB coupler. Half of the received signal enters the O/E converter and the data and clock signals extracted for BER measurements, and the other half is used to monitor the received optical power (see figure 3.2). The 3 dB output is coupled directly to an optical power meter (Agilent 8163A/B Lightwave Multimeter) with a 100 msec averaging time and the optical power meter data is averaged and logged every 30 secs. The regenerated data and clock signals derived from the 2.5 Gbps (later 10 Gbps) and optical signal, were applied to the 2.5 Gbps error detector for link performance monitoring.

In the subsequent subsections, details on the BER and fiber coupled received power when the antenna miniature FPM tracking speed is set to 1 kHz under various weather and atmospheric conditions is presented.

3.4.1.1 BER and received power under low atmospheric turbulence

The BER characteristics when the antenna tracking speed is set to 1 kHz is shown in Figure 3.36 for the 2.5 Gbps transmission experiment. In this case for a 24 hour period, error free transmission is achieved which confirms the stability and good performance of the system. Similarly, using a 10 Gbps BERT measurement for the 10 Gbps transmission link was performed for a 12 hour period and the BER performance characteristics are shown in Figure 3.37. The above data for 2.5 Gbps and 10 Gbps transmission experiment was measured when the atmospheric condition can be considered to be clear and quiet with low to moderate atmospheric turbulence. The minimum receiving signal power (receiver sensitivity) at 10^{-12} BER is -30 dBm.

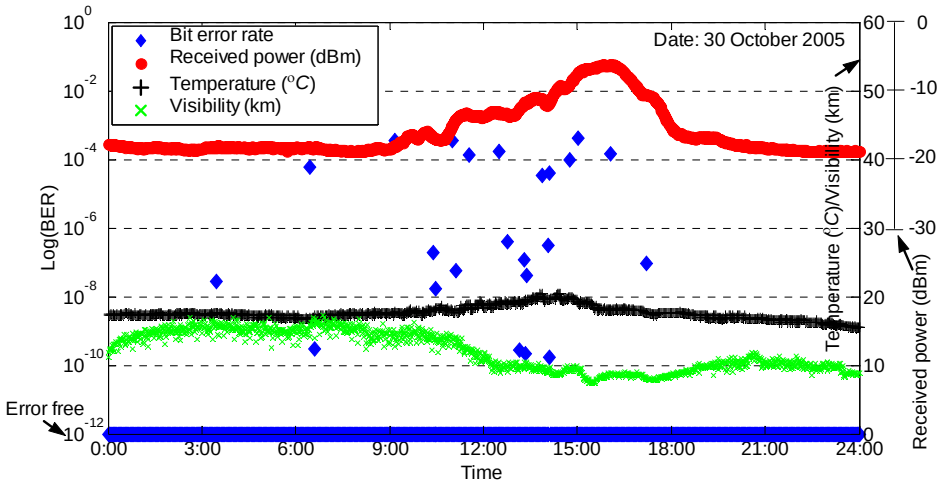

Figure 3.36: Single channel 2.5 Gbps transmission bit error rate characteristics

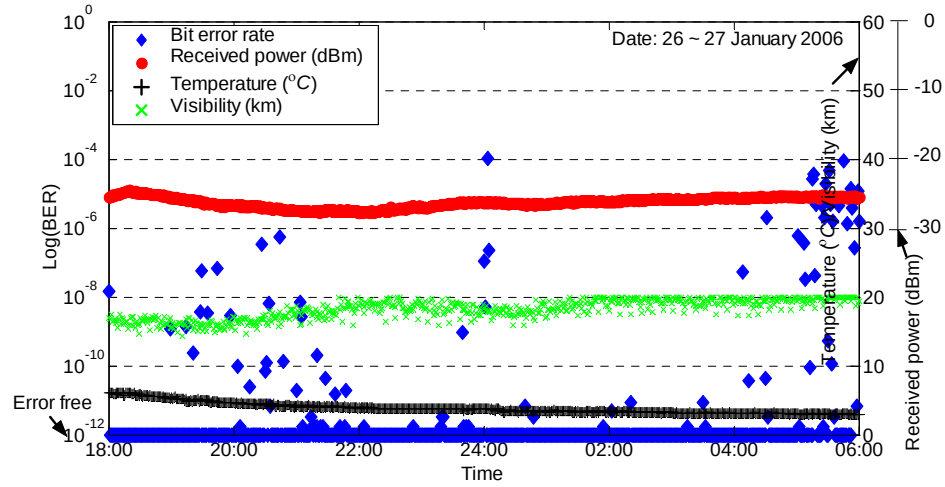

Figure 3.37: Single channel 10 Gbps transmission bit error rate characteristics

Even though the antenna tracking speed is enough to compensate for atmospheric turbulence effects, occasional burst errors occur as shown in figures 3.36 and 3.37 for single channel 2.5 Gbps and 10 Gbps transmission test respectively. These burst errors are possibly attributed to the non-linearity in the tracking system or the tracking dynamic range might be insufficient in situations of strong turbulence (the QAPD and QPD field of view is insufficient). Another likely cause of the burst errors is phase scintillation due to atmospheric turbulence of the incoming signal beam resulting in the decrease of the received power. These occasional burst errors have negligible influence on the performance of the FSO system and the system can be used for reliable stable communication.

3.4.1.2 BER and received power under varying atmospheric turbulence

During the periods of strong atmospheric turbulence ($C_n^2 \geq 10^{-13} m^{-2/3}$) and increasing changing atmospheric conditions, occasionaly the miniature FPM temporarily looses its tracking capability and burst errors occur as depicted in Figure 3.38 for data collected for a 24 hour period from 19:45 pm on 9^{th} October 2005. The weather forecast for the time the particular data was collected was cloudy/rain. This figure shows the worst case scenario with almost continuous occurrence of bit errors in the link. For a period between 9:00 am and 12:00 am burst errors are observed even though the recorded averaged received power appears to be sufficient. By observing the instantaneous recorded power (setting the power meter to 100 msec averaging time), the burst errors can be observed more closely. This is shown in Figure 3.39 (a) and (b) for two consecutive data collected for 2 hours. Figure 3.39 (a) and (b) top shows the BER characteristics (one recording every minute) while Figure 3.39 (a) and (b) below shows the corresponding instantaneous received power. The instantaneous power fades which results in bit errors can not be easily observed in Figure 3.38 but can easily be differentiated in Figure 3.39. The burst errors can be attributed to the fact that the FPM is incapable of wave-front correction beyond aberrations caused by tip and tilt errors.

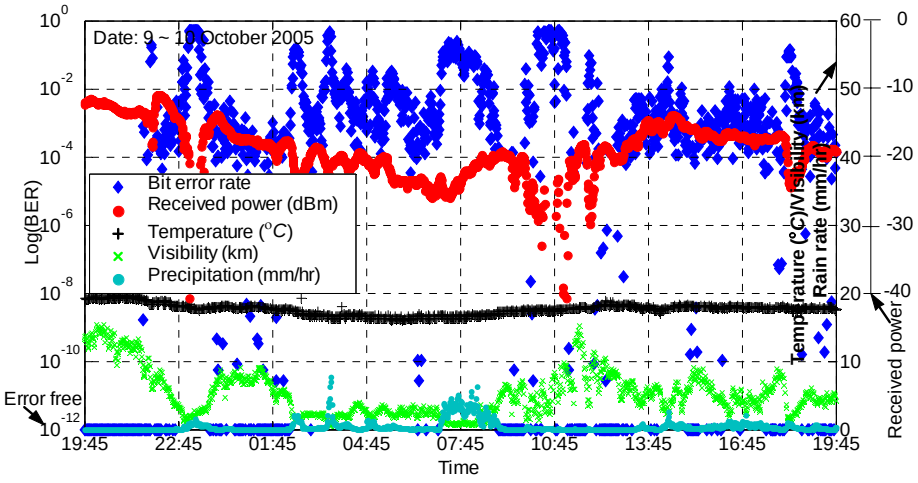

Figure 3.38: Single channel 2.5 Gbps transmission bit error rate characteristics showing bursts errors

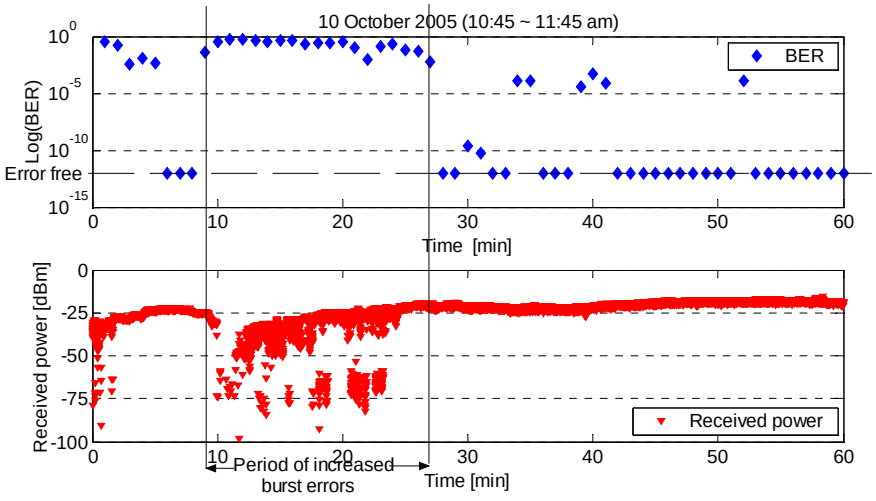

(a)

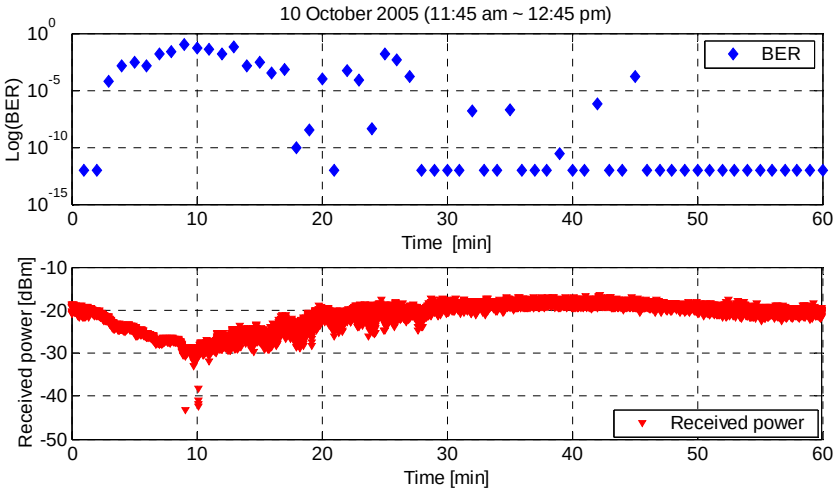

(b)

Figure 3.39: Single channel 2.5 Gbps transmission bit error rate characteristics showing bursts errors with instantaneous measured power

3.4.1.3 BER and received power under different weather conditions

As previously described, because the air needs time to heat up, atmospheric turbulence is typically greatest in the middle of the afternoon and weakest an hour after sunrise or sunset. Figure 3.40 depicts the FSO communication system BER and received power characteristics with variations in the temperature and visibility. From the figure it is observed that there is increased number of errors in the link from a period starting from around 08:30 am to about 17:00 pm even though the fiber coupled received power shows an improving trend. The occurrence of errors is more pronounced between 10:30 pm and 13:30 pm followed by a bit of improvements but experiencing more bursts errors again for a short period between 16:00 pm to around 16:30 pm. The reason for the increased

number of errors between this period can be attributed to the increased degree of scintillation fluctuation as a result of temperature changes. There is a rapid increase of temperature between 08:30 am to about 13:30 pm where it then remains at almost constant value for sometime before starting to drop again from 16:30 pm which is confirmed by the increase of bit errors in the system. The weather forecast for this day can be considered as clear with high visibility throughout as shown by the visibility curve in the same figure. The occurence of burst errors at around 16:00 pm show in the figure is due to incorrect tracking because the sun was directly opposite the receive antenna.

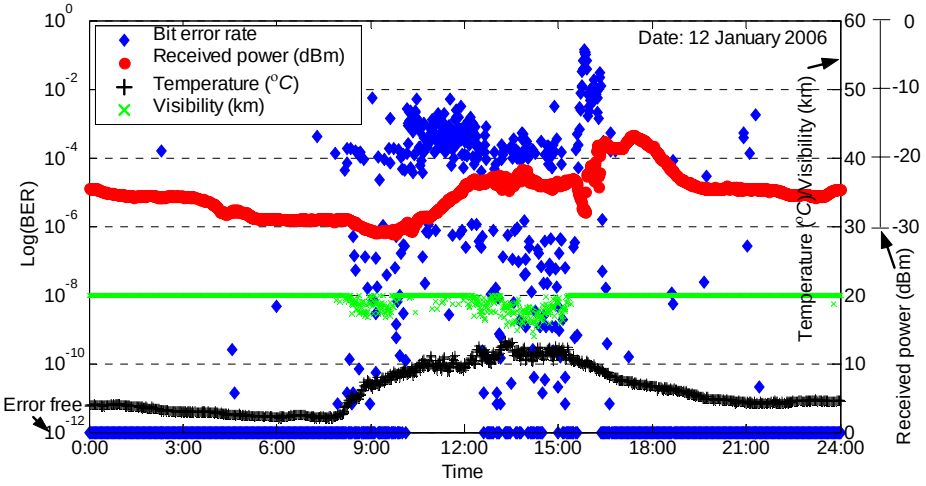

Figure 3.40: Bit error rate, received power, visibility and temperature variations characteristics

An example of the FSO system performance under a different weather condition is shown in Figure 3.41. The weather condition of this particular day was heavy rain with thunderstorms. Error free transmission with an exception of very few burst errors is observed from midnight (0:00 am) to about 13:00 pm just before the onset of rain. With the increasing rainfall the system experiences deterioration in the link quality which is depicted by the rapid occurrence of errors and the fall in the received power. Total link cut-off (unavailability) occurs at around 16:30 pm. The recorded visibility on this day is also very poor which severely affects the propagation characteristics of the 1550 nm wavelength beam contributing to the link poor performance. From around 20:45 pm the link begins to recover with improvements in the fiber coupled received power and total link recovery at around 22:30 pm. The rate of rainfall begins to drop and the visibility also improves as depicted in the figure. It should be noted that the link attenuation during rainfall has two components - link path attenuation due to rain and attenuation due to heavy rain falling on the

FSO transceiver window. During heavy rain it is expected that attenuation due to water on the FSO transceiver window will be worst especially when the wind speed is high and the wind is blowing normally towards the FSO window that explains the significant losses depicted in Figure 3.41. There is a model adopted in [106] which proposes the following expression for the optical link path attenuation, L in terms of the rainfall rate (integrated over 10 minutes), R_{10m}

$$L = 4.9 {R_{10m}}^{0.63} \text{ dB/km} \tag{27}$$

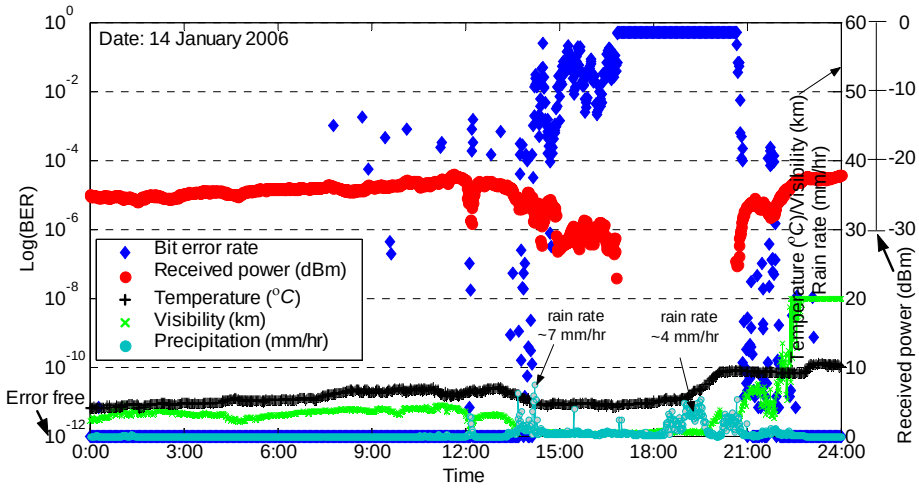

Figure 3.41: FSO system performance in terms of BER during rain condition

The FSO system performance on the two days outlined above (January 12^{th} and 14^{th}, 2006) can also be explained by looking at the variation of the degree of scintillation together with the recorded temperature. This is depicted in Figure 3.42. It is possible to obtain a direct correlation between the variation of the degree of scintillation, the rainfall rate and the performance in terms of BER of the FSO communication link. The variation of the degree of scintillation recorded on January 12^{th} is greater than the variations recorded for January 14^{th}. This is because the temperature difference (the days maximum and minimum temperature) on 12^{th} January is higher than that recorded on the 14^{th} January (minimum temperature 2^oC and maximum temperature of 12^oC). The weather condition on January 12^{th} was clear weather with high visibility whereas the weather condition on January 14^{th} was heavy rain with thunderstorms. The degree of scintillation is less on 14^{th} January because the days temperature difference is not very high, varying from a minimum of 4^oC to 10^oC. The rapid increase of the degree of scintillation fluctuation on the 12^{th} January shown in Figure 3.42 confirms the increased in the errors in the FSO communication system shown in Figure 3.40.

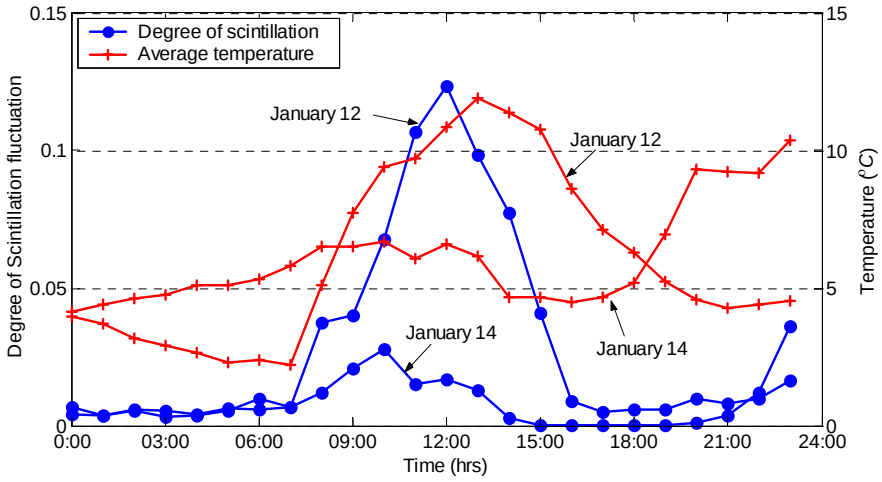

Figure 3.42: Variation of degree of scintillation with temperature for January 12th and 14th (2006) recorded using 800 nm antenna

The effect on the BER and fiber received power during snow event is depicted in Figure 3.43. This data is recorded on 21^{st} and 22^{nd} January 2006. Before the onset of snow on 21^{st} January 2006 (shown in Figure 3.43 (a)) just before 3:00 am, the fiber received power and BER characteristics show typical performance i.e. error free transmission and about -25 dBm received power. But at around 3:00 am the visibility begins to deteriorate and errors in the link increase as the fiber received power drops. Complete link cut-off is experienced at around 4:40 am and the temperature drops to negative values. Figure 3.40 (b) shows the link recovering at around 13:38 pm the next day (22^{nd} January 2006) after the temperature climbing to about 10^{o}C.

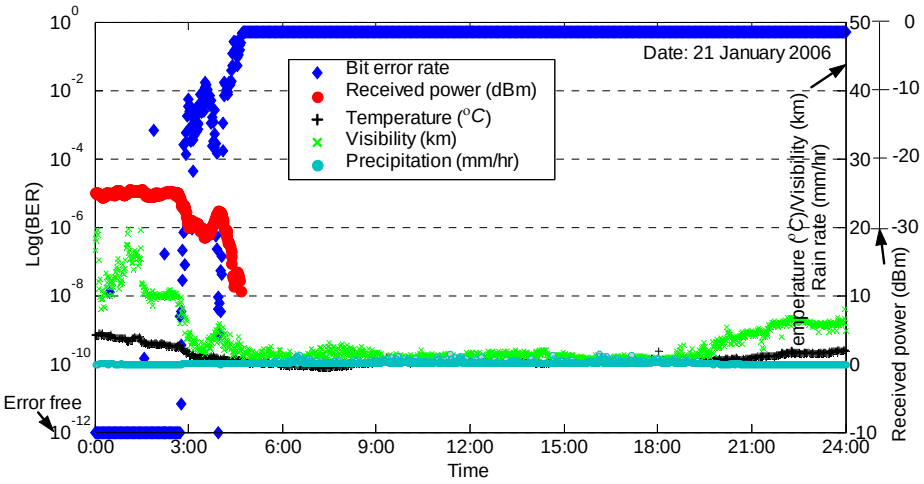

(a)

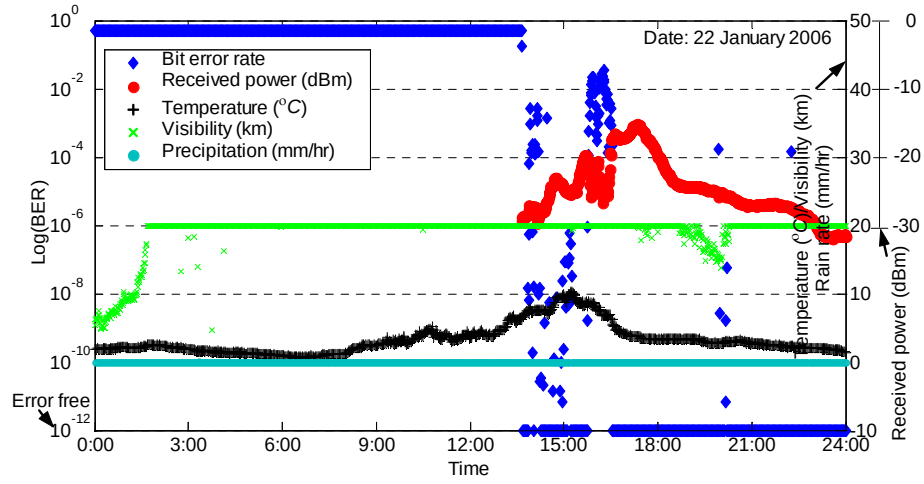

(b)

Figure 3.43: FSO system performance in terms of BER during snow event

The reason for the delay in the link recovering can be explained by Figure 3.44. Figure 3.44 shows the QAPD tracking characteristics for the antennas in Nishi Waseda and Okubo campuses. The QAPD tracking of Nishi Waseda is automatically enabled, that is why it recovers sooner than the Okubo QAPD tracking. The tracking circuit in Nishi Waseda receovered at 19:30 pm when it stopped snowing and the visibility had also improved. On the other hand, the recovering of the tracking at Nishi Waseda was delayed. This is why the FSO link recovered at around 13:38 pm when the Okubo QAPD tracking capability was restored. From this result was later discovered that the adjustment of the tracking control circuit was inadequate in extreme cold weather.

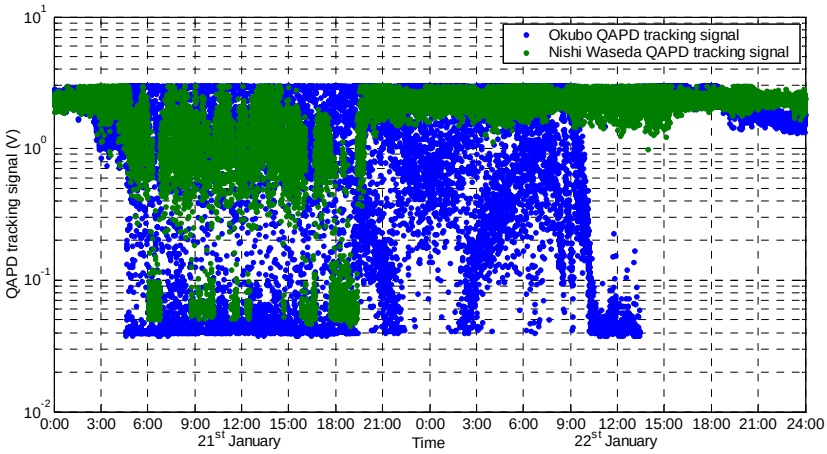

Figure 3.44: FSO system QAPD tracking during snow event

3.4.2 Eye pattern measurement

By using a digital communication analyzer the data handling capability of the FSO communication system was evaluated using the eye pattern technique. The eye pattern technique is a qualitative measure of the system performance. In the experimental FSO system the essential eye pattern key wave shape parameters including period, rise/fall time, clock to data jitter, overshoot, ringing, noise and signal to noise ratio for 2.5 Gbps and 10 Gbps transmission are within acceptable tolerance. This is depicted in Figure 3.45 (a) for the 2.5 Gbps single channel 1550 nm transmission for typical case (collected over a period of 30 minutes) and Figure 3.46 depicting eye pattern for a single channel 1550 nm data link operating at 10 Gbps transmission (collected for 1 minute). Figure 3.45 (b) depicts the case when there is strong atmospheric turbulence. Typical results by comparing the Eye pattern before and after transmission shows no degradation of the signal waveform. This confirms that under clear weather conditions in the absence of strong atmospheric turbulence, this FSO communication system can be used for stable and reliable high-speed data transmission.

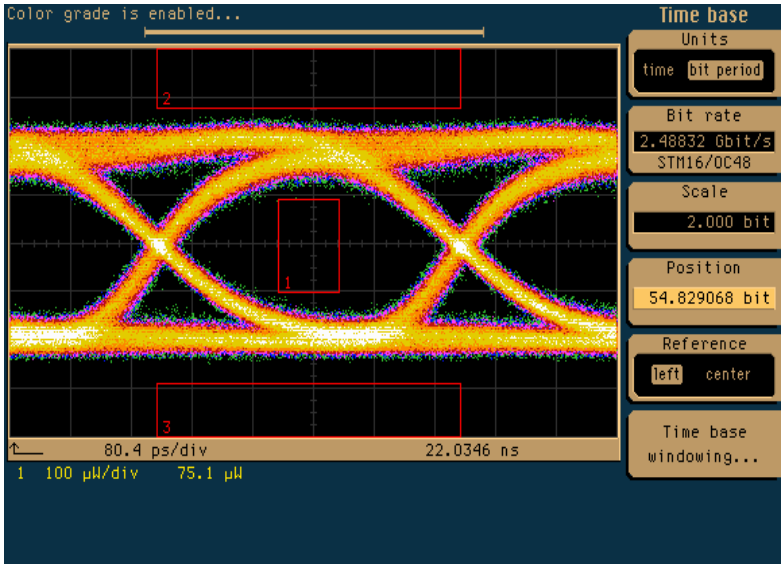

(a)

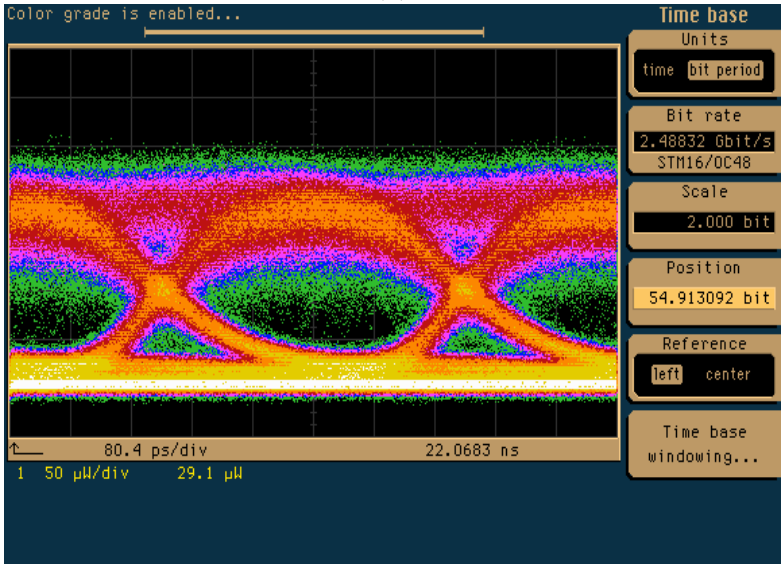

(b)

Figure 3.45: Eye pattern with a Mask showing a standard STM16/OC48 test for 2.5 Gbps transmission (a) typical case with no transmission impairment and (b) worst case scenario during strong atmospheric turbulence

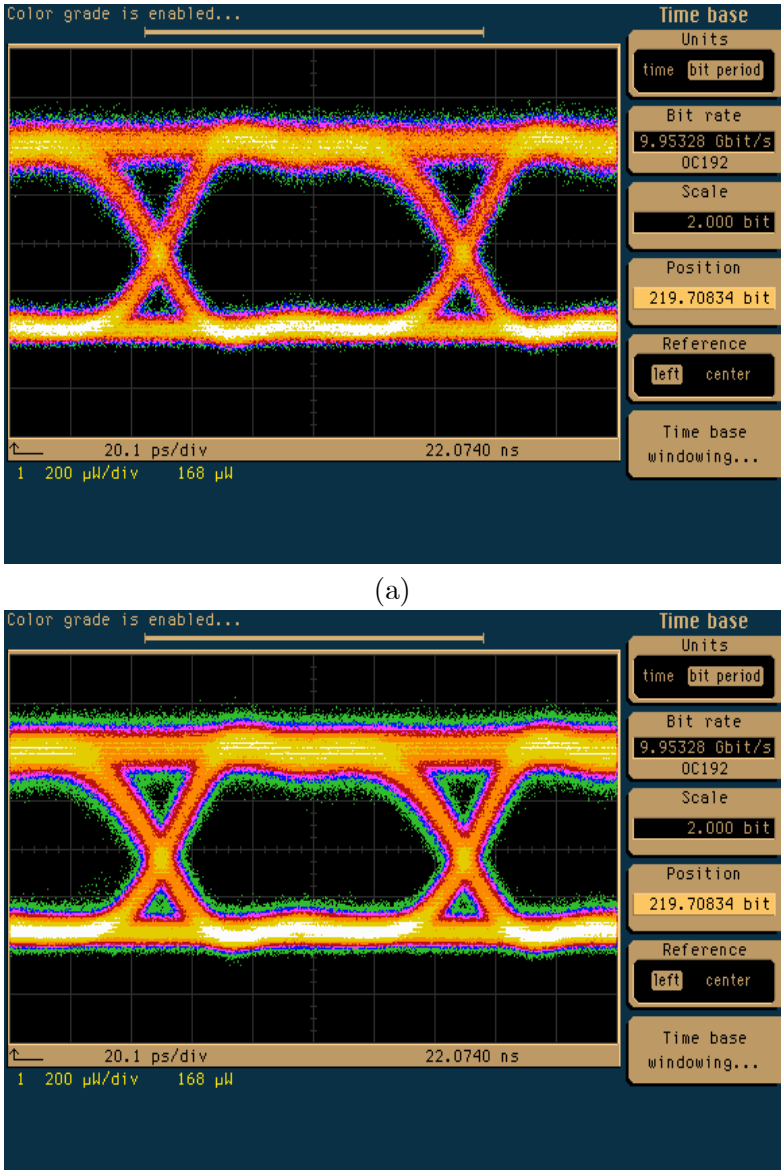

(a)

(b)

Figure 3.46: 10 Gbps transmission eye pattern figure (a) before transmission (b) after transmission

3.4.3 WDM experiment

Alternatively, by using a relatively straightforward method of increasing the system bandwidth by employing WDM technology, four 2.5 Gbps individual channels with an output power of 100 mW per wavelength can be realised. The four 2.5 Gbps channels where combined for a total wireless throughput of 10 Gbps. By employing this technique stable communication was accomplished without any fluctuation or interferences between wavelengths as shown in Figure 3.47. The total bandwidth of the FSO communication system can be increased considerably as more channels are

activated in dense wavelength division multiplexing (DWDM) schemes. The BER characteristics taken during the WDM transmission experiment is shown in Figure 3.48. The increased in the number of burst errors shown by the 1550.1 nm wavelength channel is a result of a 3 dB attenuator which was placed before the post-amp in Nishi Waseda setup.

This experiment demonstrated that DWDM is possible with this free-space optical system as means of increasing capacity.

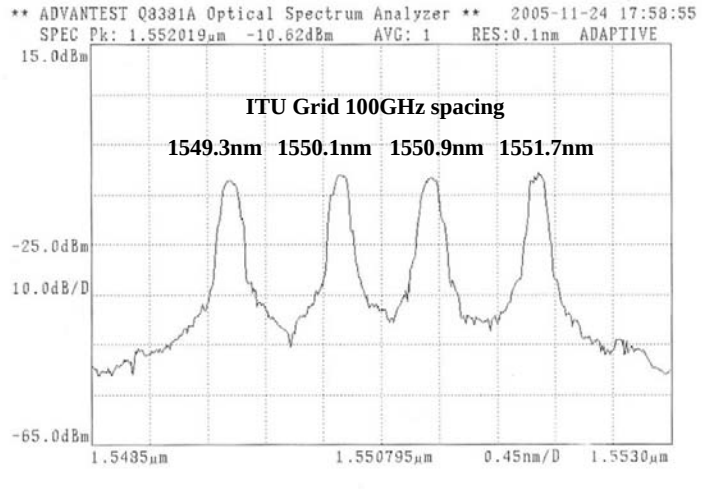

Figure 3.47: WDM received signal spectrum

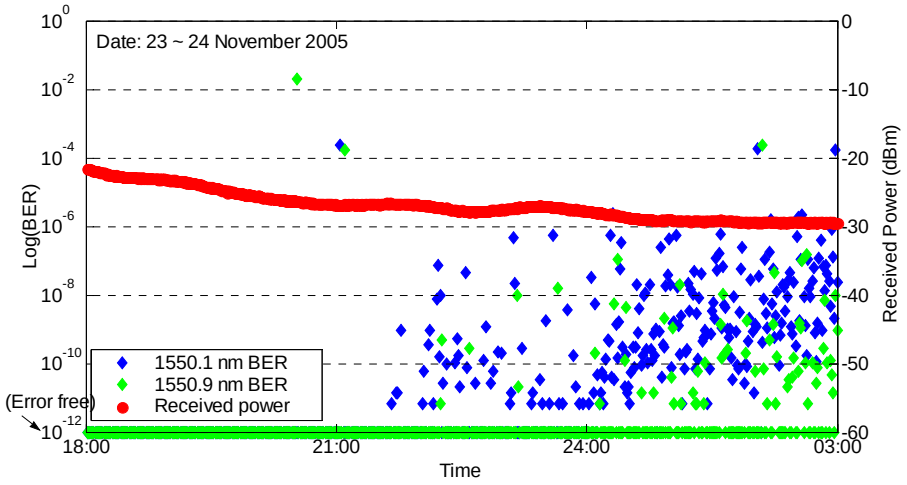

Figure 3.48: BER during WDM transmission (2.5 Gbps with output power 100 mW/wavelength

3.4.4 Application experiment

The system performance using simple network monitoring tools was also verified. This application experiment was conducted using PCs connected to Gigabit switches installed at both sites (Nishi Waseda and Okubo campuses). Connection of the Gigabit switch to the optical network is achieved by using a media converter. One experiment conducted is measurement of throughput by using the TCP protocol. The choice of TCP/IP protocol is because it is a popular reliable transport protocol for applications over the Internet. The next experiment is measurement of ping response characteristics using ping packet length of 1,500 Byte continuously. The ping packet loss rate is recorded for every minute. In order to monitor the link state while conducting the application experiments the system BER characteristics is also collected at the same time. So, an experiment system composed of WDM with G-Ethernet and a 2.5 Gbps BERT monitor is employed.

Figure 3.49 is data showing the link throughput measurement for a 2.5 Gbps WDM channel. The transferred file size is 1 MByte with a packet size 8 KByte. The recorded transmit and received throughput averages about 92 Mbps. This is because the computers used for the test had only a 100 Mbps Ethernet card (100Base-T) interface. From the Figure 3.49 it is observed that even in the presence of burst errors in the link (observed between 18:00 pm and 19:30 pm when the link quality deteriorates) the system throughput is not affected. Usually when there is a presence of random errors in the transmission channel and the quality deteriorates to around 10^{-4} congestion as a result of retransmission of errored packets causes sudden fall of the throughput. In this case, this phenomenon is not observed.

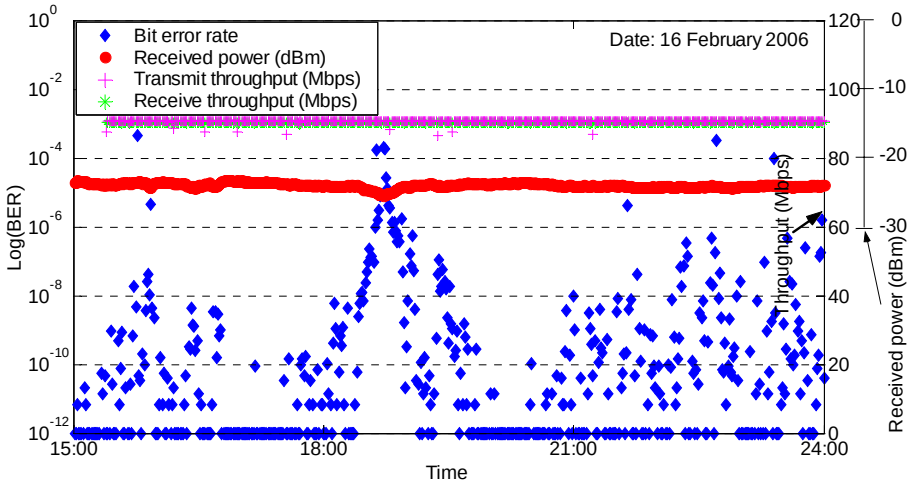

Figure 3.49: TCP throughput experiment showing BER and received power characteristics

Figure 3.50 depicts the ping packet loss rate with the BER characteristics. This data was recorded during a rain event which will account for the increased bursts errors and increased ping packet loss rate. In order to increase the probability of detecting the outbreak of error in the link, continuous transmission of ping packets of size 1,500 Byte is performed. Furthermore, in the 1 minute period detecting ping response while transmitting, at the very most 5000 ping packets can be sent therefore the smallest detection loss ratio it approximately 2×10^{-4}. Since the received optical power deteriorates because of the rainfall as shown in Figure 3.50 the increase in the BER as the ping packet loss rate are also observed.

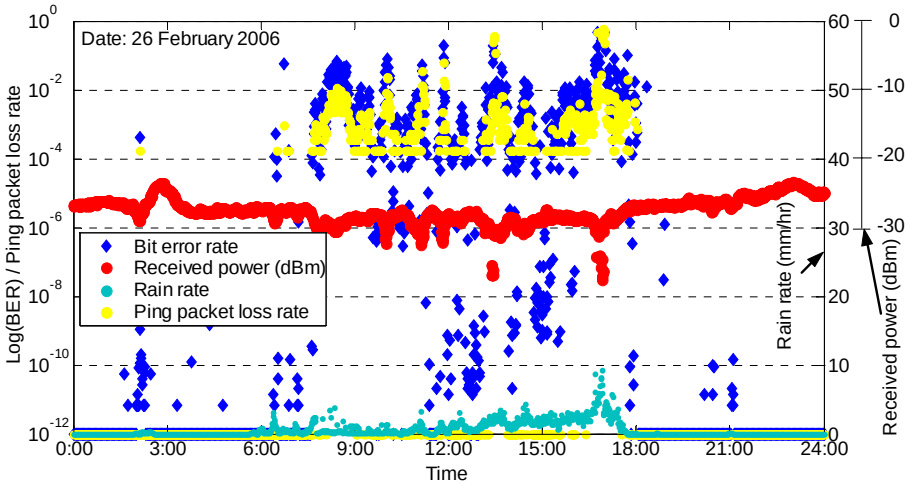

Figure 3.50: Ping packet loss experiment showing BER and received power characteristics under rain weather condition

As shown by the result in Figure 3.49, even when the BER deteriorates, the user will not necessarily experience deterioration of the link quality. When the ping packet loss rate is 1% or more, the drop of the speed of response of application will be experienced.

3.4.5 Communication quality stability

The system stability is discussed based on the BER results given above. From the application experiment when the BER becomes worse than 10^{-2} it is possible that the TCP/IP transmission rate will be affected. In addition, even when the BER deteriorates there is very little influence in the data handling capability of the communication system. On the other hand, the effective communication speed is influenced by the time which the error occurs. Taking this in consideration, in the BER measurement taken at 1 minute intervals, the period in which the BER drops below

10^{-2} and half a minute (30 seconds) in which error occurred was measured (EFS < 30) during the experimental operation period.

For the experimental period, the percentage the communication quality drops below the above described conditions is collected and compiled in month as well as time. These results is summarized in Table 3.5. For the first month (September), the performance is poor because it the start of the experiment and it is the trial period which involved a lot of system adjustment including tracking adjustment. Furthermore, the period before mid October, the EDFA was not installed. The performance for October was relative good. However, the effect of temperature characteristics on the tracking system begins to affect the performance of the system in November and becomes particularly worse in December. However, good results is achieved after correcting the temperature characteristics of the tracking system by installing a heater.

Month	The percentage in 1 min interval measurement where the BER $> 10^{-2}$ and EFS < 30
September (from 15th)	44.96 %
October	18.38 %
November	24.78 %
December	43.46 %
January	9.70 %
February	18.66 %
Total	25.63 %

Table 3.5: Monthly link operating rate

The communication quality deterioration separated into different period of the day for the entire experiment observation period are summarized in Table 3.6. In particular, during sunshine period, when the temperature difference is big, it results in strong atmospheric turbulence fluctuation. In this situation, the tracking suppression capability of the fine pointing mirror is reduced. In addition, at night time during the cold winter months, the tracking control circuit temperature characteristic problem arises. When the temperature drops and the circuit becomes cold the tracking characteristics changes.

Hour	The percentage in 1 min interval measurement where the BER $> 10^{-2}$ and EFS < 30
0:00 ~6:00	3.92 %
6:00 ~12:00	9.01 %
12:00 ~18:00	9.57 %
18:00 ~24:00	3.13 %
Total	25.63 %

Table 3.6: System operating rate at different hours

Data collected showing the system BER performance for a one week period (including the day when there was snow event) is shown in Figure 3.53. The BER performance can be correlated with the atmospheric and weather events. The increased in the number of burst errors is observed in the mid afternoon time. This is because of the changes in the ambient temperature which results in increased atmospheric turbulence. The fine pointing tracking mechanism can not suppress the rapid beam angle of arrival changes as a result of this increased atmospheric turbulence therefore the burst errors. On 21^{st} January, there was snow fall and as explained earlier this resulted in poor visibility and link complete unavailability.

The reason why the FPM can not suppress the rapid beam angle-of-arrival changes which occur during high atmospheric turbulence ($C_n^2 \geq 1{\cdot}10^{-13}$) situations can be shown by Figure 3.51[8]. The figure demonstrates the power spectrum magnitude for performance improvement in the 1552 nm signal beam when the FPM tracking is set to OFF and ON. From the figure, the improvement when the FPM is OFF and when the tracking is set to ON is not so significant. Only a small improvement in signal intensity at low frequency region was observed. Same comparison for the tracking error spectrum in the azimuth direction is shown in Figure 3.52. The reason for the insignificant improvement in the signal intensity is because of the poor correlation between signal beam and beacon beam.

[8] This is for data collected at 5:00 pm on 31 July 2006.

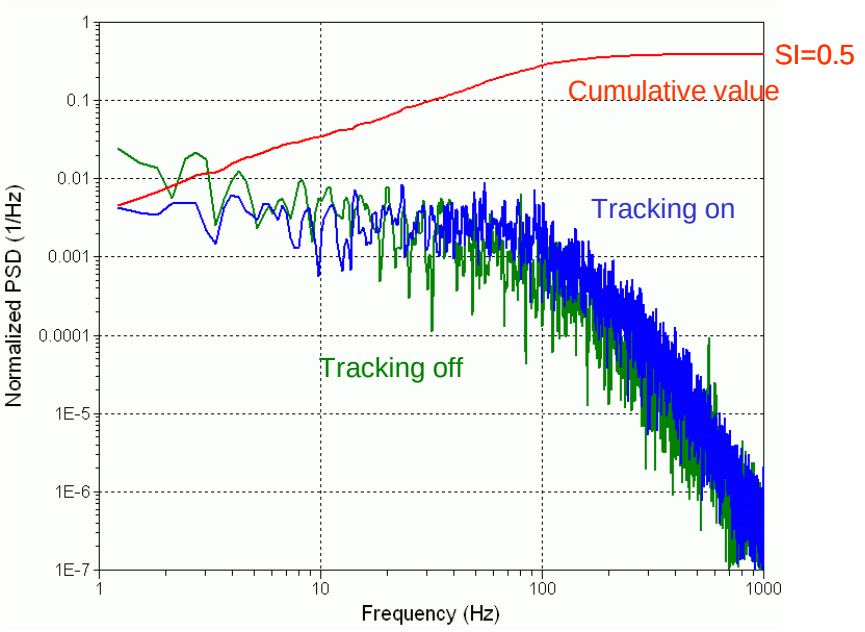

Figure 3.51: Signal intensity at 1552nm

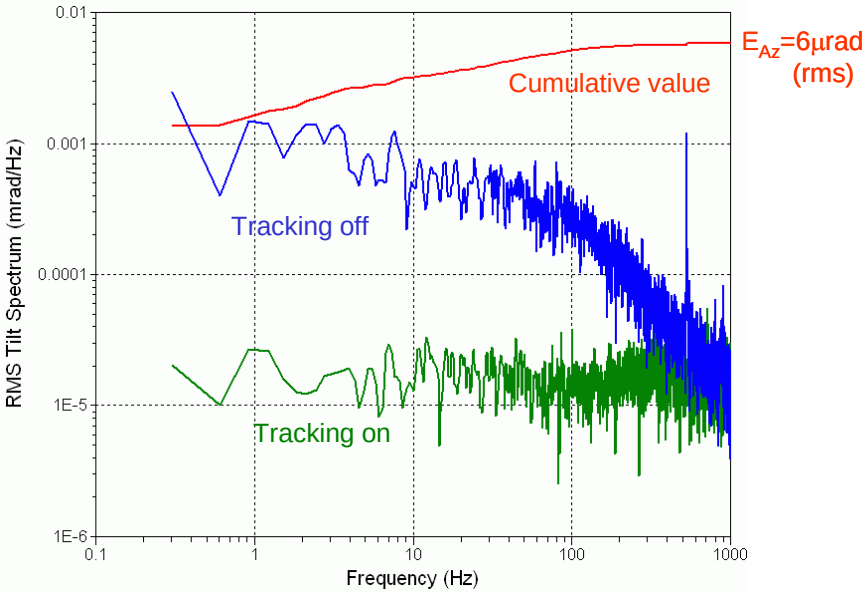

Figure 3.52: Tracking error (in Az) at 980 nm

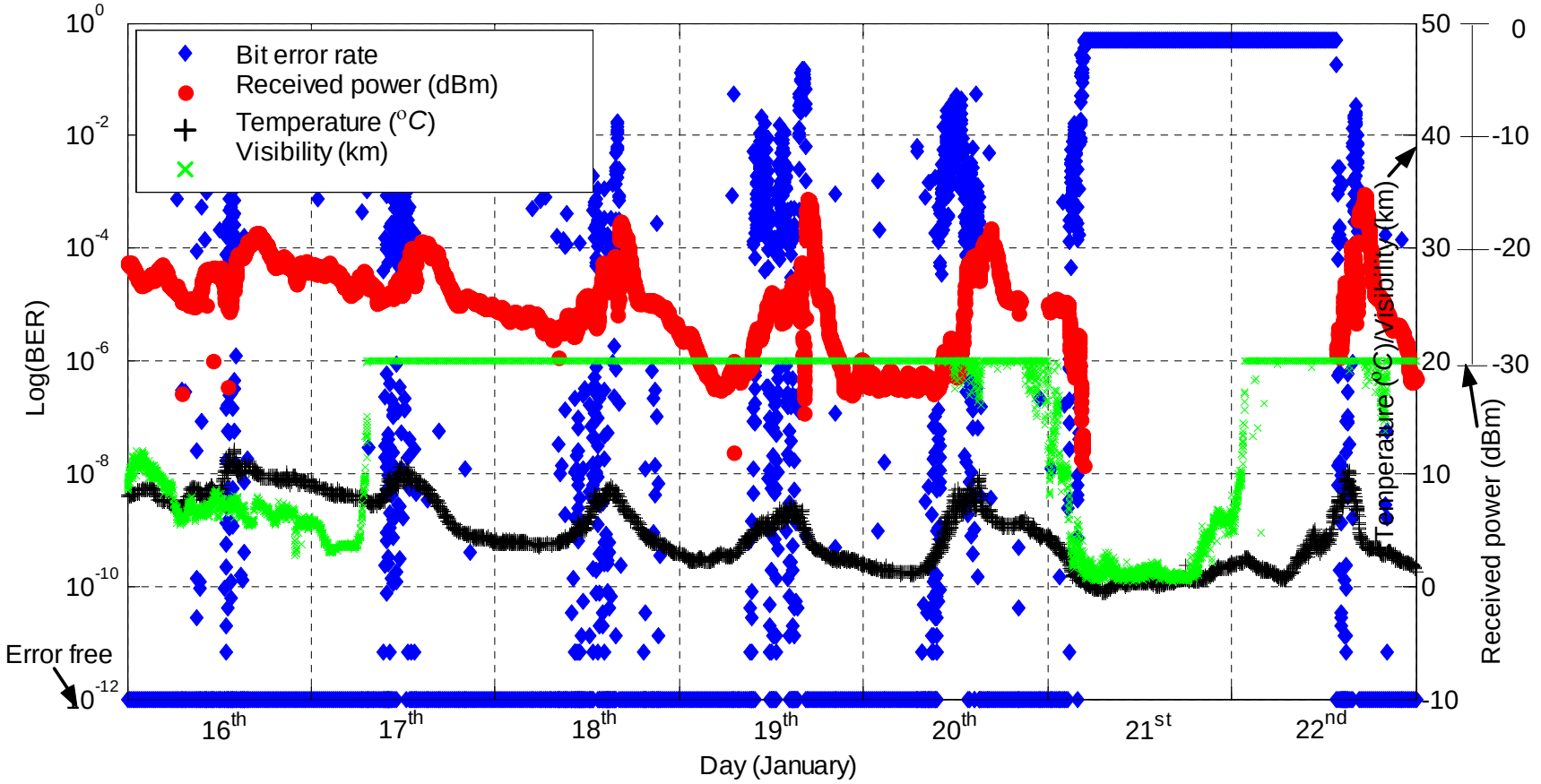

Figure 3.53: System performance data collected over a one week period

3.5 Conclusion

In this chapter the performance evaluation of the FSO system installed in the Waseda University campus has been presented. The effects of atmospheric turbulence on the 785 nm and 1550 nm wavelength systems has been measured, characterized and quantified. It has been shown that the magnitude of scintillation is a strong function of time of day and ambient temperature and significant diurnal and seasonal variations have been clearly demonstrated. Furthermore the refractive index structure constant parameter, C_n^2, neccessary to characterize the effects of atmospheric turbulence has been measured during the experiment period. The midday maximum value of C_n^2 has been found to change by a factor of 2.3 from arbitrary chosen summer and winter months. The accuracy of the C_n^2 values if subject for further analysis and they can correctly at this point be assumed to be approximate values. Future work will focus in model validation for more accurate computation of C_n^2 values. Several important parameters like the calibration constant which is dependent of the receiving and transmitting apertures as well as height scaling factor need to be accurately determined.

Moreover, 785 nm wavelength beam measured intensity fluctuation as a result of scintillation effects has been compared to the intensity variation of the 1550 nm beam caused by AOA fluctuations. The two wavelengths signal spectral density showing the intensity at different frequency exhibit similar characteristics and can be said to be correlated. The antennas' miniature FPM tracking speed of 1 kHz to successfully suppress atmospheric induced turbulence effects has been approximated using this result.

The comparison in terms of propagations characteristics of the 785 nm and 1550 nnm wavelength systems has also been studied and presented. The two systems has been compared under various weather conditions. When the optical power attenuation characteristic as a function of visibility was evaluated, the received optical power was confirmed to closely correspond to the theoretical value. Therefore, considering the same propagation path and data collected at the same time, based on optical power measurement for 785 nm and 1550 nm wavelength systems, both wavelength comparison evaluation result (disregarding the full optical connection free-space optical system tracking problem) the 1550 nm attenuation characteristics using theoretical derived equations was confirmed. The comparison can not be extensively explored due to insufficient data at the moment as well as the difference in the physical nature of the two systems i.e. the 785 nm systems uses photo detector while the 1550 nm the signal is directly fiber coupled.

Extensive BER and received power performance characteristics for the full-optical seamless connection 1550 nm wavelength system was also conducted. The system was observed to offer stable and reliable communication at both 2.5 Gbps and 10 Gbps single channel 1550 nm transmission under quiet weather condition considered to be of low atmospheric turbulence. The antennas' miniature FPM tracking speed of 1 kHz (currently 2 kHz) is sufficient to suppress the effects of atmospheric turbulence

Under strong atmospheric turbulence (C_n^2 values greater than 10^{-13} $m^{-2/3}$), which was generally recorded during midday in the summer months, increased BER was observed. This is because the tracking dynamic range of the antenna FPM tracking dynamic range (QAPD FOV) is not sufficient and the non liniearity in the tracking system.

Rain and snow significantly influences the performance of the 1550 nm wavelenth system. During rain and snow, the visibility is severly affected which results in the deterioration of the received signal power. The deterioration of the link quality during snow event is also attributed to the tracking circuit temperature characteristics. Extreme cold temperatures affect the tracking circuit performance.

By using the eye pattern technique, the system performance for single channel 2.5 Gbps and 10 Gbps transmission has been evaluated and demonstrated stable communication in the absence of strong atmospheric turbulence. Stable performance was also observed during the WDM experiment where the system bandwidth was increased using WDM technology.

The application experiments using throughput measurement and ping packet loss rate has shown that the system can be used for stable and reliable communications in absence of severe atmospheric conditions including snow, heavy rain and strong atmospheric turbulence. The burst errors which have been occurring during midday because of the higher scintillation amount have been shown to have little effect on the application performance.

Finally, the communication quality stability was evaluated for the period from mid September 2005 to end of March 2006. A communication quality of over 90 % was recorded in January 2006 after careful adjusting the antenna FPM tracking system. The communication quality of 90 % achieved for the month of January 2006 can also be attributed to the absence of strong atmospheric turbulence. The occurence of C_n^2 values greater than 10^{-13} $m^{-2/3}$ was less than 3 %.

Well engineered FSO system which properly account for statistical occurence of fog can achieve an availability of 99.9 %, or even full carrier class availability of 99.999 % with a (lower capacity) RF link or DSL backup [107]. The FSO system performance availability attained for the month

of January also accounts for time the system was down due to adjustment work. It is practically possible for the system after carefull adjustments to achieve consistent performance of above 95 % or more in the absence of severe atmospheric conditions or weather..

Monitoring the BER and other propagation characteristics over a long period of time using one or more transmission channels at 1550 nm each operating at 10 Gbps as well as the 785 nm wavelength system is considered as future work. This measured data will be correlated with atmospheric events.

CHAPTER 4

PERFORMANCE ENHANCEMENT PROPOSAL

As outlined in the previous chapters, the deterioration and deformation of a free-space optical beam wave-front as it propagates through the atmosphere can reduce the link availability and may introduce burst errors thus degrading the performance of the system. In subsection 2.2 conventional techniques used to improve the reliability of FSO communications systems have been discussed. These techniques suppress the effect of atmospheric turbulence and therefore lead to the improvement in the performance of the FSO systems. In this chapter the suitability of utilizing soft-computing (SC) based tools for improving performance of free-space optical (FSO) communications systems is explored [108], [109]. The SC based tools are used for the prediction of key parameters of a FSO communications system. Measured data collected from the experimental FSO communication system is used as training and testing data for a proposed multi-layer neural network predictor (MNNP) used to predict future parameter values. The predicted parameters are essential for reducing transmission errors by improving the antenna's accuracy of tracking data beams. This is particularly essential for periods considered to be of strong atmospheric turbulence (C_n^2 of $10^{-13}\mathrm{m}^{-2/3}$). From computer simulation parameter values predicted using the proposed tool have shown acceptable conformity with original measurements.

4.1 Soft Computing

Soft Computing differs from conventional (hard) computing in that, unlike hard computing, it is tolerant of imprecision, uncertainty, partial truth, and approximation. To that end, Soft Computing exploits the tolerance for imprecision, uncertainty, partial truth, and approximation to achieve tractability, robustness and low solution cost. The principal constituents of Soft Computing (SC) are Fuzzy Logic (FL), Neural Computing (NC), Evolutionary Computation (EC) Machine Learning (ML) and Probabilistic Reasoning (PR), with the latter subsuming belief networks, chaos theory and parts of learning theory [110], [111]. The principal constituent methodologies in SC are complementary rather than competitive. Furthermore, soft computing may be viewed as a foundation component for the emerging field of conceptual intelligence.

Soft computing methods are gradually penetrating industrial application and they are mainly utilized to improve the performance of conventional hard computing (HC) algorithms or even replacing them. In [112] research using neural networks for modeling, prediction, and control, exploits the complementarity of the neural and conventional paradigms to address realistic problem situations. A general framework for identifying the possible ways of combining neural networks is developed with physical models, model-based estimators, and conventional controllers. Hybrid systems are expected to have such valuable characteristics that would not be either possible or practical to obtain by just using one system.

4.2 Predictor implementation

In the antenna under investigation, rough or coarse beam tracking is achieved by moving the antenna using 2-axis gimbals controlled by position information that is derived from charge-coupled devices (CCD) arrays. Finer tracking is enabled when actuators move the miniature fine pointing mirror (FPM) in azimuth and elevation angles depending on the incident beam's angle-of-arrival. This minimizes the power coupling losses as the FPM directs a beam in to a 8 - 10 μm diameter core of a SMF with high ccuracy. The actuator drive voltages are computed from the voltage outputs P_1 to P_4 produced the four detector elements of a quadrant detector (QD). The QD is able to track the incident beam's location depending on the movement of the beam spot focused on the detector. A more illustrative description of the antenna's schematic representing the beam tracking and control setup is depicted in Figure 4.1.

The FPM actuator drive voltages V_x and V_y trigger an actuator to move the FPM by changing

its azimuth and elevation angles respectively. These voltages are directly evaluated from the QD output voltages by

$$V_x = \frac{(P_2 + P_4) - (P_1 + P_3)}{\sum_{i=1}^{4} P_i} \ , \tag{28}$$

$$Vy = \frac{(P_1 + P_2) - (P_3 + P_4)}{\sum_{i=1}^{4} P_i} \ , \tag{29}$$

Considering the narrow acceptance angle of SMFs which has a core diameter of 8.2 μm and a numerical aperture of 0.13 the fiber connection incident angle is $\pm$7.47 degrees, the V_x and V_y error tolerance is low since the sensitivity of the FPM angular motion in azimuth and elevation angles is only about – 150 mV/deg and + 150 mV/deg respectively.

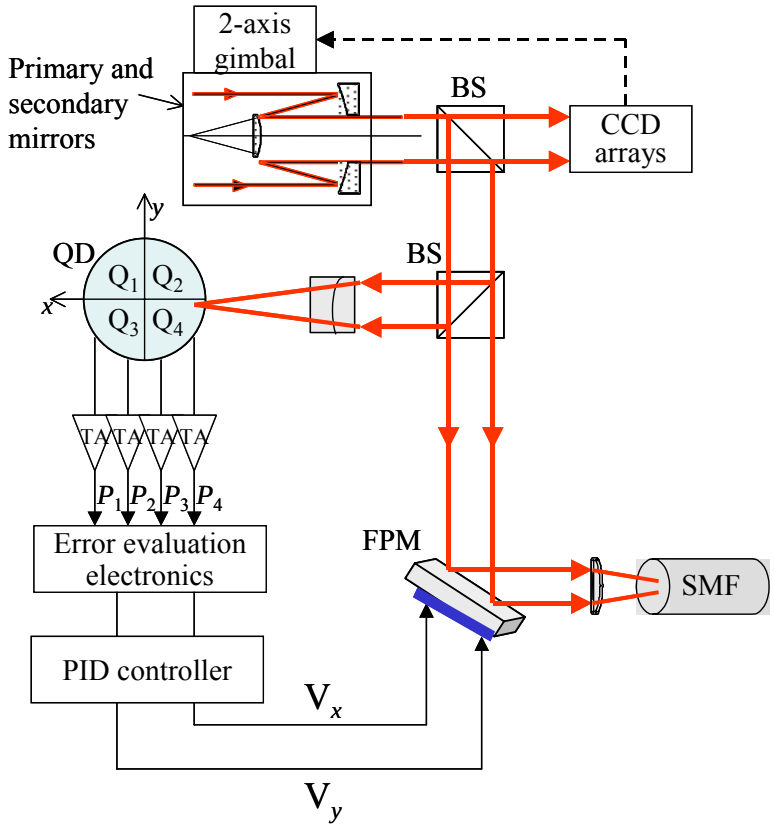

BS	Beam splitter
FPM	Fine pointing mirror
TA	Transimpedance amplifier
CCD	Charge coupled device
SMF	Single mode fiber
PID	Proportional-Integral derivative
QD	Quadrant detector

Figure 4.1: Configuration of internal antenna optical devices

The tracking controller schematic is shown in Figure 4.2 (a) and the actual circuit implementation itself is shown in the photo in Figure 4.2 (b). The beam changes as a result of angle-of-arrival (AOA) fluctuations are detected by the silicon quadrant detector. A proportional-integral-derivative (PID) controller is employed to improve the transient response of tracking control system. The PID is implemented using hard computing (HC) control algorithm for the transient response. PID characteristics features include simplified linear approximation, manual tunability and high computational efficiency.

The roles of the separate parts of the controller is as follows:

- The proportional part of the controller reduces error responses to disturbances.

- The term proportional to the integral of the error eliminates steady state error and
- The term proportional to the derivative of the error dampens the dynamic response and thereby improves stability of the system.

The PID controller is widely used because the proportional part estimates the system at present, the integral part takes the past into account and the derivative part estimates what will happen in the future. This results in control that is much more stable than control that uses only one or two of these features [113]. However, in some cases the control performance may not be suffient by using just fixed linear approximation unaccompanied. In hybrid systems of SC and HC, the soft computing constituent is tuning the PI(D) control parameters either incrementally or continuously. To ensure the stability of the auto-tuning PI(D) systems, the range and tuning intervals of control parameters must be constrained appropriately [114].

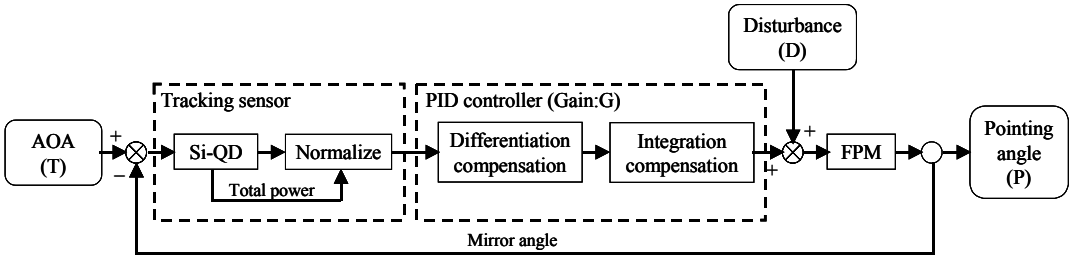

(a)

AOA	Angle of arrival
Si-QD	Silicon quadrant detector
PID controller	Proportional integral derivative controller
FPM	Fine pointing mirror

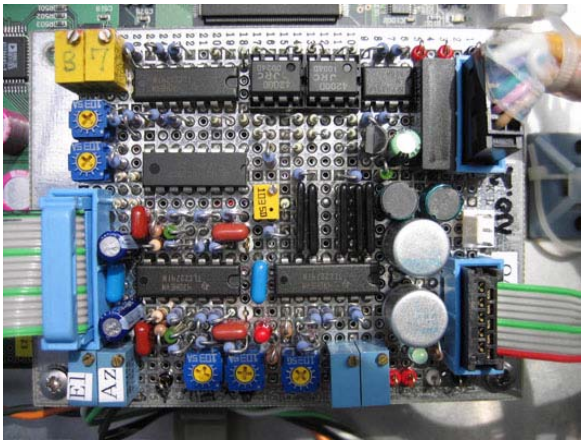

(b)

Figure 4.2: Tracking controller (a) schematic diagram and (b) photo of actual tracking controller circuit

4.2.1 Multi-layer neural network predictor structure

A soft computing based parameter predictor has the potential to complement the existing antenna's hard computing based tracking system. The resulting composite system could provide even better tracking capabilities with improved performance due to precise beam tracking even in periods of high turbulence. In [115] a neural network which can be trained to operate over a wide range of conditions is applied to improve the performance of wave-front reconstruction process in adaptive optical system for ground-based astronomical telescope has been proposed. The neural network offer a viable solution for prediction of wave front sensor slope measurements that helps compensate for system time-delay effects, especially in the presence of noise. The soft-computing tool considered for implementing the predictors in this study are neural networks [116]. By using data obtained from previous parameter measurements, a neural network can be trained to predict future parameter values. Figure 4.3 depicts the structure of a multi-layer neural network predictor (MNNP). It is composed of multiple neurons in the input and hidden layers, and a single neuron in the output layer.

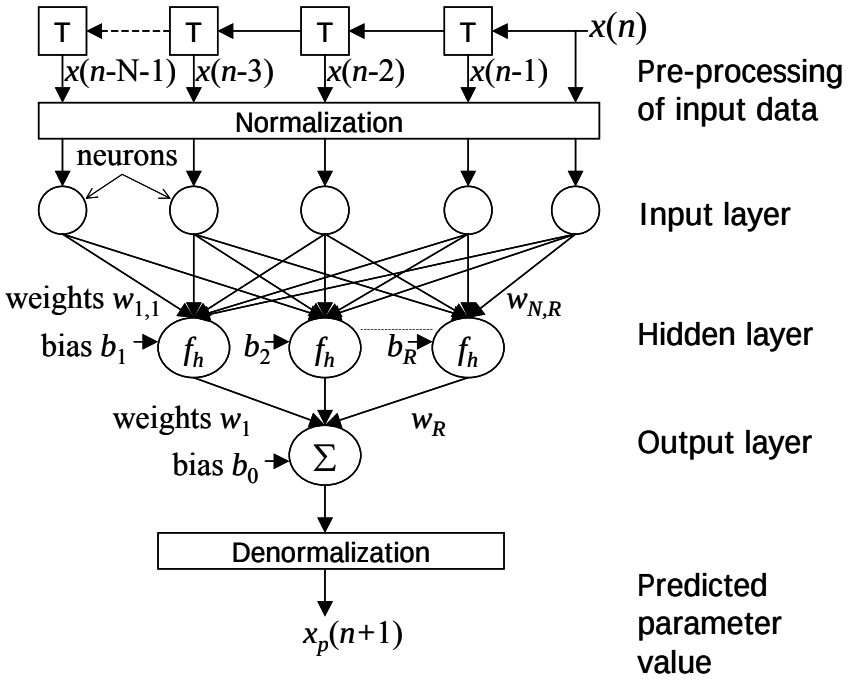

Figure 4.3: The structure of a Multi Layer Neural Network predictor

The MNNP structure is usually described by $N - R - T$ nomenclature, where N, R and T is number of neurons in the input, hidden and output layers respectively. The MNNP with N neurons

in the input layer can be trained by a supervised learning algorithm using N previous and current measured parameters $x(n-N-1)$,...,$x(n-1)$,$x(n)$ to predict a future value $x_p(n+1)$. The learning procedure is a multi-dimensional optimization problem whereby the weights and bias are varied to minimize the minimum square error (MSE) expressed by

$$MSE = \frac{1}{M}\sum_{n=1}^{M}(x(n) - x_p(n))^2 \ , \tag{30}$$

where M is the number of samples in one epoch (optimization step). The Levenberg-Marquardt algorithm is employed as the learning algorithm due to its rapid convergence and accuracy in comparison to other commonly used learning algorithms [117]. The output $h_j(n)$ of the jth hidden neuron for a MNNP input $x(n)$ is given by

$$h_j(n) = f_h(\sum_{i=1}^{N} w_{ji}x(n-1-i)) + b_j \ , \tag{31}$$

where b_j is the bias at the jth hidden neuron, w_{ji} is the connection weight between the ith input and jth hidden neuron and f_h is the activation function employed by the hidden layer neurons. In this investigation, f_h is a bipolar hyperbolic tan-sigmoid function given by

$$f_h(x) = \frac{2}{1+e^{-x}} - 1 \ . \tag{32}$$

This nonlinear function ensures the predictability of the nonlinearity in the input time series. The motivation for choosing the bipolar (-1 to +1 range) hyperbolic tan-sigmoid function as the activation function is that it offers a good balance between speed of training and accuracy. By contrast, the conventional unipolar (0 to 1 range) tan-sigmoid function that provides slightly more accuracy but has longer training times. This slower training speed may not be suited for periods with more chaotic turbulence. Past studies indicate that the reason for the difference in speed is that for a tan-sigmoid function a 0 input value is mapped to a 0 output value which leads to no weight change. On the other hand a 0 input value is mapped to -1 for the bipolar hyperbolic function, resulting in weight change.

The output layer of a MNNP for single parameter prediction has only one neuron ($T = 1$). The neuron employs a linear summation as the activation function giving an output expressed by

$$y(n) = \sum_{j=1}^{R} w_j h_j(n) + b_0 \ , \tag{33}$$

where b_0 is the bias at output neuron and w_j is the connection weight between the jth hidden neuron and the output neuron. This output represents the next predicted value in the time series, that is, $x_p(n+1) = y(n)$.

The MNNP basic algorithm loop structure can be represented by the following program fragment

```
initialize weights
repeat
    for each training pattern
        train on the pattern
    end for loop
until the error is acceptably low
```

4.2.2 MNNP integration with existing controller

Several methodologies exist for integrating soft and hard computing systems to combined system with superior performance compared to systems performing individually [[114], Chapt. 1]. The soft computing system considered here is the MNNP while the hard computing system is the existing tracking and control unit (TCU) in the test antenna. The possible integration configurations are (but not limited to):

4.2.2.1 Parallel redundancy configurations:

The MNNP is called into action when TCU loses track of the beam momentarily or fails completely. The changeover could be triggered by detected beam power falling below a certain threshold. In this parallel connected topology, the SC-based MNNP is complementing the behaviour and capabilities of the primary HC-based TCU (see Figure 4.4).

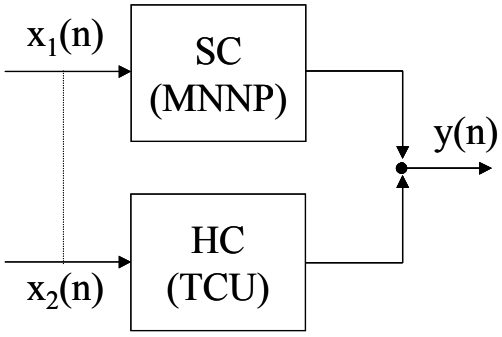

Figure 4.4: Soft computing and hard computing in parallel

This kind of parallel SC and HC based system are often considered to be easier to design and more efficient to implement than pure HC systems with comparable performance. In this important category the fusion grade is moderate. The characteristic function of SC/HC is defined as [114]

$$y(n) = f_{SC}(\theta_{SC}; x_1(n)) \oplus f_{HC}(\theta_{HC}; x_2(n)) \tag{34}$$

where the merging operator, $\oplus$, denotes either addition or combining data/signal vectors, that is, $a \oplus b$ is either $a + b$ or [ab], where a and b are arbitrary row/column vectors.

4.2.2.2 Feedback parallel configuration

The MNNP output is fed back into the TCU or vice versa as shown in Figure 4.5. The aim is to provide improved transient performance of the closed loop controller implemented in the TCU. In this case the output of the TCU feedback or MNNP feedback is added to the input of the primary MNNP and TCU\ blocks respectively.

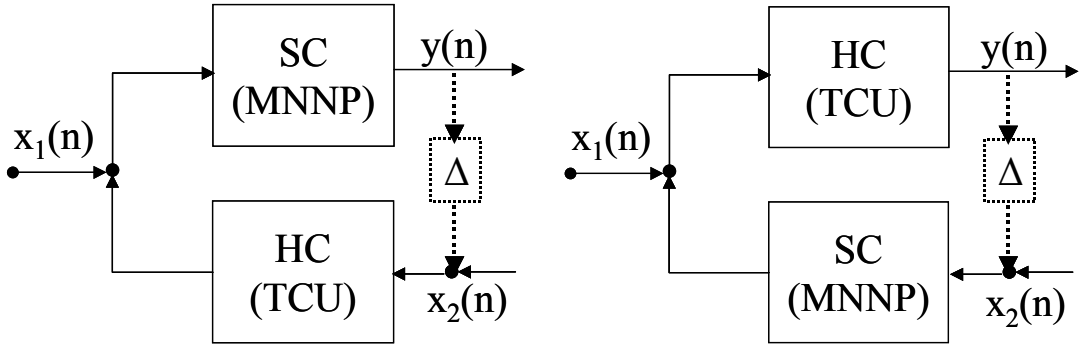

Figure 4.5: Feedback parallel configuration (a) SC with HC feedback and (b) HC with SC feedback

All SC and HC fusion structures require a delay element Δ on the feedback loop to make the system realizable. The input-output mappings of SC\HC and HC\SC can be expressed in the following compact form [114]

$$y(n) = f_{SC}(\theta_{SC}; [x_1(n) \oplus f_{HC}(\theta_{HC}; x_2(n))]) \tag{35}$$

$$y(n) = f_{HC}(\theta_{HC}; [x_1(n) \oplus f_{SC}(\theta_{SC}; x_2(n))]) \tag{36}$$

4.2.2.3 Serial configuration

The MNNP and TUC are arranged in cascade, with preceding system acting as a preprocessor for the next system. This kind of configuration acts as a dual stage optimization procedure where the initial optimization phase can be carried out by evelotionry computation (global search), and the intermediate result is then refined by some gradient basedalgorith (local search) to yield the final optimum.

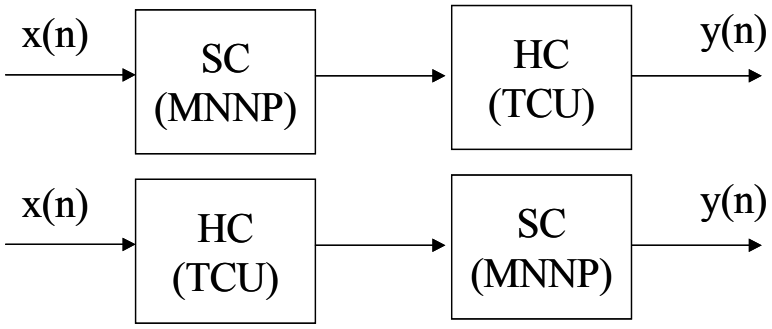

Figure 4.6: Serial configuration of SC and HC

Even though this dual-stage optimization procedure may offer clear advantages in specific applications, it is not as a general purpose a technique for evolutionary computing alone. Moreover, rather than using the gradient-based algorithm in the second optimisation stage, also other local-information-based algorithms (e.g., the simplex algorithm) are applicable. The equations which describe the cascade structure SC-HC and HC-SC, respectively are given below [114]:

$$y(n) = f_{HC}(\theta_{HC}; f_{SC}(\theta_{SC}; x(n))) \tag{37}$$

$$y(n) = f_{SC}(\theta_{SC}; f_{HC}(\theta_{HC}; x(n))) \tag{38}$$

4.2.2.4 Assisted configuration

The MNNP processes the internal parameters of an active TCU prior to the TCU completing its main task. This configuration is like a master-slave type structure which are moderately or sparsely used in real-world applications. In HC/SC some internal data is first extracted from the SC algorithm (master), processed by the specific HC algorithm (slave), and fed back into the SC algorithm, which completes the primary task. Therefore the HC constituent is an intergral part

of the computational procedure. The input-output mappings for this kind of SC and HC fusion is given by [114]

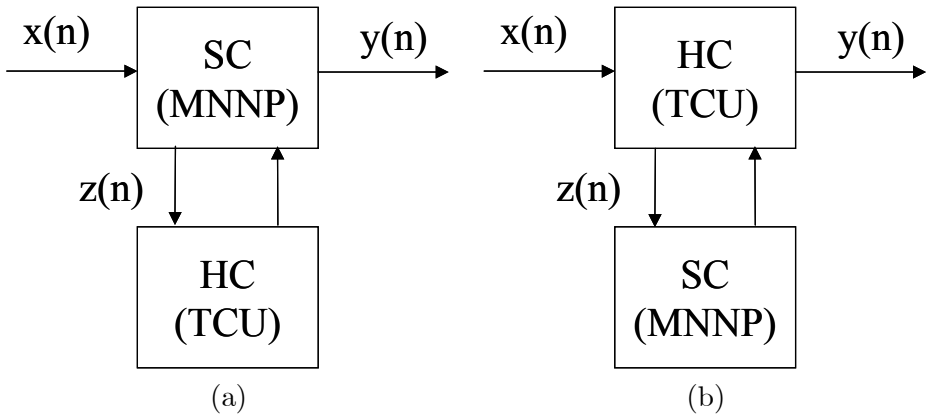

Figure 4.7: Assisted configuration (a) HC assisted SC and (b) SC assisted HC

$$y(n) = f_{SC}\left(\underset{\sim}{\theta}_{SC}; \overbrace{x(n), f_{HC}(\theta_{HC}; z(n))}^{Inputs}\right) \tag{39}$$

$$y(n) = f_{HC}\left(\underset{\sim}{\theta}_{HC}; \overbrace{x(n), f_{SC}(\theta_{SC}; z(n))}^{Inputs}\right) \tag{40}$$

4.3 Simulation test results

Measurement of both the training and testing data were performed in the afternoon, a period considered to be of strong turbulence causing significant errors in the link due to frequent ignal fading. As an illustration of this case the system performance characteristics in terms of bit error rate (BER), measured received fiber-coupled power, and day temperature variations measured over a period of 24 hours is shown in Figure 4.8. Further details on how the experimental data was collected for the FSO system performance evaluation can be found in [75]. From the figure, it is clear that significant BER performance degradation occurs in the period from around 12:00 pm to about 14:00 pm. This is the period considered to be of strong atmospheric turbulence influence because of the big temperature difference between the ground and the air. The big temperature difference results into increase in the degree of scintillation fluctuation therefore the link deterioration resulting to burst errors. These burst errors have been attributed to either the non-linearity in the TCU and/or the limited tracking dynamic range in situations of strong turbulence [75]. The burst errors

can also be because of the excessive delay between measurement of the aberrated wavefront and implementation of propoer correctuve action.

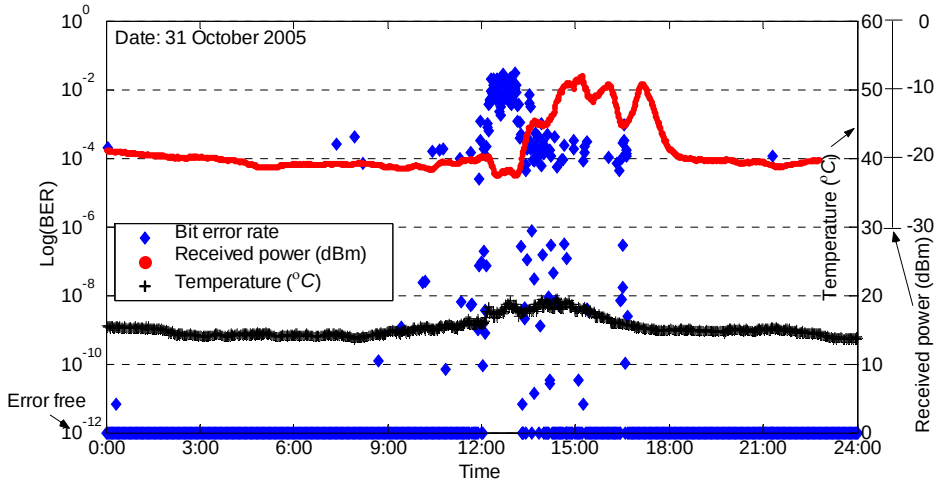

Figure 4.8: Bit error rate characteristics and fiber received power under strong atmospheric condition

The time series data of the AOA fluctuation measurement is shown in Figure 4.8. This data is recorded after every 5 minutes in the current experimental setup. The 5 minute periods are split into blocks of 3 seconds wherein the sampling rate is 10 kHz. A 3 second ($3\text{x}10^{-4}$ samples) AOA fluctuation data block (shown in Figure 4.9) is used in the training phase while the subsequent 3 second block is used for the test phase. Although the FPM tracking speed is set at 1 KHz, the actuator drive voltage data is only recorded once per second. This V_x and V_y data is bundled in to 305 second blocks (305 samples), whereby a single block was used for the training phase (see Figure 4.10) and subsequent block for the testing phase.

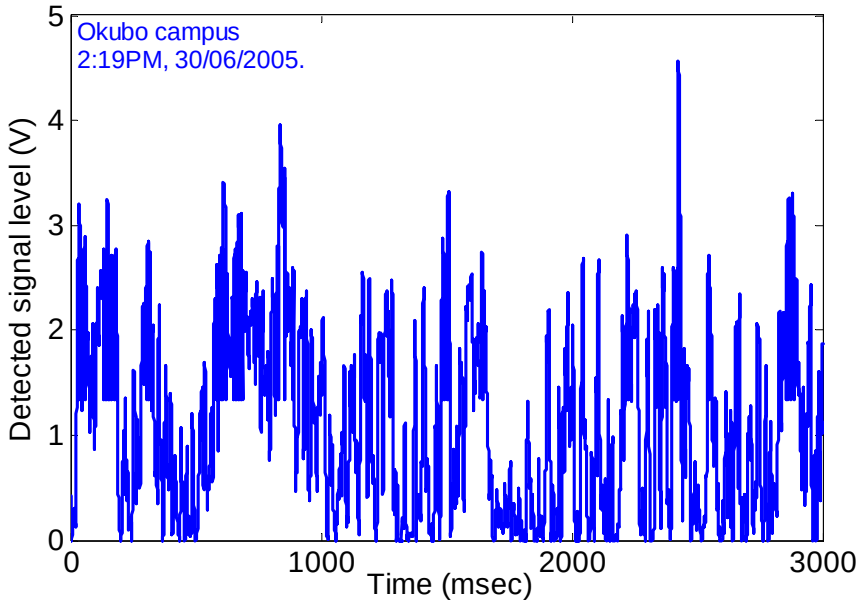

Figure 4.9: Predictor training data for AOA fluctuation

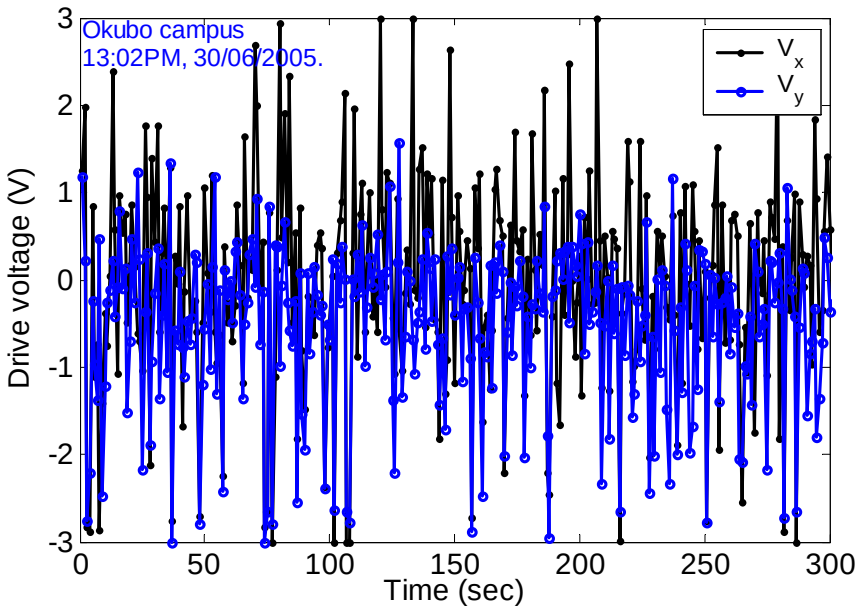

Figure 4.10: Predictor training data for FPM actuator drive voltages

After repeated trials a 5 – 20 – 1 MNNP was selected for prediction of both the AOA fluctuation and FPM actuator drive voltages. The respective prediction errors for test data are shown in Figures 4.11 and 4.12. Mean prediction errors for V_x and V_y are – 35.1 μV and – 0.4 μV respectively. This implies that typical FPM angular motion errors caused by the predictor are only – 4 μrad (azimuth)

and – 0.05 μrad (elevation) obtained from the average prediction errors of the FPM actuator voltages and using the values of the sensitivity of the FPM angular motion in azimuth and elevation quoted in section 3.2.

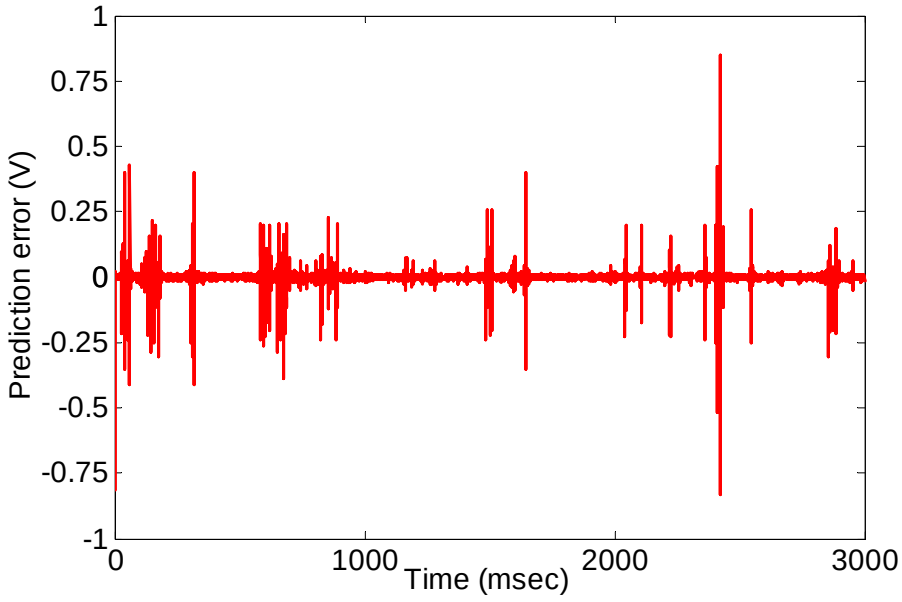

Figure 4.11: Error in the test prediction for detected voltage variation due to AOA fluctuation

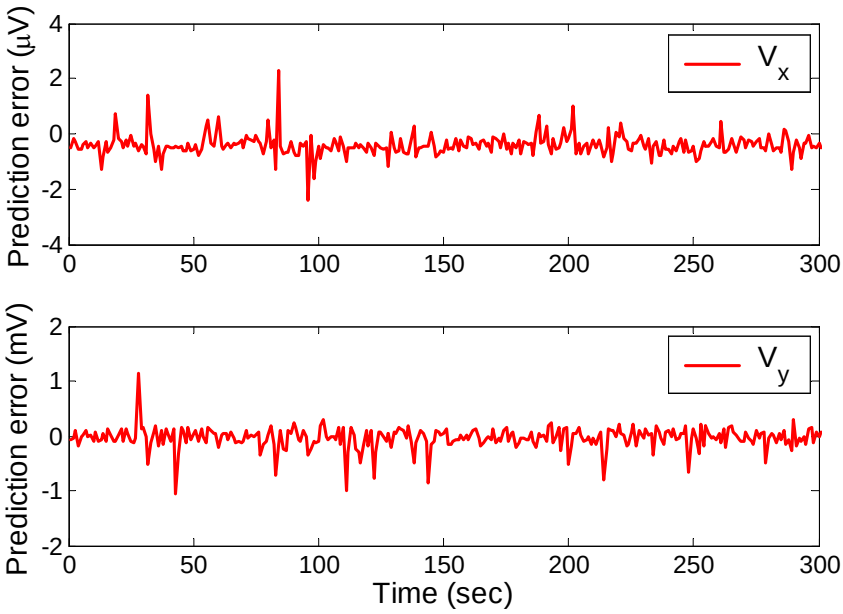

Figure 4.12: Errors in the test predictions for FPM actuator drive voltage

Plotting on the same axis it is easier to compare the measured data and the predicted data (see

Figure 4.13). The two curves exhibit almost idetentical characteristics which demonstrate that the predicted data very closely resembles the original measured data.

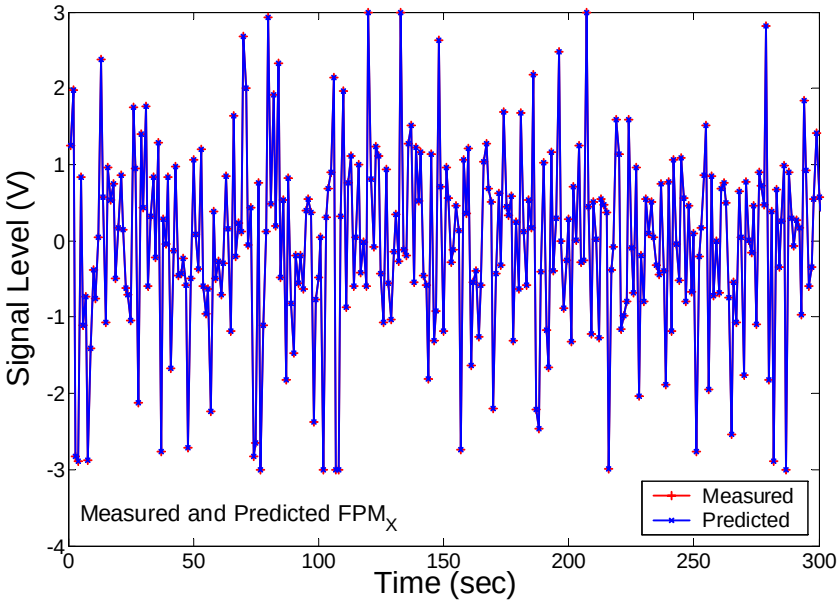

Figure 4.13: Comparison of FPM x-direction voltage for measured and predicted data

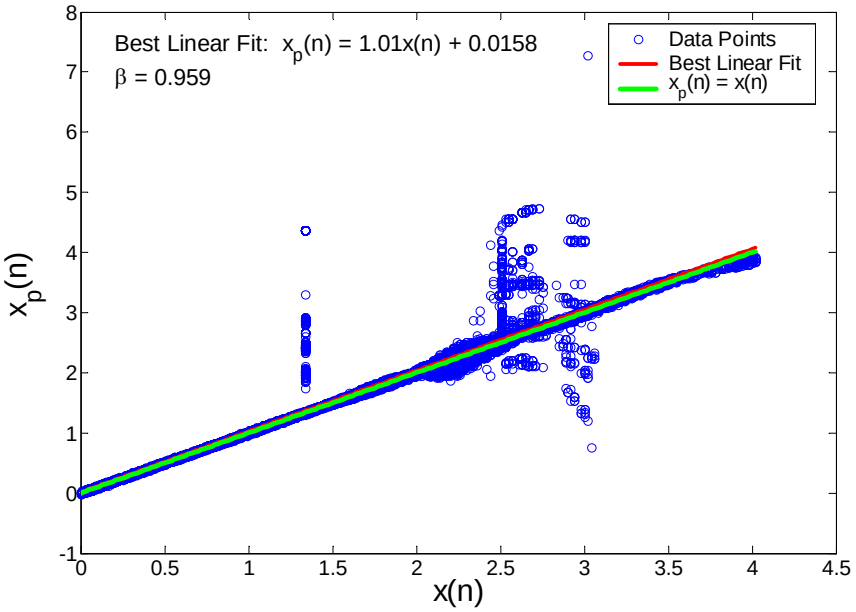

Figure 4.14: AOA intensity fluctuation prediction regression analysis

Figure 4.14 shows the AOA intensity fluctuation prediction regression analysis[1]. For this particular case the best linear fit if found to be

$$x_p(n) = 1.01x(n) + 0.0158 \tag{41}$$

where the correlation coefficient, β, is 0.959 and the y-intercept $a = x_p|_{x=0}$ is 0.0258 and the slope $r = \frac{\Delta x_p}{\Delta x}$ is 1.01. A perfect prediction of the parameter test values would return the values $\beta = 1.0$, $\alpha = 0$ and $r = 1.0$.

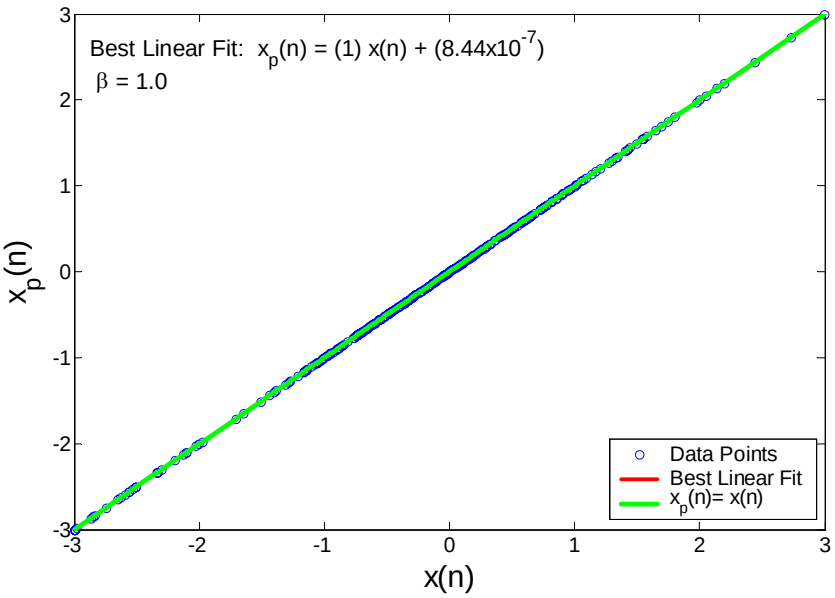

Figure 4.15: FPM x-direction test prediction regression analysis

Figure 4.15 shows the FPM y-direction test prediction regression analysis. For this particular case the best linear fit if found to be

$$x_p(n) = (1)x(n) + (-9.64 \times 10^{-6}) \tag{42}$$

where the correlation coefficient, β, is 1 and the y-intercept $a = x_p|_{x=0}$ is -9.64×10^{-6} and the slope $r = \frac{\Delta x_p}{\Delta x}$ is 1. Showing that the prediction values

very closely relate to the test parameters values.

[1]Regression analysis is a method for determining the association between a dependent variable and one or more independent variables.

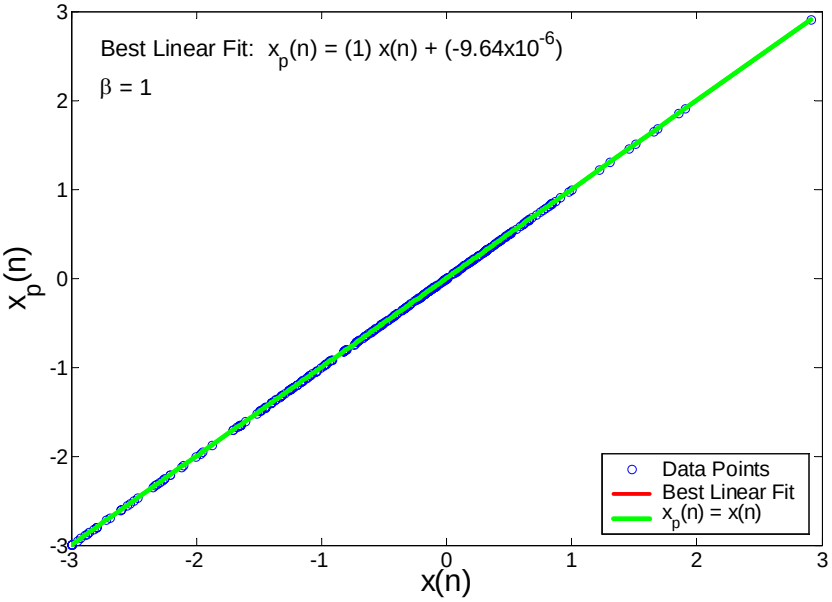

Figure 4.16: FPM y-direction test prediction regression analysis

A more clear view of the accuracy of the MNNP is provided by regression analysis between the predicted values and the test data. The analysis produces three results: the correlation-coefficient β, the y-intercept $a = x_p|_{x=0}$ and the slope $r = \frac{\Delta x_p}{\Delta x}$ of the best linear regression between the measured and predicted values. The results in Table \ref% {opticsEast_Tab_RegressionAnalysisResults} indicate the high accuracy of all prediction tests performed.

Predicted parameter	α	β	r
AOA fluctuation	0.0158	0.959	1.01
FPM actuator drive voltage V_x	8.44 x 10^{-7}	1.0	1.0
FPM actuator drive voltage V_y	-9.64 x 10^{-6}	1.0	1.0

Table 4.1: Summary of regression analysis results

4.4 Conclusions

The idea of an FSO antenna that can be trained directly with previous measurements may be realized using MNNPs. By employing the future parameter values, the errors that occur during the periods of high turbulence may be reduced. This is possible by enabling the antenna control system to utilize predicted values when there are excessive hard computing delays or uncertainties in the original tracking devices. Furthermore, the MNNP implementations are low cost and could be engineered to provide predictions with minimal time delay.

There are several kinds of fusion of SC and HC which are not covered in this thesis. The central motivation behind fusing elemental SC and HC methods is the aim of overcoming the limitations of the indivivual methods which in this case are the individual limitations of the SC-based on MNNP and HC-based TCU. The resulting hybrid systems are expected to have such valuable characteristics that will not be either possible or practical to obtain using a single methodological class only. The choice of a particular MNNP/TCU configuration will depend on several factors such as reliability, evaluation accuracy and computational delays together with the easiness to design, and efficiency in implementation.

Future work involves designing the predictor circuit and making a hardware implementation into the antenna tracking and control mechanism. Experiments on the performance improvements after intergrating the MNNP to the antenna will be conducted.

CHAPTER 5

CONCLUSION

In this section, the main results of the presented work are summarized and critically analysed. An overview of the future research topics building on this work is also presented.

5.1 Summary of the studies

The major source of errors in FSO communications systems is atmospheric turbulence manifested as beam wander and scintillation effects. It is therefore neccessary to measure, characterize and quantify the influence of atmospheric effects so as to be able to account for them in the design of FSO communication system. To improve the performance and reliability of FSO systems, techniques to suppress atmospheric turbulence are necessary to be incorporated in the system design.

This dissertion has outlined the experimental studies of techniques to enhance the performance and reliability of FSO communication systems. A technique which employs a high-speed beam tracking miniature FPM has been investigated and its capability for suppressing atmospheric induced turbulence for improved FSO link reliability demonstrated. Compared to other techniques used to mitigate atmospheric effects, the fast beam steering miniature FPM has several advantages including, achieving a compact size antenna, with less electronics overhead and design complexities. Extensive experiments to demonstrate the perfomance in terms of BER and fiber received power under various weather conditions have been conducted and presented.

Because it is difficult to directly measure the received beam angle-of-arrival (AOA) fluctuation, this thesis proposes a technique to determine the antennas miniature FPM optimum tracking speed required to suppress the atmospheric induced beam intensity variations because of AOA. The techniques compares the beam intensity fluctuations as a result of of scintillation effects to the received

intensity variations caused by AOA fluctuations. By comparing the power spectrum, similarities between the frequency characterics of the intensity fluctuations as a result of scintillation and AOA fluctuations is deduced. The optimum miniature FPM tracking speed can be approximated from the derived power spectrum of the AOA fluctuations. In this case the antenna's miniature FPM optimum tracking speed was found to be 1 kHz.

By comparing the refractive-index structure parameter, C_n^2, which is considered to be the most critical parameter along the propagation path in characterizing the effects of atmospheric turbulence, it was found that the values of the noon maximum of C_n^2 measured for arbitrary chosen summer and winter months changed by a factor of 2.3. This explains the increase in the number of burst errors in the transmission link for the 1550 nm FSO system during the summer months because the FPM could not suppress the effects of increased atmospheric turbulence (C_n^2 values greater than 10^{-13} $\mathrm{m}^{-2/3}$).

The comparison in terms of propagations characteristics of the 785 nm and 1550 nm wavelength systems has also been studied and presented. The two systems have been compared under various weather conditions. When the optical power attenuation characteristic as a function of visibility was evaluated, the received optical power was confirmed to closely correspond to the theoretical value. Therefore, considering the same propagation path and data collected at the same time, based on optical power measurement for 785 nm and 1550 nm wavelength systems, both wavelength comparison evaluation result, except for the full optical connection free-space optical system tracking problem, the 1550 nm attenuation characteristics using theoretical derived equations was confirmed. The comparison can not be extensively explored due to insufficient data at the moment as well as the difference in the physical nature of the two systems i.e. the 785 nm systems uses photo detector while the 1550 nm the signal is directly fiber coupled.

To further enhance the performance of the FSO communication systems especially in presence of strong atmospheric turbulence (turbulence strength of $C_n^2 \geq 10^{-13}$ $\mathrm{m}^{-2/3}$), where the miniature FPM tracking mechanism can temporary loose tracking resulting in burst errors it is proposed to use soft-computing based tools. By using MATLAB simulation tool a soft computing based multi-layer neural network predictor (MNNP) used to predict key parameters of the FSO system is studied. From the simulation results the predicted parameter value of the FSO system have shown acceptable conformity with the original measurements. It is envisaged that by incorporating the MMNP to the existing tracking and control unit, a more robust and reliable FSO communication system can be achieved.

5.2 Critical analysis of results

Several critical comments maybe be made to highlight the limitations of research results and proposals covered in this thesis.

The method proposed to determine the optimum miniature fine pointing mirror (FPM) tracking speed does not yield the absolute result but rather just an approximation. This is true because of the fact that the intensity fluctuations as a result of scintillation effects in the atmosphere was measured using a 785 nm wavelength FSO antenna. The intensity variations as a result of AOA fluctuations was measured using the 1550 nm wavelength experimental antenna. Even though the two antennas are installed and operating in the same propagation path the difference in the optical devices and the wavelength leads to only an approximate results rather than absolute accuracy. A more accurate result could have been obtained if both antennas had the same specification as well as operating in the same wavelength.

The accuracy of the C_n^2 values determined by using the measured 785 nm wavelength FSO system intensity fluctuation data is subject to further analysis. Model validation which will include determination of the calibration constant and height scaling factor for more accurate computation of C_n^2 values is neccessary.

The suitability of the proposed soft computing based multi-layer neural network predictor (MNNP) for FSO communication system performance and reliability enhancement has been confirmed by using a simulation tool. The proposed key parameters to be predicted include the AOA fluctuations and the miniature FPM mirror actuator drive voltage. It is believed that accurate performance can be achieved if more system parameters (such as temperature, wind, weather condition etc) are included in the predictor. Even though simulation is used extensively during the many phases of a system design process and deployment, it is still not a replacement of traditional analysis or hardware measurements. Therefore, the acceptable conformity with the original measurements data demonstrated by the proposed MNNP should be complemented by hard ware implementation and repeated simulation to allow critical parameters of the system to be identified and for the predictor to be simplified.

5.3 Future work

Investigate on the possibility of implementing adaptive atmospheric turbulence effects mitigation techniques that optimize link performance using electrical, optical, and network modalities. Explore the possibility of designing an autonomous controller that modifies terminal characteristics to compensate for atmospheric channel variations and adjust according to user requirements. Next-generation ultra high-speed FSO communications terminals must dynamically react to changing atmospheric conditions in order to optimize overall system performance.

Implement the MNNP and integrate it to the existing tracking and control unit. Experimental performance evaluation after predictor implementations as well as exploring the different MNNP intergration outlined in this thesis work.

.

REFERENCES

[1] G. Keiser, *Optical Fiber Communications*. Mc Graw Hill, first ed., 2003.

[2] P. C. Becker, N. A. Olsson, and J. R. Simpson, *Erbium-Doped Fiber Amplifiers: Fundamentals and Technology*. San Diego: Academic Press, March 1999.

[3] A. Stok and E. Sargent, "Lighting the local area: optical code-division multiple access and quality of service provisioning," *IEEE Trans. Netw*, vol. 14, pp. 42 – 46, Nov./Dec. 2000.

[4] S. S. C.L. HO, "Modified prime codes for CDMA Optical Communication Systems," *Journal of optical communications*, vol. 20, pp. 150–152, 1999.

[5] T. G. Kang and Y. W. Choi, "Significantly enhanced fiber optic code-division multiple-access system using a novel optical decoder with an AND-gate logic element Paper," *Optical Eng.*, vol. 45, pp. 065002–1 – 065002–6, June 2006.

[6] E. Mutafungwa, *Design and Performance Analysis of Pure and Hybrid WDM Optical Networks*. PhD thesis, Helsinki University of Technology, Espoo, Finland, 2004.

[7] M. Nohara, Y. Arimoto, W. Chujo, and M. Fjise, "A Link Study of a Low-Earth Orbit Satellite Communications System Using Optical Intersatellite Links," *IEICE Trans. Commun.*, vol. E76-B, pp. 536–543, May 1993.

[8] T. H. Carbonneau and D. R. Wisely, "Opportunities and challenges for optical wireless: the competitive advantage of free space telecommunications links in today's crowded marketplace," in *Wireless Technologies and Systems: Millimeter-Wave and Optical* (P. Christopher, L. Langston, and G. S. Mecherle, eds.), vol. 3232, pp. 119 – 128, SPIE, Jan. 1998.

[9] Heinz Willebrand and Baksheesh Ghuman, "Fiber optics without fiber," *IEEE Spectrum*, vol. 38, pp. 40–45, Aug. 2001.

[10] S. Bloom, E. Korevaar, J. Schuster, and H. Willebrand, "Understanding the performance of free-space optics," *Journal of Optical Networking*, vol. 2, pp. 178–200, June 2003.

[11] P. Eardley and D. Wisely, "1 Gbit/s optical free space link operating over 40 m - system and applications," in *IEE Optoelectron*, vol. 143, pp. 330–333, Dec. 1996.

[12] O. Bouchet, H. Sizun, C. Boisrobert, F. de Fornel, and P. N. Favennec, *Free-Space Optics Propagation and Communication*. ISTE, 2006.

[13] H. Willebrand and B. Ghuman, *Free Space Optics: Enabling Optical Connectivity in Today's Networks*. Sams Publishing, 2002.

[14] Free-Space Optical Alliance. `http://www.wcai.com/fsoalliance`.

[15] Free-Space Optics. `http://www.freespaceoptics.org/freespaceoptics/default.cfm`.

[16] FSONA Free Space Optics. `http://www.free-space-optics.org/index.php`.

[17] D. Begley, "Free-space laser communications: a historical perspective," in *The 15th Annual Meeting of the IEEE Lasers and Electro-Optics Society (LEOS 2002)*, vol. 2, pp. 391–392, Nov. 2002.

[18] D. Kedar and S. Arnon, "Urban optical wireless communication networks: the main challenges and possible solutions," *IEEE Optical Communications Magazine*, vol. 42, pp. S2–S7, May 2004.

[19] L. M. Wasiczko, *Techniques to mitigate the effects of Atmospheric turbulence on free space Optical communication links*. PhD thesis, Univ. of Maryland, College Park, 2004.

[20] R. Lawrence and J. Strohbehn, "A survey of clear-air propagation effects relevant to optical communications," *Proceedings of the IEEE*, vol. 58, pp. 1523 – 1545, Oct. 1970.

[21] H. Weichel, *Laser Beam Propagation in the Atmosphere*. SPIE Optical Engineering Press, first ed., 1990.

[22] I. I. Kim, J. Koontz, H. Hakakha, P. Adhikari, R. Stieger, C. Moursund, M. Barclay, A. Stanford, R. Ruigrok, J. J. Schuster, and E. J. Korevaar, "Measurement of scintillation and link

margin for the TerraLink laser communication system," in *Wireless Technologies and Systems: Millimeter-Wave and Optical* (P. Christopher, L. Langston, and G. S. Mecherle, eds.), vol. 3232, pp. 100 – 118, SPIE, Jan. 1998.

[23] L. C. Andrews and R. L. Phillips, *Laser Beam Propagation Through Random Media*. SPIE-International Society for Optical Engineering, first ed., 1998.

[24] I. I. Kim, M. Mitchel, and E. Korevaar, "Measurement of Scintillation for Free-space Laser Communication at 785nm and 1550nm," in *Optical Wireless Communications II* (E. J. Korevaar, ed.), vol. 3850, (Boston, Massachusetts), pp. 49 – 62, SPIE, Sept. 1999.

[25] Y. Arimoto, Y. Hayano, and W. Klaus, "High-speed optical feeder-link system using adaptive optics," in *Free-Space Laser Communication Technologies IX* (G. S. Mecherle, ed.), vol. 2990, (San Jose, CA, USA), pp. 142–151, SPIE, Apr. 1997.

[26] T. Weyrauch and M. A. Vorontsov, "Free-space laser communications with adaptive optics: Atmospheric compensation experiments," *Journal of Optical and Fiber Communications Reports*, vol. 1, pp. 355–379, Dec. 2004.

[27] G. S. Mecherle, "Mitigation of atmospheric effects on terrestrial free-space optical communication systems," in *Free-Space Laser Communication Technologies XVI* (G. S. Mecherle, C. Y. Young, and J. S. Stryjewski, eds.), vol. 5338, pp. 102 – 117, SPIE, Jan. 2004.

[28] T. S. Rappaport, *Wireless Communications Principles and Practices*. Prentice Hall Communiciations Engineering and Emerging Technology Series, second ed., 2002.

[29] W. Honcharenko, J. Kruys, D. Lee, and N. Shah, "Broadband wireless access," *IEEE Communications Magazine*, vol. 35, pp. 20–26, Jan. 1997.

[30] A. Siamarou, "Broadband wireless local-area networks at millimeter waves around 60 GHz," *IEEE Antennas and Propagation Magazine*, vol. 45, pp. 177–181, Feb. 2003.

[31] L. M. Correia and R. Prasad, "An Overview of Wireless Broadband Communications," *IEEE Communications Magazine*, vol. 35, pp. 28–33, Jan. 1997.

[32] E. Leitgeb, M. Gebhart, and U. Birnbacher, "Optical networks, last mile access and applications," *Journal of Optical and Fiber Communications Reports*, vol. 2, pp. 56 – 85, Mar. 2005.

[33] D. B. Medved and L. Davidovich, "Optical wireless communications to OC-768 and beyond," in *Wireless and Mobile Communications* (H. Wu and J. Vaario, eds.), vol. 4586, pp. 35–42, SPIE, Oct. 2001.

[34] A. Biswas, M. W. Wright, B. Sanii, and N. A. Page, "45-km horizontal path optical link demonstration," in *Free-Space Laser Communication Technologies XIII* (G. S. Mecherle, ed.), vol. 4272, pp. 60 – 71, SPIE, June 2001.

[35] I. I. Smolyaninov, L. Wasiczko, K. Cho, and C. C. Davis, "Long-distance 1.2 Gb/s optical wireless communication link at 1550 nm," in *Free-Space Laser Communication and Laser Imaging* (D. G. Voelz and J. C. Ricklin, eds.), vol. 4489, (San Diego, CA, USA), pp. 241–250, SPIE, Jan. 2002.

[36] Y. Aburakawa and T. Otsu, "Dense Wavelength Division Multiplexed Optical Wireless Link Towards Terabit Transmission," in *International Topical Meeting on Microwave Photonics (MWP2003)*, (Budapest, Hungary), pp. 135–138, Sept. 2003.

[37] Infrared Communication Systems Association. `http://www.icsa.org.jp`.

[38] M. Kunigonis, "FTTH Explained: Delivering Efficient Customer Bandwidth and Enhanced Services." `http://www.iec.org/online/tutorials/fiber_home/topic05.html`.

[39] G. Nykolak, G. Raybon, B. Mikkelsen, B. B. Brown, P. F. Szajowski, J. J. Auborn, and H. M. Presby, "A 160 Gb/s free space transmission link," in *Optical Wireless Communications III* (E. J. Korevaar, ed.), vol. 4214, pp. 11 – 13, SPIE, Feb. 2001.

[40] K. Tsukamoto, "Software Definable Radio Networks for the Ubiquitous Networks," in *XXVI-IIth General Assembly of International Union of Radio Science (URSI)*, vol. 1, p. 205, Oct. 2005.

[41] R. Hudson, *Infrared Systems Engineering*. John Wiley and Sons, 1969.

[42] The International Electrotechnical Commission (IEC). `http://www.iec.ch/`.

[43] American National Standards Institute (ANSI). `http://www.ansi.org/`.

[44] European Committee for Electrotechnical Standardization (CENELEC). `http://www.cenelec.org/`.

[45] Japanese Industrial Standards Committee (JISC). http://www.jisc.go.jp/.

[46] D. A. Rockwell and G. S. Mecherle, "Wavelength selection for optical wireless communications systems," in *Optical Wireless Communications IV* (E. J. Korevaar, ed.), vol. 4530, pp. 27–35, SPIE, Nov. 2001.

[47] LightPointe. http://www.lightpointe.com/home.cfm.

[48] Terabeam, Inc. http://www.terabeam.com/.

[49] Proxim Wireless. http://www.proxim.com/.

[50] Canon. http://www.usa.canon.com/.

[51] Hamamatsu Photonics. http://jp.hamamatsu.com/.

[52] MRV Communications, Inc. http://www.mrv.com/technology/fso.php.

[53] I. S. Reed and X. Chen, *Error-Control Coding for Data Networks*. Kluwer Academic Publishers, 1999.

[54] D. L. Fried, "Aperture averaging of scintillation," *Journal of Optical Society of America*, vol. 57, pp. 169–175, Feb. 1967.

[55] L. C. Andrews, R. L. Phillips, and C. Y. Hopen, *Laser Beam Scintillation with Applications*. Bellingham, Washington: SPIE-International Society for Optical Engineering, first ed., 2001.

[56] H. Yuksel, C. C. Davis, and L. Wasiczko, "Aperture averaging experiment for optimizing receiver design and analyzing turbulence on free space optical communication links," in *Conference on Lasers and Electro-Optics(CLEO 2005)*, vol. 1, pp. 743–745, May 2005.

[57] X. Zhu and J. M. Kahn, "Free-space optical communication through atmospheric turbulence channels," *IEEE Transactions on Communications*, vol. 50, pp. 1293–1300, Aug. 2002.

[58] X. Zhu, J. M. Kahn, and J. Wang, "Mitigation of turbulence-induced scintillation noise in free-space optical links using temporal-domain detection techniques," *IEEE Photonics Technology Letters*, vol. 15, pp. 623–625, Apr. 2003.

[59] S. C. Wilks, J. R. Morris, J. M. Brase, S. S. Olivier, J. R. Henderson, C. A. Thompson, M. W. Kartz, and A. J. Ruggerio, "Modeling of adaptive optics-based free-space communications

systems," in *Free-Space Laser Communication and Laser Imaging II* (J. C. Ricklin and D. G. Voelz, eds.), vol. 4821, (Seattle, WA, USA), pp. 121–128, SPIE, Dec. 2002.

[60] T. Weyrauch, M. A. Vorontsov, J. Gowens, and T. G. Bifano, "Fiber coupling with adaptive optics for free-space optical communication," in *Free-Space Laser Communication and Laser Imaging* (D. G. Voelz and J. C. Ricklin, eds.), vol. 4489, (San Diego, CA, USA), pp. 177–184, SPIE, Jan. 2002.

[61] J. E. Graves and S. Drenker, "Advancing free-space optical communications with adaptive optics." `http://www.aoptix.com/`.

[62] C. A. Thompson, S. C. Wilks, J. M. Brase, R. A. Young, G. Johnson, and A. J. Ruggiero, "Horizontal Path Laser Communications Employing MEMS Adaptive Optics Correction," in *46th Annual Meeting International Symposium on Optical Science and Technology*, (San Diego, CA, USA), July/Aug. 2001.

[63] C. A. Thompson, M. W. Kartz, L. M. Flath, S. C. Wilks, R. A. Young, G. W. Johnson, and A. J. Ruggiero, "Free space optical communications utilizing MEMS adaptive optics correction," in *Free-Space Laser Communication and Laser Imaging II* (J. C. Ricklin and D. G. Voelz, eds.), vol. 4821, (Seattle, WA, USA), pp. 129–138, SPIE, Dec. 2002.

[64] B. Sklar, *Digital Communications: Fundamentals and Applications*. Prentice Hall, second ed., 2001.

[65] K. Wakamori, T. Hayashi, K. Kitamura, K. Kanda, K. Magima, and Y. Hoshino, "Development of a Digital Optical FPU," *The Institute of Image Information and Television Engineers*, vol. 52, no. 11, pp. 1630–1636, 1998.

[66] J. Kim, K. Lee, and Y. Kim, "A performance analysis of wireless optical communication with convolutional code in turbulence atmosphere," in *International Technical Conference on Circuits Systems, Computers and Communications (ITC-CSCC'97)*, (Okinawa, Japan), pp. 15–18, July 1997.

[67] T. Ohtsuki, "Turbo-coded atmospheric optical communication systems," in *IEEE International Conference on Communications (ICC 2002)*, vol. 5, pp. 2938–2942, Apr./May 2002.

[68] X. Zhu and J. M. Kahn, "Pairwise codeword error probability for coded free-space optical communication through atmospheric turbulence channels," in *Proc. IEEE International Conference on Communications(ICC 2001)*, vol. 1, pp. 161–164, June 2001.

[69] X. Zhu and J. M. Kahn, "Performance bounds for coded free-space optical communications through atmospheric turbulence channels," *IEEE Transactions on Communications*, vol. 51, pp. 1233–1239, Aug. 2003.

[70] X. Zhu and J. M. Kahn, "Markov chain model in maximum-likelihood sequence detection for free-space optical communication through atmospheric turbulence channels," *IEEE Transactions on Communications*, vol. 51, pp. 509–516, Mar. 2003.

[71] K. Kiasaleh, "Performance of coherent dpsk free-space optical communication systems in k-distributed turbulence," *IEEE Transactions on Communications*, vol. 54, pp. 604–607, Apr. 2006.

[72] K. Kiasaleh, "Performance of APD-based, PPM free-space optical communication systems in atmospheric turbulence," *IEEE Transactions on Communications*, vol. 53, pp. 1455–1461, Sept. 2005.

[73] K. Kazaura, K. Omae, T. Suzuki, M. Matsumoto, E. Mutafungwa, K. Asatani, T. Murakami, K. Takahashi, H. Matsumoto, K. Wakamori, and Y. Arimoto, "Experimental demonstration of next-generation FSO communication system," in *Broadband Access Communication Technologies* (R. Jain, B. B. Dingel, S. Komaki, and S. Ovadia, eds.), vol. 6390, (Boston, MA), SPIE, Oct. 2006.

[74] K. Kazaura, K. Omae, T. Suzuki, M. Matsumoto, E. Mutafungwa, T. Murakami, H. Matsumoto, K. Wakamori, and Y. Arimoto, "FSO antenna with high speed tracking for improved atmospheric turbulence effects mitigation," *J. Jpn. Soc. Infrared Science and Technology*, Feb. 2006.

[75] K. Kazaura, K. Omae, T. Suzuki, M. Matsumoto, T. Sato, K. Asatani, M. Hatori, T. Murakami, K. Takahashi, H. Matsumoto, K. Wakamori, and Y. Arimoto, "Mitigation of atmospheric effects on terrestrial FSO communication systems by using high-speed beam tracking antenna," in *Free-Space Laser Communication Technologies XVIII* (G. S. Mecherle, ed.), vol. 6105, (San Jose, California), pp. 167 – 176, SPIE, Jan. 2006.

[76] Y. Koyama, E. Morikawa, K. Shiratama, R. Suzuki, and Y. Yasuda, "Optical terminal for NeLS in-orbit demonstration," in *Free-Space Laser Communication Technologies XVI* (G. S. Mecherle, C. Y. Young, and J. S. Stryjewski, eds.), vol. 5338, (San Jose, CA, USA), pp. 29–36, SPIE, June 2004.

[77] K. Kazaura, K. Omae, T. Suzuki, M. Matsumoto, E. Mutafungwa, T. Murakami, K. Takahashi, H. Matsumoto, K. Wakamori, and Y. Arimoto, "Experimental Performance Evaluation of Next Generation FSO Communication System," in *Proc. Asia-Pacific Microwave Photonics Conference (AP-MWP 2006))*, (Kobe, Japan), pp. 289–292, Apr. 2006.

[78] V. Draganov and D. G. James, "Compact telescope for free-space communications Paper," in *Current Developments in Lens Design and Optical Engineering III* (R. E. Fischer, W. J. Smith, and R. B. Johnson, eds.), vol. 4767, pp. 151 – 158, SPIE, Oct. 2002.

[79] J. C. Minano, P. Benitez, R. M. Arroyo, J. L. Alvarez, M. Hernandez, J.-C. Gonzalez, K. Hirohashi, and S. Toguchi, "Ultracompact optics for optical wireless communications," in *Optical Wireless Communications II* (E. J. Korevaar, ed.), vol. 3850, (Boston, Massachusetts), pp. 80 – 90, SPIE, Sept. 1999.

[80] D. Korsch, "Design and optimization technique for three-mirror telescopes," *Applied Optics*, vol. 19, pp. 3640–3645, Nov. 1980.

[81] J. Chen, Z. Liu, and Z. Huang, "Design of transmitting optical antenna of a terrestrial line-sight optical communication," in *2nd International Symposium on Advanced Optical Manufacturing and Testing Technologies: Advanced Optical Manufacturing Technologies* (L. Yang, S. Wen, Y. Chen, and E. B. Kley, eds.), vol. 6149, SPIE, Feb. 2006.

[82] K. Takahashi and Y. Arimoto, "Development of optical antennas utilizing free form surface optics for the high speed laser communication systems," in *Free-Space Laser Communication Technologies XVIII* (G. S. Mecherle, ed.), vol. 6105, (San Jose, California), pp. 40 – 49, SPIE, Jan. 2006.

[83] Y. Arimoto, "Multi-gigabit free-space optical communication system with bi-directional beacon tracking," *IEEJ Transactions*, submitted for publication.

[84] S. Bloom, "The physics of free-space optics." `http://www.systemsupportsolutions.com/whitepapers/Physics%20of%20Free-space%20Optics.pdf`.

[85] P. F. Szajowski, G. Nykolak, J. J. Auborn, H. M. Presby, G. E. Tourgee, E. J. Korevaar, J. J. Schuster, and I. I. Kim, "2.4-km free-space optical communication 1550-nm transmission link operating at 2.5 Gb/s: experimental results," in *Optical Wireless Communications* (E. J. Korevaar, ed.), vol. 3532, (Boston, MA, USA), pp. 29–40, SPIE, Jan. 1999.

[86] I. I. Kim, P. Adhikari, M. Chevitarese, R. Doshi, J. Koontz, and R. R. Rao, "Quantifying the effects of weather and scintillation on the network performance of the San Diego LaserNet," in *Optical Wireless Communications* (E. J. Korevaar, ed.), vol. 3532, (Boston, MA, USA), pp. 6–15, SPIE, Jan. 1999.

[87] J. Kerr, P. Titterton, A. Kraemer, and C. Cooke, "Atmospheric optical communications systems," *Proceedings of the IEEE*, vol. 58, pp. 1691 – 1709, Oct. 1970.

[88] E. Brookner, "Atmosphere Propagation and Communication Channel Model for Laser Wavelengths," *IEEE Transactions on Communications*, vol. 18, pp. 396 – 416, Aug. 1970.

[89] M. Born and E. Wolf, *Principles of Optics*. Cambridge U. Press, 7th (expanded) ed., 1999.

[90] J. Goodman, *Statistical Optics*. John Wiley and Sons, 1985.

[91] A. Ishimaru, *Wave Propagation and Scattering in Random Media*. IEEE Press-Oxford University Press, 1997.

[92] S. Karp, R. Gagliardi, S. E. Moran, and L. B. Stotts, *Optical Channels*. Plenum, 1988.

[93] P. Kruse, L. McGlauchlin, and R. McQuistan, *Elements of infrared technology: Generation, Transmission and Detection*. John Wiley and Sons, 1962.

[94] K. Morita and F. Yoshida, "Light wave attenuation characteristics in propagation through the atmosphere," *Review of Electrical Comm. Labs. Japan*, vol. 18, p. 1165, 1969.

[95] K. Wakamori, H. Matsumoto, M. Asano, T. Otobe, A. Samejima, T. Suzuki, M. Hattori, and M. Nauri, "Study of the Laser Transmission Characteristics through the Atmosphere for the Free-space Optical Communication Systems," *Tec. report of IEICE*, vol. 103, pp. 143–148, 2003.

[96] T. i Wang, G. R. Ochs, and S. F. Clifford, "A saturation-resistant optical scintillometer to measure C2/n," *J. Opt. Soc. Am.*, vol. 68, pp. 334–338, Mar. 1978.

[97] J. H. Churnside and R. J. Lataitis, "Wander of an optical beam in the turbulent atmosphere," *Applied Optics*, vol. 29, pp. 926 – 930, Mar. 1990.

[98] F. M. Davidson, S. Bucaille, G. C. Gilbreath, and E. Oh, "Measurements of intensity scintillations and probability density functions of retroreflected broadband 980-nm laser light in atmospheric turbulence," *Optical Eng.*, vol. 43, pp. 2689–2695, Nov. 2004.

[99] J. Ong, K. Timothy, J. Chong, and S. Rao, "Heavy rain effects on the propagation of free space optical links in singapore," in *Twelfth International Conference on Antennas and Propagation (ICAP 2003)*, vol. 1, pp. 365–368, 2003.

[100] K. Weiss-Wrana and L. S. Balfour, "Statistical analysis of measurements of atmospheric turbulence in different climates," in *Optics in Atmospheric Propagation and Adaptive Systems IV* (A. Kohnle, J. D. Gonglewski, and T. J. Schmugge, eds.), vol. 4538, pp. 93–101, SPIE, Aug. 2002.

[101] K. R. Weiss-Wrana, "Turbulence statistics applied to calculate expected turbulence-induced scintillation effects on electro-optical systems in different climatic regions," in *Atmospheric Optical Modeling, Measurement, and Simulation* (S. M. Doss-Hammel and A. Kohnle, eds.), vol. 5891, p. 58910D, SPIE, Aug. 2005.

[102] J. H. Churnside, "Aperture averaging of optical scintillations in the turbulent atmosphere," *Applied Optics*, vol. 30, pp. 1982–1994, Mar. 1991.

[103] D. Tsintikidis, S. Doss-Hammel, M. Jablecki, C. Miscisin, and I. Bendall, "Scintillation quantification during the VAMPIRA '04 field campaign," in *Atmospheric Optical Modeling, Measurement, and Simulation* (S. M. Doss-Hammel and A. Kohnle, eds.), vol. 5891, p. 589105, SPIE, Aug. 2005.

[104] M. Aakiba and S. I. Kazuhiko Wakamori, "Measurement of Optical Propagation Characteristics for Free-Space Optical Communications during Rainfall," *LETTER Optical Wireless Communications*, vol. E87-B, pp. 2053–2056, July 2004.

[105] Isaac I. Kim and Bruce McArthur and Eric J. Korevaar, "Comparison of laser beam propagation at 785 nm and 1550 nm in fog and haze for optical wireless communications," in *Optical Wireless Communications III* (E. J. Korevaar, ed.), vol. 4214, pp. 100 – 118, SPIE, Feb. 2001.

[106] K. Wakamori, T. Hayashi, H. Yamashita, Y. Kimura, and M. Hosoda, "155-Mbps ATM Backbone for an Interbuilding Intranet Using an Optical Wireless System," in *10th International Symposium on Personal, Indoor and Mobile Radio Communications (PIMRC99)*, vol. 1, pp. 85–90, Sept. 1999.

[107] D. A. Rockwell and G. S. Mecherle, "Optical wireless: low-cost high-speed optical access," in *Wireless and Mobile Communications* (H. Wu and J. Vaario, eds.), vol. 4586, pp. 1–10, SPIE, Oct. 2001.

[108] E. Mutafungwa, K. Kazaura, K. Omae, T. Suzuki, M. Matsumoto, T. O. Korhonen, T. Murakami, K. Takahashi, H. Matsumoto, K. Wakamori, and Y. Arimoto, "Soft Computing-based Predictions to Enhance Performance of Next Generation FSO Communication Systems," in *Proc. Asia-Pacific Microwave Photonics Conference (AP-MWP 2006))*, (Kobe, Japan), pp. 59–62, Apr. 2006.

[109] K. Kazaura, K. Omae, T. Suzuki, M. Matsumoto, E. Mutafungwa, T. O. Korhonen, T. Murakami, K. Takahashi, H. Matsumoto, and K. Wakamori, "Enhancing performance of next generation FSO communication systems using soft computing-based predictions," *Optics Express*, vol. 14, pp. 4958–4968, June 2006.

[110] I. Hayashi, M. Umano, T. Maeda, A. Bastian, and L. C. Jain, "Acquisition of Fuzzy Knowledge by NN and GA - A Survey of the Fusion and Union Methods Proposed in Japan ," in *Proc. of Second International Conference on Knowledge-Based Electronic Systems (KES'98)*, (Adelaide, Australia), pp. 69–78, Apr. 1998.

[111] S. J. Ovaska, A. Kamiya, and Y. Chen, "Fusion of Soft Computing and Hard Computing: Computational Structures and Characteristic Features," *IEEE Transactions on systems, Man, and Cybernetics*, vol. 36, pp. 439–448, May 2006.

[112] M. Agarwal, "Combining neural and conventional paradigms for modeling,prediction, and control," in *Proceedings of the 4th IEEE Conference on Control Applications*, (Albany, NY, USA), pp. 566–571, Sept. 1995.

[113] P. V. Rensburg, I. Shaw, and J. V. Wyk, "Adaptive PID control using a genetic algorithm," in *Proc. of Second International Conference on Knowledge-Based Electronic Systems (KES'98)*, vol. 2, (Adelaide, Australia), pp. 133–138, Apr. 1998.

[114] S. J. Ovaska, ed., *Computationally Intelligent Hybrid Systems: The Fusion of Soft Computing and Hard Computing*. Wiley-IEEE Press, 2005.

[115] D. A. Montera, B. M. Welsh, M. C. Roggemann, and D. W. Ruck, "Prediction of wave-front sensor slope measurements with artificial neural networks ," *Applied Optics*, vol. 36, pp. 675–681, Jan. 1997.

[116] K. Gurney, *An Introduction to Neural Networks*. London: UCL Press, 1997.

[117] The Mathworks Inc., *Neural Networks Toolbox User Guide*. Massachusetts: Mathworks, 2005.

APPENDIX A. Summary of publications

A.1 Publication 1

K. Kazaura, K. Omae, T. Suzuki, M. Matsumoto, T. Murakami, K. Takahashi, H. Matsumoto, K. Wakamori and Y. Arimoto, "FSO antenna with high speed tracking for improved atmospheric turbulence effects mitigation," *J. Jpn. Soc. Infrared Science and Technology*, Feb. 2006

Abstract: When a free-space optical beam propagates through the atmosphere it experiences deterioration and deformation of its wave-front caused from small scale, randomly localized changes in the atmospheric index of refraction. This results in beam wander and scintillation effects which can reduce the link vailability and may introduce burst errors. This paper outlines experimental work on a free-space optical (FSO) communication system which connects an optical beam directly to a single-mode fiber (SMF) without any optical-to-electrical (O-E) conversion. In order to effectively couple the 1550 nm transmitted optical beam to a SMF it is necessary to be able to track and control the beam angle-of-arrival (AOA) changes. To achieve this, we have developed an optical antenna which uses a fine pointing mirror (FPM) capable of performing high-speed beam tracking and steering thus reducing to a great extent the optical power fluctuations of the received beam coupled to the SMF. This optical power fluctuation is partly a result of beam angle-of-arrival fluctuations caused by atmospheric turbulence. From our experiments we have demonstrated the relation between the AOA fluctuations and the frequency characteristics of the scintillation effects for a free-space optical beam propagating through a turbulent atmosphere. We use this information to determine the optimum antenna tracking speed for improved performance and error free transmission.

Synopsis: In this publication the external parameters (environment specific parameters) which influence the performance of FSO communications systems are studied. The effect of atmospheric turbulence on the free-space optical beam in the FSO system deployment environment are measure and characterized. A method to determine the antenna's FPM tracking speed sufficient to suppress

(mitigate) the received beam intensity variations as result of AOA fluctuations if proposed and confirmed. This method is important because technically it is not possible to measure a free-space optic wave-front phase changes (AOA), so an alternative, easy, convenient and fast way to determine the magnitude of the influence of AOA changes on the received optical beam is necessary.

A.2 Publication 2

K. Kazaura, K. Omae, T. Suzuki, M. Matsumoto, E. Mutafungwa, T. Murakami, K. Takahashi, H Matsumoto, K. Wakamori, and Y. Arimoto, "Performance Evaluation of Next Generation Free-Space Optical Communication System", *IEICE Trans. on Electron. Special Section on Evolution of Microwave and Millimeter-Wave Photonics Technology*, vol. E90-C, no. 2, Feb. 2007.

Abstract: Free-space optical communication systems can provide high-speed, improved capacity, cost effective and easy to deploy wireless networks. Experimental investigation on the next generation free-space optical (FSO) communication system utilizing seamless connection of free-space and optical fiber links is presented. A compact antenna which utilizes a miniature fine pointing mirror (FPM) for high-speed beam control and steering is described. The effect of atmospheric turbulence on the beam angle-of-arrival (AOA) fluctuations is shown. The FPM is able to mitigate the power fluctuations at the fiber coupling port caused by this beam angle-of-arrival fluctuations. Experimental results of the FSO system capable of offering stable performance in terms of measured bit-error-rate (BER) showing error free transmission at 2.5 Gbps over extended period of time and improved fiber received power are presented. Also presented are performance results showing stable operation when increasing the FSO communication system data rate from 2.5 Gbps to 10 Gbps as well as WDM experiments.

Synopsis: In this publication the performance evaluation of a multi-gigabit per second FSO optical communication system is presented. The optical antenna design highlight and techniques to suppress atmospheric turbulence effects is outlined. The capability of the miniature fast beam tracking FPM to mitigate the rapid beam intensity variations as a result of AOA fluctuations is confirmed. Stable and reliable communication at data rates of up to 10 Gbps is presented. Even though the miniature FPM is able to suppress with a very high degree of success the atmospheric induced beam wander and scintillation effects, occasionally in situations of strong atmospheric turbulence, sometimes it looses tracking and burst errors occur. This is the reason of proposing using SC based tools (proposed in [Publication 3]), to mitigate the errors which occur in the system

during strong atmospheric turbulence.

A.3 Publication 3

K. Kazaura, K. Omae, T. Suzuki, M. Matsumoto, E. Mutafungwa, T. O. Korhonen, T. Murakami, K. Takahashi, H Matsumoto, K. Wakamori, "Enhancing performance of next generation FSO communication systems using soft computing-based predictions,", *Optics Express*, vol. 14, no. 12, pp. 4958–4968, Jun. 2006

Abstract:The deterioration and deformation of a free-space optical beam wave-front as it propagates through the atmosphere can reduce the link availability and may introduce burst errors thus degrading the performance of the system. We investigate the suitability of utilizing soft-computing (SC) based tools for improving performance of free-space optical (FSO) communications systems. The SC based tools are used for the prediction of key parameters of a FSO communications system. Measured data collected from an experimental FSO communication system is used as training and testing data for a proposed multi-layer neural network predictor (MNNP) used to predict future parameter values. The predicted parameters are essential for reducing transmission errors by improving the antenna's accuracy of tracking data beams. This is particularly essential for periods considered to be of strong atmospheric turbulence. The parameter values predicted using the proposed tool show acceptable conformity with original measurements.

Synopsis: In this publication a technique to enhance the performance of FSO communication system using Soft-Computing based tools is proposed. A multi-layer neural network predictor (MNNP) is used for training and predicting key parameters of a FSO system. Data collected from the experimental FSO communication systems deployed at the Waseda Campus is used for training and testing. The goal of using SC based MNNP is to reduce errors induced by the current tracking and control unit by the time delay between wave-front sensing and sending out a corrective signal. This is particularly vital in periods of strong atmospheric turbulence when the FPM can sometimes be overwhelmed with computations and can momentarily loose track of the beam position changes.

A.4 Author's contribution to published work

The author's contribution has been paramount for the above mentioned publications. The author of the thesis is solely responsible for the ideas, writing, overviews, analysis, propositions, simulations and conclusions presented in this work. External assistance for the authoring is acknowledged in terms of supervision, writing and document formatting to all the co-authors. Also

the co-authors are credited for contributing expert advice on FSO communications systems and experimental measurement.

.

APPENDIX B. List of academic achievements

Category (Subheadings)	
Articles in refereed journals	O K. Kazaura, K. Omae, T. Suzuki, M. Matsumoto, E. Mutafungwa, T. Murakami, K. Takahashi, H. Matsumoto, K. Wakamori, and Y. Arimoto, "Performance Evaluation of Next Generation Free-Space Optical Communication System," (forthcoming *IEICE Transactions on Electronics Special Section on Evolution of Microwave and Millimeter-Wave Photonics Technology*, vol. E90-C, no. 2, February 2007) O K. Kazaura, K. Omae, T. Suzuki, M. Matsumoto, E. Mutafungwa, T.O. Korhonen, T. Murakami, K. Takahashi, H. Matsumoto and K. Wakamori, "Enhancing Performance of Next Generation FSO Communication Systems using Soft Computing-Based Predictions," *Optics Express – International Journal of Optics*, vol. 14, no. 12, pp. 4958-4968, June, 2006. O K. Kazaura, K. Omae, T. Suzuki, M. Matsumoto, E. Mutafungwa, T. Murakami, K. Takahashi, H. Matsumoto, K. Wakamori, and Y. Arimoto, "Free Space Optical Antenna with High Speed Tracking for Improved Atmospheric Turbulence Mitigation," *Journal of the Japan Society of Infrared Science and Technology*, vol. 15, No. 1+2, pp. 1-6, Dec, 2005.
Presentations at International conferences	O K. Kazaura, K. Omae, T. Suzuki, M. Matsumoto, E. Mutafungwa, T. Murakami, K. Takahashi, H. Matsumoto, K. Wakamori, and Y. Arimoto, "Experimental Demonstration of Next Generation FSO Communication system," *SPIE Optics East 2006 Conference*, (Hynes Convention Centre, Boston, Massachusetts), 1~4 October 2006. O K. Kazaura, K. Omae, T. Suzuki, M. Matsumoto, E. Mutafungwa, T. Murakami, K. Takahashi, H. Matsumoto, K. Wakamori, and Y. Arimoto, "Experimental Performance Evaluation of Next Generation FSO Communication System," *Asia Pacific Microwave Photonics Conference (AP-MWP 2006)*, (Kobe, Japan), pp. 289-292, 24~26 April 2006. O K. Kazaura, K. Omae, T. Suzuki, M. Matsumoto, T. Murakami, K. Takahashi, H. Matsumoto, K. Wakamori, and Y. Arimoto, "Mitigation of Atmospheric Effects on Terrestrial FSO Communication Systems by Using High-speed Beam Tracking Antenna," *SPIE Photonic West LASE 2006 Conference*, (San Jose California), pp. 167-176, 24~26 January 2006.
Presentations at domestic academic meetings held by study groups	K. Kazaura, K. Omae, M. Matsumoto, A. Samejima, T. Suzuki, K. Takahashi, H. Matsumoto and K. Wakamori, "Study on the Development of Free Space Optical Antenna with Transparency of fiber, Telecom Summit," *6th Academy and Industry Symposium (CINAG)*, (Yokosuka, Japan), pp. 112-113, 15~16 June 2005.
Presentations at domestic conferences	K. Kazaura, K. Omae, T. Suzuki, M. Matsumoto, E. Mutafungwa, T. Murakami, K. Takahashi, H. Matsumoto, K. Wakamori, and Y. Arimoto, "Quantifying Effects of Atmospheric Turbulence in FSO Communications System," *IEICE General Meeting*, pp. B-1-25, Kokushikan Univ. Setagaya, 24~27 March 2006.

	K. Kazaura, K. Omae, T. Suzuki, M. Matsumoto, T. Sato, M. Hatori, T. Murakami, K. Takahashi, H. Matsumoto, K. Wakamori, and Y. Arimoto, "Study of Free-space Optical Communication System with transparency of fiber (3) – Scintillation Measurement for FSO Communication System," *IEICE Society Meeting*, Hokkaido Univ.、 Hokkaido, 20~23 September 2005. K. Kazaura, K. Omae, M. Matsumoto, T. Sato, K. Asatani, M. Hatori, A. Samejima, T. Suzuki, K. Takahashi, H. Matsumoto and K. Wakamori, "Study of Free-space Optical Communication Systems with transparency of fiber," *IEICE General Meeting*, Osaka, 21~24 March 2005.
Others	K. Kazaura, "Experimental Study on Next Generation Free-Space Optical Communication System," Technical Lecture given at the meeting of the Institution of Engineering and Technology, Japan Centre, Tokyo, 6 September 2006.
'Other achievements'	K. Kazaura, L. Jun and M. Matsumoto, "A Simulation Based Evaluation on the Performance of Integrated 3G – Wireless LAN Networks," *IEEE International Technical Conference (TENCON 2004*), Chiang Mai, Thailand, 21~24 November 2004.
Presentations at International conferences	K. Kazaura, E. Mutafungwa and M. Matsumoto, "An Investigation into the Optimum Integration Scenario. For Traffic Handling in a Combined 3G – WLAN Network System," *The Sixth International Symposium on Wireless Personal Multimedia Communications (WPMC03)*, Yokosuka, Japan, 19~22 October 2003. K. Kazaura, E. Mutafungwa P. Ulanga, T. Wakahara and M. Matsumoto, "Delivering Wireless Data Application in East Africa: Opportunities provided by MM-Wave Communication Systems," *The East African Telecommunications, Broadcasting Conference*, Nairobi, Kenya, 7~9 March 2002. K. Kazaura, T. Mwakabaga, E. Mutafungwa and M. Matsumoto, "Investigation on the Efficient Multimedia Traffic Handling for an Integrated 3G – WLAN Network," *The 2003 International Conference on Electrical Engineering and Technology (ICEET03)*, Dar Es Salaam, Tanzania, 18~19 August 2003.
Presentations at domestic academic meetings held by study groups	K. Kazaura, L. Jun and M. Matsumoto, "Deployment Strategies for Optimal Performance in Integrated Wireless LAN and 3G Cellular Networks," *Telecom Summit, 5th Academy and Industry Symposium (CINAG)*, (Yokosuka, Japan), 7~8 July 2004
Presentations at domestic conferences	K. Kazaura, T. Wakahara and M. Matsumoto, "Delivery of Multimedia Using High-Speed Millimeter Wave Communication Links," 2002 画像電子学会第 30 回年次大会画像電子学会&GITS/GITI 合同セッション 2 pp. 147-148, 2002.6. K. Kazaura, T. Wakahara and M. Matsumoto, "Modeling of High Speed Campus Network Using Millimeter Wave Communication Links," 年電子情報通信学会総 合大会 SB-12-6, 2002.3. カザウラカムギシャ、対馬正宏、若原俊彦、松本充 司, "60GHz Millimeter Wave Communication Links for High Speed Point-to-Point Communications – Waseda University Campus Network Case Study," 2001 年電子情報通信学会ソサイチィ大会 B-5-45, 2001. 9.

Others	カザウラカムギシャ、対馬正宏、若原俊彦、松本充 司, 60GHz 無線におけるポイントトポイント通信のシミュレーション検討, 2001 年電子情報通信学会総 合大会 B-5-233, 2001. カザウラカムギシャ、三宅、若原俊彦、松本充 司, “Experimental Study of Wireless Lecture Support System,” 画像電子学会第 28 回年次大会, pp. 1-2 (2000) E. Mutafungwa, K. Kazaura, K. Omae, T. Suzuki, M. Matsumoto, T.O. Korhonen, T. Murakami, K. Takahashi, H. Matsumoto, K. Wakamori, and y. Arimoto: Soft Computing-based Prediction to Enhance Performance of Next Generation FSO Communication Systems, Asia Pacific Microwave Photonics Conference (AP-MWP 2006), (Kobe, Japan), pp. 59-62, 24~26 April 2006. 鈴木 敏司, カザウラカムギシャ, 松本充 司, 村上匡亮, 大前和憲, 高橋浩一, 松本秀樹, 若森和彦, “光無線と光ファイバのフル光接続技術の研究開発”, 電子情報通信学会 MWP 研究会 於, 神戸, 2001.11 大前 和憲, 鈴木敏司, カザウラカムギシャ, 松本充 司, 佐藤 拓朗, 淺谷 耕一, 羽鳥 光俊, 村上 匡亮, 高橋 浩一, 松本 秀樹, 若森 和彦, “光波とミリ波の相互補完性に関する一検討”, 電子情報通信学会総 合大会, 世田谷, 2006.3 松本秀樹, 大前和憲, カザウラカムギシャ, 松本充 司, 鈴木敏司, 羽鳥光俊, 村上匡亮, 高橋浩一, 若森和彦, 有本好徳, ” フル光接続光無線システムの有効性評価”, 電子情報通信学会総 合大会, 世田谷, 2006.3 若森 和彦, 高橋浩一, 松本秀樹, 村上 匡亮, 羽鳥光俊, カザウラカムギシャ, 大前和憲, 松本充 司, 鈴木敏司, 有本好徳, “次世代光無線システムの研究開発”, 電子情報通信学会総 合大会, 世田谷, 2006.3 鈴木敏司, カザウラカムギシャ, 松本充 司, 佐藤拓朗, 淺谷耕一, 羽鳥光俊, 鮫島彰孝, 大前和憲, 高橋浩一, 松本秀樹, 若森和彦, “フル光接続光無線システムの研究開発(1) － 光無線と 60GHz 帯ミリ波無線との併用に関する評価の一検討(1) －”, 電子情報通信学会 ソサエティ大会 於, 2005.9 大前和憲, 鈴木敏司, カザウラカムギシャ, 松本充 司, 佐藤拓朗, 淺谷耕一, 羽鳥光俊, 村上匡亮, 高橋浩一, 松本秀樹, 若森和彦, “フル光接続光無線システムの研究開発(2) － 光無線と 60GHz 帯ミリ波無線との併用に関する評価の一検討(2)－”, 電子情報通信学会 ソサエティ大会 於, 2005.9 松本秀樹, 大前和憲, カザウラカムギシャ, 松本充 司, 佐藤拓朗, 鈴木敏司, 羽鳥光俊, 村上匡亮, 高橋浩一, 若森和彦, 有本好徳, “フル光接続光無線システムの研究開発(4) －光軸追尾と BER 計測システム－”, 電子情報通信学会 ソサエティ大会 於, 2005.9

	高橋浩一, 松本秀樹, 若森和彦, 羽鳥光俊, 村上匡亮, 有本好徳, 大前和憲, カザウラカムギシャ, 松本充司, 佐藤拓朗, 鈴木敏司, “フル光接続光無線システムの研究開発(5) －光学システム系概要－”, 電子情報通信学会 ソサエティ大会 於, 2005. 9 村上匡亮, 村上匡亮, 大前和憲, カザウラカムギシャ, 松本充司, 佐藤拓朗, 鈴木敏司, 羽鳥光俊, 高橋浩一, 松本秀樹, 若森和彦, 有本好徳, “フル光接続光無線システムの研究開発(6) －光波伝搬特性評価のための, 気象計測システムの評価－”, 電子情報通信学会 ソサエティ大会 於, 2005. 9 大前和憲, カザウラカムギシャ, 松本充司, 佐藤拓朗, 淺谷耕一, 羽鳥光俊, 村上匡亮, 鈴木敏司, 高橋浩一, 松本秀樹, 若森和彦, “フル光接続光無線システムの回線設計における一検討”, 画像電子学会 年次大会 於, 長野, 2005. 6 大前和憲, カザウラカムギシャ, 松本充司, 佐藤拓朗, 淺谷耕一, 羽鳥光俊, 鮫島彰孝, 鈴木敏司, 高橋浩一, 松本秀樹, 若森和彦, “フル光接続光無線システムの研究開発(1) － ファイバ直接受光型光無線装置の開発及び評価の一検討 －”, 電子情報通信学会 総合大会 於, 大阪, 2005. 3 L. Jun, K. Kazaura and M. Matsumoto: An Approach for Providing Location Information in IP Enabled Emergency Communication Service, IASTED International Conference on Communication Systems and Application (CSA 2004), July, 2004, Banff, Canada. L. Jun, K. Kazaura and M. Matsumoto: A low latency inter-system handover scheme for multiple interfaces terminal, IEEE 6th Circuits and Systems Workshop/Symposium on Emerging Technologies, Shanghai, 2004, China, May. T. Wakahara, Y. Meng, K. Kazaura, M. Matsumoto and T. Shimizu: A Voice Quality Measurement Method for PHS over IP Communication, 18th International Conference on Advanced Information Networking and Applications (AINA 2004), March 2004, Fukuoka Japan, pp 29- 31. L. Jun, K. Kazaura and M. Matsumoto: Location management of the emergency caller IP-based E911 network, IEICE/COMSOC Proceedings, Tokyo, March, 2004 L. Jun, K. Kazaura and M. Matsumoto: QoS Consideration for Intersystem handover in Heteregeneous Networks, IEICE 1st QoS Workshop, February, 2004. E. Mutafungwa, S.J. Halme, K. Kazaura, M. Matsumoto and T. Wakahara: Millimeter-wave over Fiber Systems Using Hybrid OCDM/WDM Transmission;, International Journal of Infrared and Millimeter waves, vol. 24, no. 7, pp. 1113-1126, July 2003 E. Mutafungwa, S.J. Halme, K. Kazaura, M. Matsumoto and T. Wakahara: Strategies for resource provisioning in optical networks supporting broadband wireless access network;, Journal of Optical Networking, vol. 2, no. 3, pp. 55-68, Mar. 2003 E. Mutafungwa, S.J. Halme, K. Kazaura, M. Matsumoto and T. Wakahara: Hybrid OCDM/WDM for Broadband Wireless Access Network, The Fifth Topical Symposium on Millimeter Waves (TSMMW2003), (Yokosuka, Japan), Mar. 2003

	E. Mutafungwa, S.J. Halme, K. Kazaura, M. Matsumoto and T. Wakahara: Efficient Utilization of Wavelengths in WDM Networks Supporting Broadband Wireless Access Networks, The Fifth Topical Symposium on Millimeter Waves (TSMMW2003), (Yokosuka, Japan), Mar. 2003 Edward Mutafungwa and Kamugisha Kazaura: A Modified Optical Add-Drop Multiplexer with Improved Transmission Performance, The 7th Asia-Pacific Conference on Communications (APCC 01), (Tokyo, Japan), pp. 546-550, Sept. 2001. Edward Mutafungwa and Kamugisha Kazaura: Assessing Opportunities for Broadband Optical Wireless Local Loops in an Unbundled Access Network, Lecture Notes in Computer Science (Mobile Data Access), H. Leong, W. Lee, B. Li, and L. Yin Eds, Springer-Verlag, vol. 1748, pp. 34-44, Dec. 1999.